Aus dem

Walter-Brendel-Zentrum für Experimentelle Medizin
Ludwig-Maximilians-Universität München
Vorstand: Prof. Dr. med. Ulrich Pohl

Lentiviral Magnetic Microbubbles: A guidable tool enabling targeted gene transfer to vascular endothelium *in vivo*

Dissertation

Zum Erwerb des Doktorgrades der Humanbiologie

An der Medizinischen Fakultät der
Ludwig-Maximilians-Universität zu München

Vorgelegt von

Yvonn Heun

Aus

Bernburg (Saale)

2017

Mit Genehmigung der Medizinischen Fakultät der Universität München

Berichterstatter

Prof. Dr. med. Florian Krötz

Mitberichterstatter

Prof. Dr. Christoph Klein
Prof. Dr. Gustav Schelling
Prof. Dr. Andreas Schober

Mitbetreuung durch die promovierte Mitarbeiterin

Dr. rer. nat. Hanna Mannell

Dekan

Herr Prof. Dr. Reinhard Hickel

Tag der mündlichen Prüfung

25.09.2017

"It always seems impossible until it is done."

-Nelson Mandela-

Table of Content

1 Introduction

1.1 Vascular gene therapy

By definition, gene therapy is the delivery of recombinant nucleic acids to somatic host cells with the intention to modulate endogenous gene expression thereby achieving significant improvement or reduced progression of a disease. In addition, a successful gene therapy might yield long-term effects which may supersede the need of drugs or even surgical interventions. In general, three types of gene modifications can be distinguished:

- Replacement of a mutated gene by its intact form,
- Inactivation of 'bad' gene substantially involved in genesis or progression of a disease (knock out),
- Introduction of a 'good' gene resulting in disease regression (knock in).

However, the whole topic of gene therapy requires considerations which are much more complex than just knocking a gene out or in. Also temporal and spacial factors, such as stability and location of the transgene expression are important. Uncontrolled gene transfer to non-target cells might turn beneficial effects of a therapy into severe side effects and too low expression can make the whole intervention useless. Therefore, the development of new gene targeting strategies is an important prerequisite to make gene therapy indeed a standard procedure for clinical application.

Effectivity and specificity of an implemented genetic modification strongly depend on the route of administration. The term intravascular gene therapy involves all types of therapeutic strategies where genetic vectors are applied via the systemic circulation. This form of application seems to be most reasonable for a variety of diseases involving the circulatory system such as cardiovascular diseases and a variety of solid tumors. However, vascular gene therapy remains challenging due to conditions given in the circulation, such as shear forces due to blood flow, systemic dilution and biological clearance mechanisms resulting from protein binding or immune cell activation [1]. Altogether these factors are causative for a strongly reduced local amount and therefore ineffective quantities of the therapeutic substance at the desired site. In most cases, an increase of dose is not always a rational answer to this problem as this may result also in enhanced drug actions at unintended sites in the body thereby inducing severe systemic side effects. For that reason intravascular gene therapy is still at a disadvantage to other approaches, such as local tissue injection. However, great scientific efforts are put into the abolition of these disadvantages

to finally utilize the natural benefits given by the circulation for gene therapeutic targeting:

- Passive convective transport of injected genetic vectors,
- Close proximity to an intended area of treatment (e.g. vascular cells, organs etc.),
- Low invasiveness of intravascular injection.

The potential areas of application for vascular gene therapy are various including treatment of inherited disorders, cancer or diseases of the cardiovascular system. As such diseases oftentimes demand the treatment of a localized vascular compartment, gene targeting is desirable. In addition, the development of an effective vascular gene delivery method has a substantial value for experimental studies of certain genes and proteins *in vivo*.

However, first clinical studies did not fulfill the initial promising expectations excited by prior animal studies [2]. Humoral and cellular immune responses, inefficient gene targeting and too low transgene expression may account for this. Therefore, more effective and safer gene delivery strategies are highly demanded to establish vascular gene therapy as a general procedure of clinical therapy.

1.2 Viral vectors applied in vascular gene therapy

The hydrophobic membranes of mammalian cells represent effective barriers against the introduction of naked genetic material (e.g. DNA and RNA). Therefore, successful gene therapy using these vectors has oftentimes proven challenging [3]. To overcome this basic natural hurdle, different physical (e.g. electroporation, sonication), chemical (e.g. lipofection, polymers) or biological (e.g. viral vectors) tools have been developed and are applied by scientists, either alone or in combination [1].

In this regard, especially viruses moved into the centre of attention of scientific efforts. Due to their unique evolutionary strategy to conquer the host cell´s membrane via active or passive mechanisms, viral vectors represent perfectly suitable vehicles for gene therapy [2, 4]. Accordingly, many experimental and clinical studies already applied virus-mediated gene delivery in order to achieve therapeutic gene expression. Importantly, to increase safety of virus-mediated gene therapy in patients, recombination technologies to modify the viral genome have been implemented resulting in more secure second- and third-generation virions [5]. There, viral genes encoding components dispensable for infection (e.g. replication proteins) have been removed resulting in replication deficient viruses capable to infect host cells only once. Among the available viruses, adenoviruses, adeno-associated

viruses and lentiviruses have been used most frequently in experimental and clinical gene therapy studies [6, 7]. Due to their considerable differences regarding genome structure, way of infection and transgene expression, the choice of an adequate vector needs to be considered carefully depending on the respective aspired therapeutic aim.

Adenoviruses are non-enveloped dsDNA viruses and infect dividing and non-dividing cells mainly via endosomal entry [2]. As they do not integrate into the host genome, adenoviruses are not associated with a known risk of insertional mutagenesis or genotoxicity. However, strong activation of the innate immune system results in profound limitations. Furthermore, the extrachromosomal state of the viral genome and the resulting transient transgene expression (< 14 days [8]) excludes adenoviruses for long-term gene therapeutic applications.

Adeno-associated viruses (AAV) from the family of *Parvoviridae* are non-enveloped ssDNA viruses, which attracted considerable interest for gene therapy due to their non-pathogenicity and low immunogenicity *in vivo* [2, 9]. Similar to adenoviruses, they infect dividing as well as non-dividing cells resulting in an extrachromosomal existence. Gene expression has been shown to persist longer (3-12 month [8, 10]) compared to adenovirus-mediated transduction, however, still remains transient. So far 13 AAV serotypes are known, whereby some of them show promising cellular tropisms (e.g. cardiotropic AAV9 or hepatotrophic AAV5) advantageous for organ specific expression upon systemic application. Unfortunately a considerable prevalence of patients with pre-existing neutralizing antibodies restricts the use of these vectors for clinical application [11].

Lentiviruses from the *Retroviridae* family contain a ssRNA genome and have been advanced from the human immunodeficiency virus-1 (HIV-1) [12, 13]. The current third-generation lentiviruses contain no more than 3 of the former 9 HIV-1 genes (named *gag*, *pol* and *env*), making them safe vectors applicable for *in vivo* gene transfer [5]. They infect dividing and non-dividing cells whereby their infection spectrum was significantly enhanced by recombinant replacement of the original envelope protein (*env*) by a VSV-G envelope protein (derived from vesicular stomatitis virus). The undeniable advantage of lentiviruses for gene delivery over other virus types persists in their ability to integrate their own genome cDNA into the host's genome resulting in stable and heritable transgene expression. A detailed scheme of the lentivirus structure and infection mechanism is depicted in Figure 1.1. Importantly, it has been shown that the integration of the lentiviral genome is predominantly occurring in downstream gene regions rather than promotor regions thereby significantly decreasing the risk of genotoxicity [7]. However, the former

mentioned broad infection spectrum of lentiviruses also represents a drawback especially for their therapeutic application via the circulatory system. Without a supportive targeting and shielding system, lentiviruses become rapidly cleared by circulating immune cells as well as infect cells at unintended sites leading to severe side effects. Accordingly, no clinical studies using lentivirus-mediated intravascular gene delivery have been performed so far. However, the general benefit of lentiviruses as therapeutic vehicles for gene therapy has been proven in clinical studies facilitating *ex vivo* transduction of autologous hematopoietic stem cells following cell transplantation in patients with β-thalassemia [14], X-linked adrenoleukodystrophy (ALD) [15] and Wiskott–Aldrich syndrome (WAS) [16]. The beneficial outcomes achieved in these patients strongly support the prospect that lentiviruses may be the first-choice gene vehicles for long-term gene therapy in the near future. Therefore, the development of carrier approaches enabling targeted delivery and reduced unspecific transduction by lentiviruses *in vivo* is an important step to take.

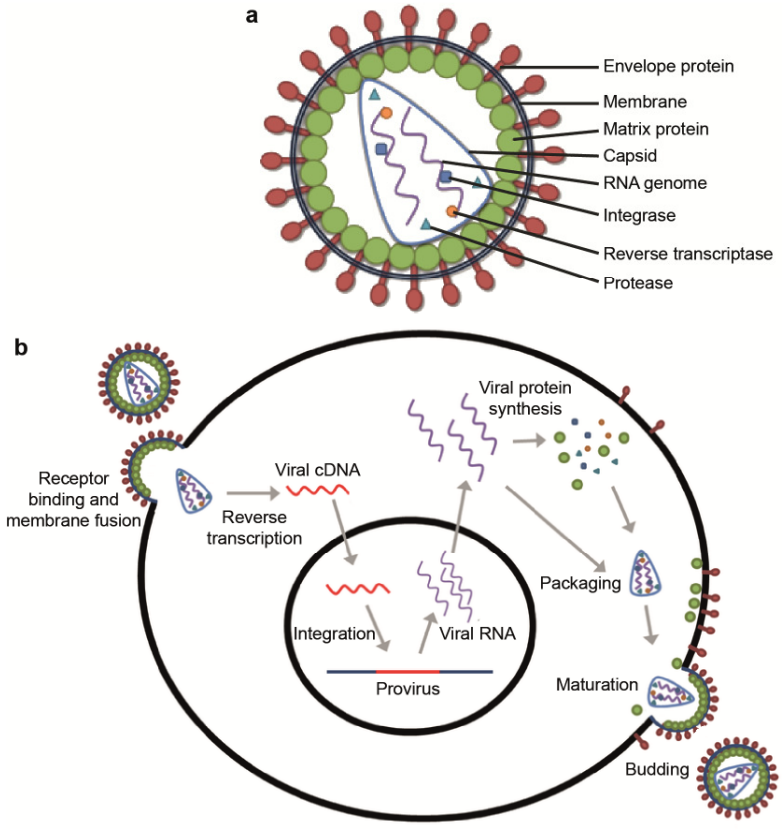

Figure 1.1. Lentivirus structure and infection/replication cycle.

(a) Unmodified lentiviruses feature an enveloped capsid core containing two copies of ssRNA as well as integrase, reverse transcriptase and proteases. **(b)** The natural infection and replication cycle of lentiviruses is shown. Recombinant lentiviral particles applied in gene therapy are deficient in viral replication and propagation. Adapted and modified from Eric P. O'Keefe, MATER METHODS 2013;3:174.

1.3 Available carrier systems for improved and guidable gene therapy

Low gene transfer and targeting efficiency are still the major obstacles limiting successful vascular gene therapy. To overcome these, supportive gene delivery systems capable of improving circulation time and drug targeting are needed. In this regard, important prerequisites such as non-toxicity, non-immunogenicity and biodegradability have to be considered before a carrier is eligible for *in vivo* and even clinical application. Furthermore, the binding behaviour between carrier and genetic vector must be effective and controllable. Thus, the binding stability between carrier and vector is as important as the triggered dissociation of both at the intended site of action. The implementation of surface modifications (charge, hydrophobicity, etc.) can substantially determine stability, binding behaviour and circulation time of the carrier and the bound therapeutic payload [1]. Also, other factors such as size and rigidity may have considerable influence on the effectivity of an intravascularly applied vector-carrier-system.

The range of available carriers, though, is as broad as the variety of genetic vectors. However, two categories have shown promising results in experimental studies and can therefore be highlighted: lipid- and nanoparticle-based gene carrier systems [1, 17]. In the context of gene therapy, lipid-based ultrasonic microbubbles and magnetic nanoparticles have been shown to be capable of binding genetic vectors and support gene transfer *in vitro* and *in vivo* [18, 19]. However, although both nanocarriers have been demonstrated to achieve targeted gene transfer upon either local ultrasound application (microbubbles) or magnetic field exposure (magnetic nanoparticles), they are still a far cry from standard procedures for clinical gene therapy. One possibility to maximize effectivity may be achieved by generating a synergistic carrier system combining the two mentioned approaches. The following sections will describe the single targeting methods in more detail and discuss the option of a combined approach.

1.3.1 Ultrasonic microbubbles – More than just contrast agents

Microbubbles have already been applied as a contrast agent in diagnostic ultrasound imaging since three decades [20]. Their additional potential as intravascular delivery vectors for biomaterials due to their unique physico-chemical properties was recognized around 15 years ago [18, 21]. In general, microbubbles can be generated from lipids, polymers or proteins, such as albumin, resulting in structures with very different physico-chemical properties [22]. All three of them have been shown to be capable to bind and deliver genetic vectors at a desired vascular site upon local application of ultrasound [22]. However, especially their excellent shell flexibility compared to the rather rigid polymer-based microbubbles as well as their high storage and circulation half life compared to protein-based microbubbles makes the lipid microbubbles splendid nanocarriers for vascular applications [22, 23]. Furthermore, lipid microbubbles are easily generated compared to other microbubble formulations as the amphiphilic lipids tend to self-assemble into small bubbles with diameters in the micrometer range around a gas-filled core, whereby the hydrophobic tails face the gas phase and interact via hydrophobic forces [23]. The gas core is thereby oftentimes filled with a poorly water-soluble gas, such as perfluorocarbon gas, increasing the stability and half-life of the microbubbles. The already mentioned high shape flexibility of lipid microbubbles enables the passage through even the smallest blood vessels (capillaries) after intravascular application. Importantly, it has been shown that microbubbles efficiently bind genetic material, such as DNA, RNA, siRNA and viral vectors, and that this binding results in reduced systemic clearance and subsequent increase in bioavailability also designated as shielding [23, 24]. By application of an acoustic pulse (ultrasound, US), the highly compressible microbubbles expand and contract. Depending on the strength of the applied US, this oscillation can be increased up to a frequency where the microbubble structure bursts. For the purpose of drug and gene targeting this disruption of microbubbles is highly desired, as it allows for controlled and localized substance release at the site of sonication. In addition, microbubble sonication has been shown to result in enhanced cellular uptake of the bound vectors due to temporal induction of cellular pores and intercellular cavities, a process called sonoporation [25]. Although a certain site-specificity of gene transfer can be achieved by locally applied ultrasound, systemic dilution strongly hampers the benefits given by this approach. As only a minor fraction of microbubbles are abundant at the site of ultrasound application after systemic injection, a higher dose is required to achieve sufficient vector concentrations at the desired

tissue location and therefore efficient gene transfer to cells and tissues. In addition, longer sonication times, to enable disruption of a higher fraction of microbubbles, may cause unintended tissue damage and vessel leakage. Therefore, targeting mechanisms, supplemental to localized ultrasound application are under intense investigations [1, 26].

1.3.2 Magnetic nanoparticle mediated gene targeting

Magnetic nanoparticles (MNP) are nanomaterials excellently qualified for biomedical applications, such as magnetic resonance imaging [27], tumour hyperthermia [28] and drug targeting [19]. The basic principle of directing and accumulating drug-loaded MNP by local application of an external magnetic field raised a huge scientific interest. In most experimental studies, MNP containing an iron-oxide core (also designated as superparamagnetic iron oxide nanoparticles; SPIONS) are used. In detail, iron-oxide MNP feature a γ-Fe_2O_3 (maghemite) or a Fe_3O_4 (magnetite) core resulting in intrinsic magnetism [19]. Magnetisation of the particles is exclusively induced by application of an external magnetic field with no remaining magnetic interaction upon removal of the magnetic field. Improved chemical and biological behaviour of iron-oxide MNP can be achieved by their coating with organic and inorganic materials such as PEG (polyethylene glycol), PEI (polyethylenimine) or silica. Such surface functionalizations can influence the colloidal stability and storage life, but have also substantial impact on drug binding capacity, biocompatibility and performance in complex biological environments such as blood [19]. Due to their small size they are able to pass cellular membranes whereby they potentially increase the cellular uptake of the bound substance by dragging it along. Concerning biocompatibility aspects, iron-oxide MNP have mostly been found to possess low cytotoxicity *in vitro* and *in vivo*. Especially if applied in low concentrations of <100 µg/ml relatively good compatibility and safety has been attested even in humans [29, 30]. Long-term, iron-oxide MNP are suggested to be mainly eliminated from the body via the hepatic iron metabolism resulting either in uptake to endogenous iron stores or renal excretion [31]. MNP-assisted gene transfer, so called magnetofection, is already an established approach alternatively applied to common *in vitro* transfection methods such as lipofection [32-34]. In several studies, MNP coated with viral [35, 36] and non-viral vectors [32, 37] have been tested for magnetically directed *in vivo* gene transfer. However, extensive interactions of MNP with blood cells, plasma proteins and glycocalix observed after systemic injection dampened the

initial hope of an easy guidable gene carrier system for vascular therapy [19, 27]. Therefore, the development of MNP with improved circulation time, magnetic susceptibility and vector coupling is still ongoing and also paved the way to combined approaches, such as magnetic nanocapsules, liposomes and microbubbles [19]. These, however, still need to be evaluated for their compatibility and effectivity *in vivo*.

1.3.3 Magnetic microbubbles – Combining shielding with targeting

The functionalization of microbubbles by coating them with different nanomaterials is a highly active field of research at the moment. Especially the embedding of superparamagnetic iron-oxide nanoparticles within the lipid monolayer represents a promising advancement in this regard. In the area of multi-modal imaging, such magnetic microbubbles (MMB) have been successfully tested for simultaneous magnetic resonance and ultrasound imaging after intravenous injection *in vivo* [38, 39]. Besides, the combination of ultrasound sensitive microbubbles, known for their good circulation behaviour, with magnetic nanoparticles, excellently suited for magnetic guidance and attraction even under flow conditions, may yield a synergistic gene delivery system with outstanding efficiency. MMB as nanocarriers for therapeutic genes have been addressed by some studies aiming at localized magnetic accumulation and, in some cases, their controlled ultrasonic burst [38, 40-42]. In general the MMB targeting procedures applied in these studies comprised the following components and parameters:

- Microbubbles generated from lipid solutions
- Magnetic nanoparticles for microbubble coating
- An external magnetic field gradient for accumulation of MMB
- Ultrasound for MMB rupture and release of payload
- Therapeutic payload (drug or genetic vector)

Due to the complexity of this targeting approach and the different *in vitro*, *ex vivo* and *in vivo* models used in the different studies, a direct comparison is hard to accomplish. However, only one study conducted in our group verified the functionality of MMB as guidable gene carrier system *in vivo* [40]. There, localized vascular targeting of MMB-coupled pDNA encoding a dsRed protein was successfully accomplished by application of a magnetic field and ultrasound. With the prospect to enhance vascular gene delivery, the applied MMB, prepared from a home-made phosholipid solution containing PEI-coated

MNP (Figure 1.2), has furthermore been used to generate lentiviral magnetic microbubbles in a second study [41]. Promising transduction rates have been achieved with these lentiviral PEI-Mag MMB *in vitro*, however their performance under complex *in vivo* conditions still has to be assessed. Furthermore, the constant progress of MNP development requires the regular re-evaluation of MMB-based gene carriers and their comparison to alternative compositions.

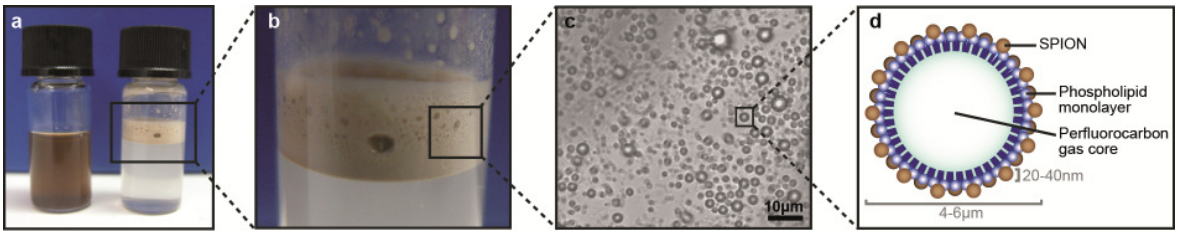

Figure 1.2. Self-assembly of magnetic microbubbles.
(a) and **(b)** Rapid shaking of a perfluorocarbon gas coated lipid-MNP mixture induces self-assembly of MNP-coated microbubbles (magnetic microbubbles, MMB) floating to the surface. **(c)** Microscopic image of MMB in solution. **(d)** Schematic illustration of a MMB featuring a gas-filled core and a phospholipid monolayer with incorporated MNP. Figure modified after Mannell et al. [40].

1.4 Targeting endothelial signaling by vascular gene therapy

The vascular system is the central organ of supply (e.g. oxygen and nutrients), elimination (e.g. CO_2 and metabolic end products) and regulation (e.g. hemostasis, immune responses and body temperature) taking part in essentially all processes of physiology. However, it is also involved in the development and progression of a variety of diseases and is therefore central object of scientific and clinical therapy. Endothelial cells are of huge interest in this regard. Due to their easy access from the blood and general importance for tissue homeostasis, endothelial cells are attractive targets for purposes regarding the therapeutic modulation of angiogenic, inflammatory or thrombotic processes.

1.4.1 The physiology and patho-physiology of vascular endothelium

The vascular endothelium, a single layer of endothelial cells sitting on a basal lamina, constitutes the inner lining of all blood vessels and therefore represents the barrier between blood and tissue. Endothelial cells are responsible for the regulation of a multitude of physiological functions regarding the circulatory system, including regulation of material transport and cell transit, adjustment of the vascular tone and maintenance of hemostasis [43]. The balance of these processes is finely adjusted by signaling processes responding to stimuli such as growth factors, cytokines and hormones, changes in shear stress or interactions with blood cells [44]. Under physiological circumstances, these signaling processes ensure an anti-thrombotic, vasodilative and anti-inflammatory state of the endothelium. However, considering this fundamentally important role of endothelial cells for the functioning of the circulatory system, it is not surprising that their dysfunction has been shown to be causative for a variety of diseases, such as peripheral vascular disease, stroke and venous thrombosis [43, 44]. In general, endothelial dysfunction can be defined as a pathological condition where the endothelium features pro-thrombotic, vasoconstrictive and/or pro-inflammatory properties.

A prevalent clinical condition, which has become interesting in the context of endothelial dysfunction, is insulin resistance, a pathological state in which the regular cellular response to insulin fails [45, 46]. Chronic insulin resistance may arise from permanent exposure of insulin responsive cells to abnormally high blood levels of insulin and glucose as can be found in pre-diabetic or obese patients. Untreated this condition may result in the full

manifestation of diabetes mellitus or metabolic syndrome. The result is a disturbed glucose homeostasis affecting the skeletal muscle, adipose tissue and liver. Furthermore, it has been shown that the incapacity of endothelial cells to respond to insulin leads to their dysfunction and is associated with deregulation of microcirculatory responses. Hence, these patients not only suffer from deregulated glucose metabolism but also develop severe secondary cardiovascular complications such as venous thrombosis, myocardial infarction, stroke and atherosclerosis [46, 47]. Furthermore, a large portion of patients featuring insulin resistance exhibit an impaired wound healing capacity [48, 49]. Explanations for this were found in a disturbed molecular equilibrium resulting in reduced production of vasoprotective substances (NO, prostacyclin) and over production of pro-inflammatory and –thrombotic factors (ROS, adhesion molecules, endothelin-1). The detailed disclosure of the molecular players involved in the development of endothelial dysfunction is the essential basis for the identification and application of new therapeutic targets.

A further, likewise important function in which endothelial cells are essentially engaged is angiogenesis, a process involving the induced proliferation and migration of endothelial cells from pre-existing vessels fundamentally important for the generation of any mature vessel [50]. The proper functioning of these processes is essential not only during embryonic development but also during adulthood e.g. for wound-healing. However, the malfunctioning of these angiogenic processes can lead to severe pathological conditions associated with either hyper- or hypovascularization, such as tumor growth or ischemic diseases, respectively [51, 52]. The therapeutic aim to treat these diseases by modulating angiogenic processes requires careful and ideally local treatment approaches.

Several therapeutic strategies, including genetic approaches, aiming for the beneficial re-equilibration of endothelial function are intensively explored and partially applied already. The therapeutic delivery of genes provides the opportunity to re-equilibrate disturbed intracellular processes thereby attenuating symptoms and progression of a disease. In addition, expression-based modulation of endothelial function may achieve efficient long-term effects, which might be otherwise only realized by constant drug application.

Furthermore, experimental gene targeting *in vivo* may help to elucidate gene and protein functions involved in endothelial patho-physiological processes. The ability to locally modulate the endothelial gene expression within a desired organ or tissue might be a powerful tool to answer complex scientific questions superseding the complicated and time consuming process of generating conditional transgenic animals.

The choice of putative targets for experimental and clinical endothelial gene therapy is

huge, especially as scientific research gains increasingly detailed information about the molecular basis of diseases. In the following two sections the focus is laid on two promising molecules which are interesting candidates being addressed as therapeutic or scientific targets to be studied by help of gene delivery approaches, such as the new lentiviral MMB technique.

1.4.2 The vascular endothelial growth factor as target for therapeutic angiogenesis

The vascular endothelial growth factor (VEGF) is a highly potent angiogenic factor with unique actions on vascular endothelium. Its secretion and recognition is crucial to initiate the formation of immature vessels by vasculogenesis or angiogenic sprouting [53]. Besides its important physiological role during embryonic development and wound healing, it is also involved during several patho-physiological conditions, such as ischemia, diabetic retinopathy and tumour vascularization [53]. Hence, VEGF has been used as a therapeutic target either to promote vascularization by its induction [54, 55] or to impair vessel growth by its inhibition [56]. In experimental studies aiming at the revascularization of ischemic tissues (e.g. hindlimb-ischemia in rabbit [57] or myocardial ischemia in pigs [58]) VEGF expression has been shown to result in long-term benefits. Accordingly, VEGF-mediated therapeutic angiogenesis by gene therapeutic approaches has been attempted in a variety of clinical phase I/II studies. There, pDNA [59-61] or adenoviral vectors [62, 63] have been used in patients with coronary heart disease or peripheral arterial disease whereby successful vector delivery was only achieved by direct tissue injection or local catheter-application of the genetic vectors [55, 64, 65]. Unfortunately, in most of these studies VEGF expression yielded only unsatisfactory patient outcomes and therefore did not reflect the beneficial effects seen in the animal studies [65]. Too low gene transfer efficiencies and accordingly insufficient VEGF expression might be the chief cause for these negative results. Therefore, an advanced intravascular targeting strategy may constitute a valuable tool to achieve effective localized modulation of angiogenesis by targeted gene delivery of VEGF via the circulation.

1.4.3 The protein-tyrosine phosphatase SHP-2 in endothelial dysfunction

The SH2 domain-containing protein tyrosine phosphatase-2 (SHP-2; synonyms: SH-PTP2, SH-PTP3, PT-P2C, PTP1D or Syp) is a cytosolic phosphatase ubiquitously expressed in virtually all types of mammalian cells [66]. On the structural level, SHP-2 possesses three functional domains: two N-terminal SH2 domains, a central catalytic phosphatase domain and two C-terminals tyrosine phosphorylation sites (Tyr^{542} and Tyr^{580}). Under basal conditions, SHP-2 is supposed to exist mainly in its auto-inhibited state as depicted in Figure 1.3. Upon cytokine or growth factor stimulation this inactive conformation is released rendering SHP-2 into a fully active enzyme or adaptor molecule [66]. Depending on the involved functional domain, SHP-2 has been shown to participate in a variety of intracellular signaling cascades including the Ras/MAPK and the PI3K/AKT pathways [66, 67] resulting in modulation of metabolic [68, 69], inflammatory [66, 70-72] and motogenic responses [73-75]. In endothelial cells, SHP-2 has been identified as an important regulator of angiogenic [75, 76] and inflammatory processes [72, 77, 78]. The development of endothelial dysfunction induced under chronically high insulin levels, as observed in the condition of insulin resistance or diabetes mellitus, has been shown to be substantially influenced by SHP-2's enzyme activity as well as by its function as an adaptor molecule [68, 69, 72]. However, the molecular mechanisms stated in these studies are partially inconsistent. To allow for a detailed elucidation of SHP-2-mediated processes during insulin resistance further detailed studies are necessary. The lentiviral MMB technique provides the opportunity to study SHP-2's function in endothelial cells *in vivo* and may potentially help to verify SHP-2 as an attractive target for vascular therapy.

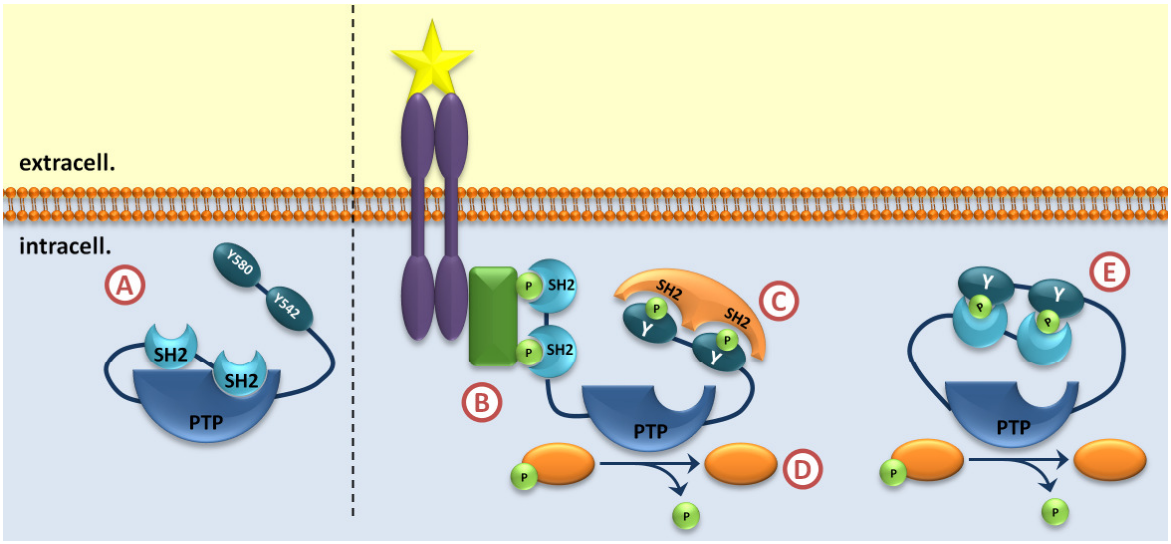

Figure 1.3. Structure and signaling mechanisms of SHP-2.

(A) SHP-2 features three functional domains, namely the two N-terminal SH2 domains, the PTP domain and two C-terminal tyrosine motifs (Y580 and Y542). In non stimulated cells SHP-2 is believed to exert rather low basal activity due to its auto-inhibitory confirmation maintained by close association of the N-SH2 and the PTP domain. **(B)** The auto-inhibitory conformation is released upon binding of SHP-2 via its SH2 motifs allowing recruitment to signaling complexes. Signals can be conducted via further recruitment of SH2 domain containing binding partners to phosphorylated tyrosine residues of SHP-2 **(C)** or by dephosphorylation of specific substrates **(D)**. **(E)** A further model suggests a self-activation mechanism of SHP-2 enzyme activity mediated by the interaction of the SH2 domains with the phosphorylated tyrosines.

1.5 Aim of the thesis and study objective

Endothelial dysfunction provides a substantial foundation for the development and progression of many cardiovascular diseases. Related therapeutic strategies oftentimes imply invasive interventions or repeated systemic drug applications known to result in side-effects due to unspecific drug uptake. For most cardiovascular pathologies, however, a local and long-lasting therapeutic strategy would be desirable. Furthermore, such an approach would represent an invaluable tool for experimental studies.

The use of MMB for the delivery of genetic vectors from the systemic circulation to a desired site of the vasculature has shown promising results in experimental studies [40, 41]. However, due to the rapid progress in the field of nanoparticle design, the MMB technique requires constant advancement and re-evaluation to provide maximal efficiency. Therefore the aim of this study was to answer the following questions:

- Can a new type of silicon-oxide coated MNP (SO-Mag MNP) be used to generate lentiviral MMB?
- Which physico-chemical (size, magnetic moment) and biological (lentivirus binding, cytotoxicity) properties do these new SO-Mag MMB possess and what are the differences compared to the formerly established PEI-Mag MMB?
- Does magnetic and ultrasonic targeting of SO-Mag MMB to cultured endothelial cells yield an improved gene delivery efficiency compared to the PEI-Mag MMB?
- How do the single technical parameters MMB, MF and US contribute to the enhanced gene transfer achieved by the lentiviral MMB technique and which cellular uptake mechanism is facilitated by MMB-mediated gene transfer?
- Does the lentiviral MMB technique also enable local transduction of the intact endothelial layer in isolated mouse aortas? Can physiologically relevant effects be achieved in these vessels by the MMB-mediated introduction of a therapeutic gene, such as VEGF?
- Which role does the protein tyrosine phosphatase SHP-2 play during endothelial insulin resistance and can these findings be translated to the *ex vivo* aorta model by using MMB-mediated gene transfer of SHP-2 mutant constructs?
- Does the magnetic and ultrasonic targeting of systemically applied lentiviral SO-Mag MMB result in localized gene expression *in vivo*?
- How do the applied MNP distribute in the body in short-term and what is the systemic expression pattern of the lentiviral vector?

2 Material and Methods

2.1 *In vitro* and *ex vivo* studies

2.1.1 Generation and production of lentiviral constructs

Plasmids encoding SHP-2 wild type (WT) and the dominant negative mutant SHP-2 CS (Cys459 to Ser459) were a kind gift from Prof. Anton M. Bennett [79]. A c-Myc-Tag sequence joined to the SHP-2 cDNA sequence allowed for distinction between endogenously and ectopically expressed SHP-2 and selective immunoprecipitation using a Myc-Tag antibody. The constitutively active mutant SHP-2 E76A (Glu76 to Ala76) was generated from SHP-2 WT using the QuikChange II XL Site-Directed Mutagenesis Kit (Agilent, CA, USA) following the manufacturer's instructions. The SHP-2 constructs as well as constructs encoding human $VEGF_{165}$, GFP and viral-enhanced firefly luciferase (veffLuc) were each subcloned into a self-inactivating RRL-lentiviral backbone under control of a CMV-promotor. SHP-2 constructs additionally contained an IRES-GFP co-expression cassette allowing for detection of positively transduced cells. Non integrating fluorescence-labeled rrl-CMV-pCHIV.eGFP lentiviral particles were generated as described by Lampe et al. [80]. Lentiviruses containing the different expression constructs were produced in cooperation with the viral vector platform of Prof. Alexander Pfeifer's group (Bonn University) within the DFG Research Unit FOR917 [81]. Depending on the respective lentiviral construct, either the biological titer or the physical titer of the viral preparations was determined. For lentiviruses including a GFP-reporter cassette (GFP LV and SHP-2 WT/CS/E76A LV), biological titers (infectious particles (IP)/µl), were assessed by application to HEK293T cells following quantification of positively transduced cells by flow cytometry [82]. For veffLuc LV, VEGF LV and pCHIV.eGFP LV the physical titer (viral particles (VP)/µl) was assessed by measuring the reverse transcriptase activity [82].

Table 2.1. List of applied lentiviral vectors.

Lentivirus	Abbreviation	Expression
rrl-CMV-SHP-2 WT/CS/E76A-IRES-GFP	SHP-2 WT/CS/E76A LV	Myc-tagged SHP-2 proteins, GFP co-expression
rrl-CMV-eGFP	GFP LV	GFP
rrl-CMV-veffLuc	veffLuc LV	Firefly luciferase
rrl-CMV-pCHIV.eGFP	pCHIV.eGFP LV	---
rrl-CMV-$VEGF_{165}$(hu)	VEGF LV	Human $VEGF_{165}$

2.1.2 Isolation and cultivation of human umbilical cord endothelial cells (HUVEC)

All procedures involving primary endothelial cells were performed in accordance with the Declaration of Helsinki. Human umbilical cord endothelial cells (HUVEC) were isolated from the veins of human umbilical cords received from a local hospital. For storage, umbilical cords were placed in screw beakers (Sarstedt, Nümbrecht, Germany) with PBS+ supplemented with 1% penicillin/streptomycin (Sigma-Aldrich, Seelze, Germany). Isolation of HUVEC was performed at the latest 48 h upon receipt. Therefore, a buttoned cannula was inserted in one end of the vein and fixed with zip tie. The vein was perfused with 10 ml PBS- to wash out residual blood and a second buttoned cannula was inserted and fixed to the other side of the vein. Three-way-valves (Braun, Melsungen, Germany) were attached to the cannulas on both sides thereby allowing for filling of the vein with 5 mg/ml Collagenase A solution (Roche, Basel Switzerland). The umbilical cord was placed in a pre-warmed waterbath (Memmert, Schwabach, Germany) at 37°C and incubated for 10 min. Detached endothelial cells were rinsed from the vessel with 10 ml DMEM (Sigma-Aldrich) and collected in a Falcon tube (Sarstedt) following centrifugation at 300 g for 5 min. Pelleted cells were resuspended in 4 ml Endopan3 medium (PAN-Biotech, Aidenbach, Germany) and transferred to a T25 tissue culture flask (Sarstedt). HUVEC were cultured in a humidified incubator (Heraeus HERAcell, ThermoFischer Scientific, Waltham, USA) under 37°C and 5% CO_2 conditions. Remaining blood cells were removed the following day by washing once with PBS+ and Endopan3 medium was exchanged daily until cells reached confluence. HUVEC were then transferred to 10 cm culture dishes (Sarstedt) and were further cultured with a 50/50 mixture of DMEM containing 20% FCS (Biochrom, Darmstadt, Germany) and Endopan3 supplemented with 1% penicillin/streptomycin (further referred to as HUVEC growth medium). For seeding, cells were washed with PBS- and detached by adding 1x trypsin/EDTA solution (Sigma-Aldrich) for 2-3 min. Detached cells were subsequently resuspended in fresh HUVEC growth medium and transferred to appropriate dishes. All experiments with HUVEC were performed up to passage 5.

→ PBS + (Phosphate buffered saline with calcium and magnesium)

136.9 mM	NaCl
2.7 mM	KCl
10.1 mM	Na_2HPO_4
1.8 mM	KH_2PO_4
0.42mM	$MgCl_2$
4.5 mM	$CaCl_2$

PBS+ was prepared in distilled water, brought to pH 7.4 and sterilized by filtration.

→ PBS- (Phosphate buffered saline without calcium and magnesium)

136.9 mM	NaCl
2.7 mM	KCl
10.1 mM	Na_2HPO_4
1.8 mM	KH_2PO_4

PBS- was prepared in distilled water, brought to pH 7.4 and sterilized by autoclaving.

2.1.3 Freezing and thawing of HUVEC

For long-term storage, cells from confluent 10 cm cell culture dishes were detached by adding 1x trypsin/EDTA solution and resuspended in 1 ml FCS supplemented with 10% DMSO (Sigma-Aldrich). Freezings were done in cryovials (Sarstedt) and gentle reduction of temperature (~1°C per minute) was achieved by using polystyrene containers (CoolCell, Biocision, San Rafael, USA). Cells were placed for 2 days in the -80°C freezer and were subsequently stored in liquid nitrogen. For restoration of cells into cell culture, the freezings were thawed quickly and added to 10 ml HUVEC growth medium in a 10 cm cell culture dish. Medium was exchanged after 4 h and cultivation was continued as described before.

2.1.4 Lentiviral transduction of HUVEC with SHP-2 mutants

Over-expression of the SHP-2 WT and its functional mutants SHP-2 CS and E76A (all featuring a c-Myc-Tag) in HUVEC was achieved by lentiviral transduction with SHP-2 WT/CS/E76A LV. In detail, IP corresponding to a multiplicity of infection (MOI) of 5 were diluted in Hank's balanced salt solution (HBSS; Biochrom, Berlin, Germany) and lentivirus solutions were applied onto subconfluent (~80%) cell cultures. After incubation for 4 h HUVEC growth medium was added and fresh medium was applied the next day. Cells were left 72 h for gene expression before assaying.

2.1.5 Analysis of adhesion molecule surface expression by flow cytometry

HUVEC grown in 6-well plates (Sarstedt) were treated with DMEM containing 15 mM glucose and 100 nM human insulin (Insuman Rapid 40 IU/ml, Sanofi Frankfurt a. Main, Germany) for 24 h and 48 h. To ensure proper bioactivity of insulin, stimulation medium on 48 h stimulated cells was refreshed after 24 h. To detect ICAM-1 and VCAM-1 surface expression, HUVEC were washed with PBS- and detached by Accutase (GE Healthcare, Solingen, Germany). Cells were then pelleted (1200 g, min), rinsed and incubated with allophycocyanin- (APC) labelled ICAM-1 and VCAM-1 antibodies (1:40 in PBS+; BD Bioscience, Heidelberg, Germany) for 30 min at room temperature in the dark. Cells were washed, resuspended in 250 µl PBS+ and transferred to FACS tubes (Sarstedt). APC-fluorescence intensities were detected by flow cytometry using a FACS Canto II (BD Bioscience). Alongside, cells incubated with an APC-labelled IgG1 isotype antibody were measured as control for unspecific antibody binding. Cells positively transduced with the SHP-2-WT/CS/E76A LV were identified by detection of co-expressed GFP. Median APC-fluorescence intensities were set relative to non stimulated controls.

Table 2.2. List of antibodies used for flow cytometry analysis.

Antibody	Label	Source/Type	Company / Cat.Nr.
α-ICAM-1 IgG_1	APC	mouse (mc)	BD Bioscience / 559771
α-VCAM-1 IgG_1	APC	mouse (mc)	BD Bioscience / 551147
IgG_1 isotype	APC	mouse (mc)	BD Bioscience / 555751

2.1.6 Synthesis of surface-modified magnetic nanoparticles

Synthesis of core–shell type iron oxide magnetic nanoparticles (MNP) has been performed in cooperation with Dr. Olga Mykhaylyk corresponding to a published protocol [83]. To improve the physico-chemical and biological properties of the synthesised MNP, surface modification were carried out. Polyethylenimine-coated (PEI-Mag) MNP were generated by combining the fluorinated surfactant ZONYL FSA (lithium-3-[2-(perfluoroalkyl)ethylthio]propionate) with 25-kDa branched polyethylenimine. Silicon oxide-coated (SO-Mag) MNP were generated by condensation of tetraethylortho-silicate and 3-(trihydroxysilyl)propylmethylphosphonate resulting in a silicon oxide layer with surface phosphonate groups. The general physico-chemical properties of SO-Mag and PEI-Mag MNP have been already described [36, 84] and are summarized in Table 2.3.

Table 2.3. Physico-chemical characteristics of SO-Mag and PEI-Mag MNP.

Characteristic	SO-Mag MNP	PEI-Mag MNP
Coating	Silicon-oxide	Polyethylenimine
ζ-Potential in ddH_2O [mV]	-38.0 ± 2.0	+55.0 ± 0.7
Magnetic moment [fAm²]	$8.7*10^{-5}$	$5.8*10^{-5}$
Iron weight per particle [µg Fe/particle]	$6.2*10^{-13}$	$1.4*10^{-12}$
Core diameter [nm]	6.8	9.0
Hydrodynamic diameter in ddH_2O [nm]	40.0 ± 14.0	28.0 ± 2.0

2.1.7 Production of lentiviral magnetic microbubbles

As basis for the production of MMB, a phospholipid solution was prepared as previously described [40]. To receive 10 ml of this phospholipid solution, 2 mg DPPE (1,2-dipalmitoyl-sn-glycero-3-phosphoethanolamine) and 10 mg DPPC (1,2-dipalmitoyl-sn-glycero-3-phosphocholine) kindly provided by Lipoid GmbH (Ludwigshafen, Germany) were given into a pear-shaped flask and 350 µl chloroform were added. The flask was attached to a rotary evaporation device (Rotavapor, Büchi Labortechnik, Essen, Germany) with connected vacuum pump. Phospholipids were allowed to completely dissolve by gentle rotation in a water bath (Weinkauf Medizintechnik, Forchheim, Germany) at 60°C for 10 min without vacuum. The chloroform was then removed by vacuum-assisted evaporation for 1.5 h under permanent rotation in a water bath at 60°C. After complete drying,

phospholipids were dissolved in 10 ml of a sterile 10% glycerine solution by rotation at 60°C for 10 min. The generated phospholipid solution was stored at 4°C for up to 3 month. To generate lentiviral MMB, MNP (SO-Mag or PEI-Mag) corresponding to a total iron weight of 150 µg or 250 µg were added to 1 ml phospholipid solution in 1.5 ml glass vials with screw caps and silicon/PTFE membranes (Omnilab, Bremen, Germany). The mixture was then covered with perfluorocarbon gas (Linde, Munich, Germany) and rapidly shaken for 20 s in a CapMix™ (3M ESPE, Neuss, Germany). Immediately before performing the experiment, lentiviral particles were added to the MMB solution in an optimal lentivirus:iron ratio given in Table 2.4. Lentivirus-MMB complex formation was left to occur for 10 min before use.

Table 2.4. Used LV:iron ratios and corresponding LV:MMB ratios.

LV	optimal LV:iron ratio	LV:MMB ratio (150 µg Fe/ml MMB)	LV:MMB ratio (250 µg Fe/ml MMB)
GFP	$3.3*10^5$ IP/µg Fe	$5*10^6$ IP/ml	
SHP-2 WT/CS/E76A	$3.3*10^5$ IP/µg Fe	$5*10^6$ IP/ml	-
pCHIV.eGFP	$3.3*10^6$ VP/µg Fe	$5*10^7$ VP/ml	-
veffLuc	$3.3*10^6$ VP/µg Fe	$5*10^7$ VP/ml	$8.3*10^7$ IP/ml
VEGF	$3.3*10^6$ VP/µg Fe	$5*10^7$ VP/ml	8.3*107 IP/ml

MMB containing 150 Fe µg/ml were used for all *in vitro* experiments. For *in vivo* experiments 250 µg Fe/ml MMB were used.
LV: lentivirus, Fe: iron, IP: infectious particle, VP: viral particle.

2.1.8 Characterisation of physico-chemical properties of MMB

Diameter (µm) and density (MB/ml) of MB in solution with or without associated MNP (SO-Mag or PEI-Mag) and lentiviruses (pCHIV.eGFP) were measured in 1:1000 dilutions in HBSS using a Casy Counter (Schärfe Systems, Roche Diagnostics, Mannheim, Germany). Mean iron content (µg Fe/MMB) and MNP content (MNP/MMB) were calculated from MMB densities (MB/ml). ζ-potentials of MMB, MNP and lentivirus in HBSS or serum were measured by photon correlation spectroscopy using a Malvern 3000 HS Zetasizer (Malvern, Herrenberg, Germany).

2.1.9 Visualization of Lentivirus-MMB complex formation

Lentivirus-MMB complex formation was visualized by fluorescence microscopy (Axiovert 200M microscope, Zeiss, Jena, Germany) using fluorescence-labelled pCHIV.eGFP lentiviral particles. Lentiviral MMB were given on a microscope slide and covered with a glass coverslip (Menzel, Braunschweig, Deutschland). Transmission light and fluorescence images were taken at 63-fold magnification (Plan-Apochromat 63x/1.4 oil immersion objective, Zeiss). Complex formation between pCHIV.eGFP and MMB was furthermore verified by flow cytometry. Therefore, MMB solutions with or without addition of lentiviruses were diluted 1:100 in HBSS and analyzed using a FACS Canto II (BD Biosciences). Median GFP-fluorescence intensities of lentivirus MMB complexes were detected in the FITC-channel.

2.1.10 MMB magnetizability and lentivirus binding capacity

To analyse if the generated MMB are capable to completely associate the applied lentiviral particles, GFP LV ($5*10^6$ IP/ml MMB) were incubated with MMB solutions (150µg Fe/ml) for 10 min. Mixtures were then exposed to a magnetic field for 15 min resulting in the generation of a MMB-free supernatant and concentrated lentiviral MMB. Meanwhile, medium on HUVEC cultured in 6-well plates (Sarstedt) was exchanged by HBSS. The MMB-free supernatants as well as the lentivirus-MMB concentrates were applied to HUVEC in separate wells. Culture plates were subsequently placed on top of a neodymium iron boron magnet (IBA Bio TAGnology, Goettingen, Germany) and US (2 W/cm², 1 MHz, 50% duty cycle; Sonitron, Rich-mar, Schwaebisch Gmuend, Germany) was applied for 30 s by submerging the transducer into the solution. After 30 min of incubation on the magnetic plate, cells were washed once with PBS+ and provided with HUVEC growth medium. GFP expression was visualized 72 h later by fluorescence microscopy (Axiovert 200M microscope, Zeiss) taking images at 10-fold magnification. Additionally, percentage of GFP-expressing cells was quantified by detaching cells with trypsin/EDTA and analysis by flow cytometry using a FACS Canto II (BD Biosciences).

2.1.11 Velocity and magnetic moment measurements of MMB

Magnetic responsiveness measurements to determine velocity and magnetic moment of the MMB under a magnetic field with a magnetic gradient of approximately 7.8 T/m were performed in cooperation with Dr. Alexandra Heidsieck from the IMETUM (Technical University, Munich) as described before [85].

2.1.12 Validation of the lentiviral MMB technique under static conditions **in vitro**

The individual gene transfer efficiencies of the two MMB types in combination with the whole targeting procedure, comprising MF and US application, were tested under static conditions using HUVEC. Therefore, medium on HUVEC cultured in 12-well plates was exchanged by HBSS and the well dish was placed on a magnet plate. Meanwhile, GFP LV was incubated with MMB solutions (150 µg Fe/ml). 2 µl of the lentivirus-MMB complexes (corresponding to $1*10^4$ IP) were added to each well and ultrasound (30 s, 2 W/cm^2, 1 MHz, 50% duty cycle) was applied. After treatment, cells were further incubated on the magnet plate for 30 min at 37°C. Cells were then rinsed with PBS+ and cultured in HUVEC growth medium for 72 h before detection of GFP expression by fluorescence microscopy and flow cytometry. Untreated cells as well as cells incubated with $1*10^4$ IP of GFP LV for 30 min were analyzed as controls. To assess the individual contribution of MMB, MF or US to the whole lentiviral MMB technique, these single method parameters were omitted from the procedure, which was otherwise kept the same.

2.1.13 Validation of the lentiviral MMB technique under flow conditions **in vitro**

To test the ability of the lentiviral MMB to be targeted by MF and US under flow conditions, perfusion experiments with HUVEC were performed. Therefore, HUVEC were grown to confluence in channel slides (µ-slides IV$^{0.4}$, IBIDI, Martinsried, Germany), which allow for the application of defined flow conditions. Channels were centrally placed above a magnet and were connected to a HBSS-filled syringe avoiding air inclusions. Perfusion of cells with HBSS was done at shear rates of 1, 5 or 7.5 dyn/cm^2 using a syringe pump (kdScientific, Holliston, MA, USA). For each channel, 20 µl of MMB solution were

preincubated with veffLuc LV ($1*10^5$ VP) for 10 min following 1:10 dilution in HBSS. Under continuous perfusion, lentivirus MMB complexes were slowly injected upstream of the cells into the tubing system. US (30 s, 1 MHz, 2 W/cm^2, 50% duty cycle) was applied at the site of MF exposure. After 2 min perfusion HUVEC growth medium was added and slides were incubated for 72 h to allow for transgene expression. To assess the individual contribution of MF or US to the efficiency of the whole lentiviral MMB technique under flow, each of these two method parameters was omitted from the procedure, which was otherwise kept the same. Furthermore, 20 µl of MNP-lipid mixture incubated with GFP LV were perfused over HUVEC and targeted as described. Luciferase activity was detected after application of VivoGlo™ luciferin (0.5 mg/ml in PBS+; Promega, Madison, USA) using an IVIS imaging system from PerkinElmer (Waltham, MA, USA) at different exposure times. Transduction efficiencies were quantified by measurement of pixel density using the Hokawo software (Hamamatsu Photonics, Hamamatsu City, Japan).

2.1.14 MTT assay

To assess if the lentiviral MMB technique has cytotoxic effects on primary endothelial cells, the MTT assay was performed as previously described [76]. This colorimetric assay allows for quantification of the metabolic activity of cells by detecting their ability to reduce the yellow MTT (3-(4,5-di**m**ethyl**t**hiazol-2-yl)-2,5-diphenyl**t**etrazolium bromide) to its insoluble purple formazan salt (see Figure 2.1). As metabolic activity is closely associated to cell viability this assay can also be applied for cytotoxicity measurements.

In detail, HUVEC cultured in 24-well plates (Sarstedt) were treated with single and combined components of the lentiviral MMB technique (GFP LV ± 150 µg Fe/ml PEI-Mag/SO-Mag MMB ± MF ± US) as described under 2.1.12. 72 h after treatment medium was removed and 500 µl of MTT solution (5 mg/ml in DMEM without phenolred; Sigma-Aldrich) were added to each well. Plates were placed in the incubator for 2 h and cells were washed with PBS+ afterwards. Generated formazan crystals were dissolved by addition of 100% 2-Propanol and 100 µl of the solution were transferred to a 96-well plate. Absorbance and background was measured at 550 nm and 620 nm, respectively, in a microplate reader (Spectra Fluor, Tecan, Maennedorf, Switzerland). Background was subtracted and absorbance values were normalized to values of untreated cells.

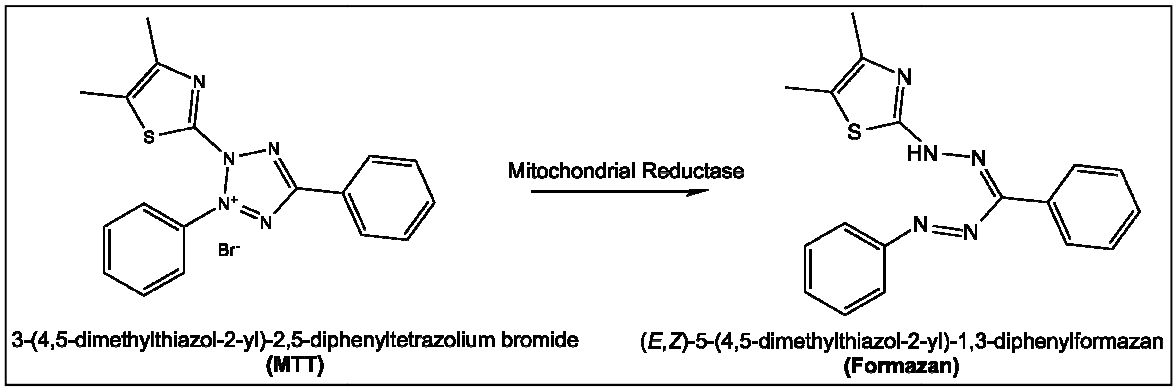

Figure 2.1. Molecular principle of the MTT Assay.
In living cells, the yellow-coloured MTT becomes reduced to its purple-coloured formazan salt by NAD(P)H-dependent cellular oxidoreductase enzymes within the mitochondria. The quantification of the formed formazan by absorbance measurements allows for indirect detection of cell viability. (Scheme adapted from Rogan Grant - Own work, CC BY-SA 4.0)

2.1.15 Identification of the cellular uptake mechanism responsible for lentiviral MMB mediated transduction

To identify the responsible mechanism of uptake relevant for lentiviral MMB-mediated gene delivery, HUVEC were incubated with specific inhibitors of different endocytic pathways previous to SO-Mag MMB mediated transduction. Caveolae-mediated endocytosis was inhibited by incubation with 10 mM methyl-β-cxclodextrin (MβCD; Sigma-Aldrich). Inhibition of phagosome-lysosome fusion was accomplished by incubation with 10 nM ammoniumchloride (NH_4Cl, Sigma-Aldrich) and 10 µM Cytochalasin B (CytoB, Sigma-Aldrich) were used to inhibit the clathrin-mediated endocytic pathway. All three inhibitors were diluted in DMEM supplemented with 20% FCS and 1% penicillin/streptomycin and preincubated on cells for 30 min. Lentiviral MMB were prepared and the transduction procedure was conducted as described under section 2.1.12. Afterwards, cells were washed once with PBS+ and maintained with HUVEC growth medium. Percentage of GFP expressing cells indicating efficiency of virus uptake was detected 72 h after transduction by flow cytometry.

Table 2.5. List of applied endocytic inhibitors and respective mechanism of action.

Inhibitor	Appl. conc.	Mechanism
Methyl-β-cyclodextrin (MβCD)	10 mM	Inhibits caveolae-mediated endocytosis by cholesterol extraction from the plasma membrane and prevention of lipid raft formation [86].
Ammoniumchloride (NH_4Cl)	10 nM	Inhibits phagosome-lysosome fusion by neutralizing the endosomal pH and prevention of viral entry dependent on vesicle acidification [87].
Cytochalasin B (CytoB)	10 µM	Inhibition of clathrin-mediated endocytosis by actin-depolymerization preventing vesicle trafficking [88].

2.1.16 Localized transduction of aortic endothelium by lentiviral MMB

For the lentiviral SO-Mag MMB mediated transduction of vascular endothelium, thoracal aortas were isolated from C57BL/6J wild type mice (Charles River, Burlington, MA, USA). Therefore, the mouse was euthanized by cervical dislocation and the thorax was opened to expose the aorta. The thoracal aorta was carefully separated from connective tissue and intercostal arteries were cauterized to prevent leakage. The aorta was bilaterally catheterized with a polyethylen tube (D_i=0.28 mm, D_o=0.61 mm; SIMS Portex, Kent, UK) and mounted above a magnet in a recirculation system constructed for MMB-mediated transduction as depicted in Figure 2.2. Aortas (diameter ~1 mm) were perfused with serum-free DMEM at around 7-8 dyn/cm². 200 µl of lentiviral MMB (corresponding to $1*10^6$ IP or $1*10^7$ VP) were diluted 1:5 in HBSS and slowly injected into the plastic tube upstream of the perfused aorta. US (30 s, 1 MHz, 2 W/cm^2, 50% duty cycle) was applied simultaneously at the site of MF application. After further 5 min of perfusion and MF exposure the aorta was placed in 500 µl DMEM supplemented with 20% FCS in a 12-well plate and maintained in a humidified incubator. To visualize the local transduction of vascular endothelium achieved with the SO-Mag MMB technique under flow conditions, GFP LV-MMB complexes were used and immunofluorescence staining was performed 6 days after transduction (see section 2.1.17). To analyse if the lentivirus-MMB mediated gene transfer is also capable to induce physiological effects in aortic endothelium, SO-Mag MMB complexed with VEGF LV or SHP-2 WT/CS/E76A LV were applied. Effects were analyzed by qRT-PCR (see Section 2.1.18), ELISA (see Section 2.1.19) and aortic ring sprouting assay (see Section 2.1.20) 3 days after transduction.

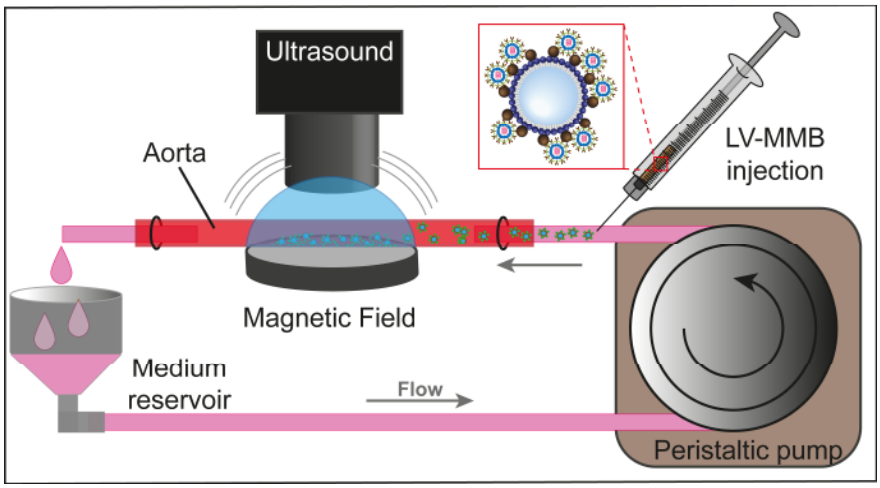

Figure 2.2. Schematic illustration of the perfusion setup applied to achieve localized lentiviral MMB mediated transduction of aortic endothelium.
The isolated aorta was continuously perfused with DMEM. Lentiviral MMB were injected in the upstream tubing with simultaneous application of MF and US targeted to the central section of the vessel.

2.1.17 Immunofluorescence staining of mouse aortas

To assess localized transgene delivery by lentiviral MMB, GFP expression in whole mouse aortas was visualized by fluorescence microscopy (Leica DMI4000B, Leica Microsystems, Wetzlar, Germany). Immunofluorescence staining was performed in cooperation with Staffan Hildebrand from the University Bonn (AG Prof. Pfeiffer). Briefly, aortas were fixed for 1 h in 2% PFA, left in 20% sucrose over night, embedded in OCT, and frozen at -80°C. 5 µm cross-sectional slices were cut with a cryotome and blocked for 30 min with 5% BSA in PBS-T (0.1% Tween-20). To stain endothelial cells, slices were incubated with a PECAM-1 antibody (1:100 dilution in PBS-T supplemented with 1% BSA) overnight. Sections were washed thrice with PBS-T and the secondary antibody dilution (1:500 in PBS-T supplemented with 1% BSA) was incubated for 2 h. After another three washing steps, the sections were incubated with Hoechst nuclear stain (50 µg/ml in PBS). The sections were then washed once more, and mounted under a coverslip. Fluorescence pictures were taken at 20-fold magnification.

Table 2.6. List of antibodies used for immunofluorescence staining of aortic cross sections.

Antibody	Label	Source	Company / Cat.Nr.
α-PECAM-1 $IgG_{2a, \kappa}$	-	rat	BD Bioscience / 553370
α-rat IgG (H+L)	Alexa Fluor®555	goat	Life Technologies / A-21434

2.1.18 RNA isolation from mouse aortas and quantitative real-time PCR

RNA from isolated mouse aortas was extracted using the peqGOLD Total RNA Kit from peqLab (Erlangen, Germany). Therefore, aortas were mechanically ground in RNA lysis buffer by addition of Precellys ceramic beads (Peqlab) and intense shaking in a CapMix (3M ESPE) for 20 s. Lysates were transferred to fresh tubes on ice and remaining chunks were removed by centrifugation at 10.000 g for 10 min at 4°C. RNA extraction from supernatants was performed following the manufacturer's instructions and concentrations were measured using a Qubit and the corresponding detection reagent (ThermoFischer Scientific, Waltham, USA). Reverse transcription and quantitative real-time PCR (qRT-PCR) were performed in cooperation with Dr. Andrea Riberio (Universitätsklinikum München) using the TaqMan real-time PCR system (Applied Biosystems) and corresponding probes (see Table 2.7).

Table 2.7. Lists of commercial and self-made TaqMan-probes used for qR-TPCR.

Probe	NCBI Ref.Seq.	Company / Cat.Nr.
murine ICAM-1	NM_010493.2	Applied Biosystems / Mm00516023_m1
murine VCAM-1	NM_011693	Applied Biosystems / MVCAM1-EX5
murine 18S rRNA	X03205.1	Applied Biosystems / 4310893E

Probe	Primer / Probe Sequences	Company
human VEGF	fw: GCCTTGCTGCTCTACCTCCAC rv: ATGATTCTGCCCTCCTCCTTCT probe: AAGTGGTCCCAGGCTGCACCCAT, FAM	Applied Biosystems

Obtained Ct-values (**C**ycle of **t**hreshold) were used to calculate the relative gene expression according to the ΔΔCt-method using the following formula:

$$\Delta\Delta Ct = 2^{-((Ct_{t\arg et} - Ct_{HK})_T - (Ct_{t\arg et} - Ct_{HK})_C)}$$

T……...treated sample
C……...untreated sample (control)
target.…target gene
HK……housekeeping gene (18S rRNA)

2.1.19 Detection of VEGF levels in supernatants of transduced mouse aortas

Amounts of VEGF generated by the endothelium of isolated mouse aortas which were transduced with VEGF LV-MMB complexes (see Section 2.1.16) were quantified using a human VEGF Quantikine® ELISA (R&D Systems, Minneapolis, UK). Therefore, treated aortas were maintained for 72 h in DMEM supplemented with 20% FCS. The medium was then collected and VEGF concentrations were analyzed in duplicates following the manufacturer's instructions. As control, VEGF levels in medium of aortas transduced with GFP LV instead of VEGF LV were analyzed in parallel.

2.1.20 Aortic ring sprouting assay

To assess the angiogenic capacity of aortic endothelial cells after lentiviral MMB treatment (VEGF LV or GFP LV), new vessel formation from aortic rings was detected. Therefore, the aortas were cut into small rings 72 h after transduction and the rings were carefully embedded in a growth factor reduced Matrigel Matrix (BD Bioscience). Incubation at 37°C in a humidified incubator for 30 min resulted in gelification of the previous free-flowing Matrigel. 200 µl DMEM supplemented with 20% FCS were added on top of the gel and the aortic rings were maintained in the incubator. The created semi-solid 3-D matrix supported sprout formation from the endothelium of the aortic rings. Pictures were taken 48 h and 72 h after embedment. Angiogenic capacity was quantified by measuring the number of sprouting tips and the total area of vascularization.

2.2 Protein biochemistry

2.2.1 Protein extraction for western blot analysis and immunoprecipitations

Cells provided for western blotting were washed with ice cold PBS+ and lysed in lysis buffer purchased from Cell Signaling Technology (Frankfurt am Main, Germany) for 10 min on ice. For SHP-2 activity measurements, cells were lysed in PTP lysis buffer (for recipe see Section 2.2.4). Cells were scraped off the dish and passed twice through a 29G needle to ensure complete lysis. Lysates were cleared by centrifugation at 14.000 g for 10 min at 4°C (Eppendorf Microcentrifuge5815R, Hamburg Germany) and supernatants were transferred to a fresh tube on ice. Protein concentrations were either analyzed directly afterwards or lysates were stored at -20°C until further handling.

2.2.2 Protein quantification

To assess the protein concentration of cell lysates the bicinchoninic acid assay (BCA; ThermoFischer Scientific) was performed following the manufacturer's instructions. The assay is based on the biuret reaction where Cu^{2+} is reduced to Cu^{1+} by proteins in alcaline medium (see Figure 2.3). The addition of bicinchoninic acid results in the formation of a purple-coloured BCA/copper-complex which is proportional to the protein concentration and can be detected colorimetrically at 562 nm.

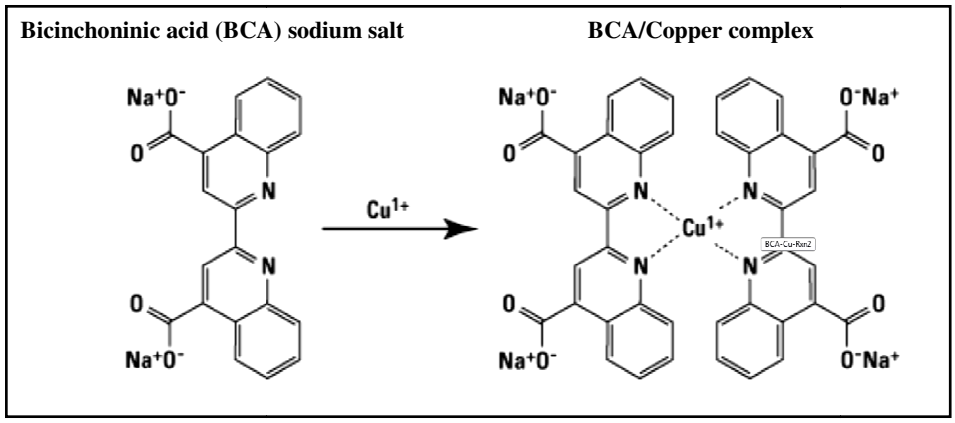

Figure 2.3. Molecular principle of the BCA kit.
Under alkaline conditions, BCA/copper-complex formation occurs directly proportional to the protein content and can be detected by absorbance measurements. (Scheme adapted from thermofisher.com)

In detail, 10 µl of protein lysate were added in duplicates to a 96-well plate (Sarstedt). BCA solution was prepared and 200 µl were added to each well. The plate was covered and incubated for 30 min at 37°C in the dark. Absorbances were measured at 550 nm (Spectra Fluor, Tecan). To establish a protein standard curve, an albumin dilution series ranging from 0 to 2 µg/µl was run alongside of each protein measurement. Protein concentrations were then calculated according to the formula:

$$y = mx+b,$$

whereby the variables **m** (slope) and **b** (intercept with the y-axis) are given by the standard curve and **y** is the measured absorbance value.

2.2.3 Western blot analysis

To allow for specific analysis of single proteins, SDS-PAGE (**s**odium **d**odecyl **s**ulphate-**p**oly**a**crylamide **g**el **e**lectrophoresis) was performed which facilitates the electrophoretic separation of different proteins depending on their molecular weight. Same amounts of protein (30 µg) were mixed with 4x loading dye and denatured at 95°C for 5 min on a heating block (Biozym Scientific, Hessisch Oldendorf, Germany). Samples were loaded onto a prepared 10% acrylamide gel placed in an electrophoresis apparatus (Peqlab) and covered with 1x running buffer. Electrophoresis was performed at 100 mV for 15 min following 200 mV until the loading dye front nearly reached the edge of the gel. Separated proteins were immediately transferred onto a nitrocellulose membrane (Peqlab) using a wet electroblotting system (Peqlab). Therefore, the acrylamide gel, nitrocellulose membrane, filter papers and sponges were soaked in 1x transfer buffer. The blotting sandwich was arranged in 1x transfer buffer as follows:

Anode

↑ Sponge
Filter papers
Nitrocellulose membrane
Gel
Filter papers
Sponge

Cathode

Air inclusions disrupting proper protein transfer were removed carefully and the blotting sandwich was placed in the blotting tank filled with 1x transfer buffer. Protein transfer was accomplished at 50 V for 2 h. Afterwards, the blotting sandwich was disassembled and the membrane with immobilized proteins was checked for proper transfer by staining with Ponceau red solution for 3 min. The membrane was washed several times with distilled water and protein traces were analyzed for equability of protein load or disturbances during transfer before proceeding. Unoccupied binding positions on the membrane were then blocked by incubation in 1x TBS-T containing 5% milk for 1 h at room temperature. To detect proteins, the membrane was incubated with a primary antibody dilution (see Table 2.8) over night at 4°C on a shaker. After washing the membrane thrice for 10 min with 1x TBS-T it was incubated with the respective horseradish peroxidase (HRP)-conjugated secondary antibody dilution (see Table 2.9) for 1 h at room temperature. The membrane was washed again thrice for 10 min with 1x TBS-T to remove any traces of unbound antibodies. The HRP signal was detected by incubating the membrane with luminol detection reagent and image acquisition at different exposure times depending on the signal intensity was performed using a bioluminescence imager (Hamamatsu Photonics, Hamamatsu City, Japan). Proteins of different molecular weight could be detected on the same membrane by consecutive antibody incubation. To verify equal protein loading and accomplish normalized protein quantification, the housekeeping protein β-actin was detected. Band intensities were assessed using the Hokawo software (Hamamatsu Photonics) and values were normalized to respective β-actin bands.

→ SDS-PAGE (10%)

<u>10% Separation gel</u>

10%	Acrylamide:Bisacrylamide (30%:0.8%)
375 mM	1.5 M Tris base, pH 8.8
0.1%	10% SDS
0.05%	10% APS
0.005%	TEMED

APS (free radical source) and TEMED (catalyst) were added directly before casting the gel. The gel was covered with 500 µl 2-Propanol to achieve a plain gel edge and exclude aerial oxygen. The 2-Propanol layer was poured off after gel solidification.

4% Stacking gel

4%	Acrylamide:Bisacrylamide, 30%:0.8%
125 mM	500 mM Tris base, pH 6.8
0.1%	10% SDS
0.05%	10% APS
0.005%	TEMED

APS and TEMED were added directly before casting the gel on top of the separation gel. A sample comb was placed in the stacking gel before solidification.

→ 4x Loading dye

250 mM	Tris base
8%	SDS
40%	Glycerol
0.02%	Bromphenol blue
400 mM	β-Mercaptoethanol

Dye was directly diluted in the sample volume.

→ 10x Running buffer (SDS-PAGE)

250 mM	Tris base
1.92 M	Glycine
10%	SDS

Buffer was diluted with distilled water.

→ 5x Transfer buffer (blotting)

125 mM	Tris base
1 M	Glycine

20% Methanol was added upon dilution with distilled water.

→ Ponceau red solution

5%	Acetic acid
0.1%	Ponceau-S

→ 10x TBS (Tris buffered saline)

500 mM	Tris base, pH 7.4
1.5 M	NaCl

0.1% Tween 20 was added upon dilution with distilled water (TBS-Tween, TBS-T).

1x TBS-T was used for washing steps, blocking solution and antibody dilution.

→ Luminol detection reagent

0.1 M	Tris base, pH 8.5
0.4 mM	p-Coumaric acid
2.5 mM	Luminol
0.08%	H_2O_2, 30%

H_2O_2 was added directly before detection.

Table 2.8. List of primary antibodies used for western blot analysis.

Antibody	Source/Type	Company / Cat.Nr.
α-β-actin (13E5)	rabbit mc	Cell Signaling Technlogy / 4790
α-pAKT (S473) (D9E)	rabbit mc	Cell Signaling Technlogy / 4060
α-VCAM-1	rabbit mc	Cell Signaling Technlogy / 12367
α-ICAM-1 (H-108)	rabbit mc	Santa Cruz Biotechnology, Inc. / sc-7891
α-GAPDH (6C5)	mouse mc	Merck Millipore / MAB374

mc: monoclonal

Table 2.9. List of secondary antibodies used for western blot analysis.

Antibody	Label	Source	Company/ Cat.Nr.
α-Mouse IgG	HRP	goat	Merck Millipore / 12-349
α -Rabbit IgG	HRP	goat	Merck Millipore / 12-348

HRP: horseradish-peroxidase

2.2.4 Immunoprecipitation and detection of SHP-2 phoshatase activity

The phosphatase activity of endogenous or ectopically expressed SHP-2 in lysates of HUVEC was assessed using the pNPP-Assay. pNPP (para-nitrophenylphosphate) is a non-proteinaceous, non-specific substrate of alkaline, acid, tyrosine and serine/threonine phosphatases [89]. The principle of the assay is based on the ability of phosphatases to catalyze the hydrolysis of pNPP to para-nitrophenol (pNP), a yellow chromogenic product with absorbance at 405 nm.

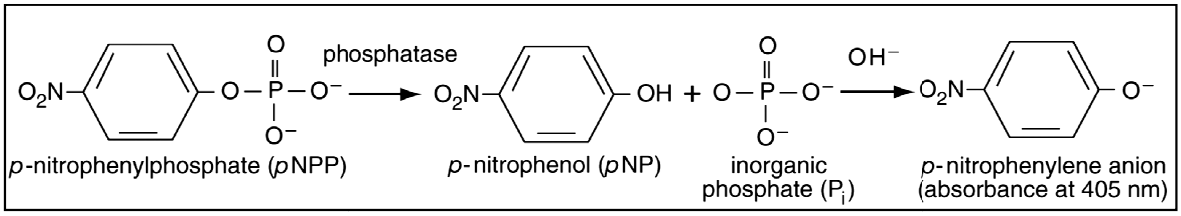

Figure 2.4. Molecular principle of the pNPP assay.
In the presence of a phosphatase, one phosphate is split from the pNPP substrate resulting in generation of pNP. The formation of pNP anion in an alkaline medium is therefore directly proportional to the phosphatase activity and can be detected by absorbance measurements. (Scheme adaped from Mercan et al. [89])

To measure the activity of one specific phosphatase its purification by immunoprecipitation from the cell lysate is necessary previous to incubation with the pNPP substrate. Isolation of SHP-2 protein from lysates of HUVEC was performed using the µMACS magnetic separation system from Miltenyi Biotec (Bergisch Gladbach, Germany). Endogenous SHP-2 was precipitated using an α-human SHP-2 antibody and Myc-tagged SHP-2 WT, CS or E76A introduced by lentiviral transduction was precipitated with an α-Myc-Tag antibody (see Table 2.10). In detail, 300 µg of total protein were incubated with 1.5 µg of the respective antibody for 1 h at 4°C on a rotation wheel. 150 µl of µMACS Protein G MicroBeads were added and the mixture was incubated for 30 min at 4°C. SHP-2/AB/bead-complexes were magnetically precipitated by applying the mixture to a µMACS separation column placed in a magnetic separator. Precipitated SHP-2 was washed thrice by applying 500 µl phosphatase buffer on top of the separation column. The SHP-2/AB/bead-complexes were eluted by placing the separation column in a tube and applying of 200 µl pNPP substrate solution (Sigma-Aldrich). The eluate was incubated for 1 h at

37°C in the dark under gentle agitation to enable an optimal enzyme reaction. Afterwards, the mixture was applied to the separation column placed in the magnetic separator and the cleared flow through was collected in a tube. 100 µl of the flow through were transferred to a 96-well plate and absorbance was measured at 405 nm (SpectraFluor, Tecan). As blank, 100 µl of pNPP substrate solution were always measured in parallel. Blank values were subtracted and absorbances were normalized to untreated control values. To inhibit the basal phosphatase activity of SHP-2 the general phosphatase inhibitor Na_3VO_4 (25mM; Sigma-Aldrich) or the specific SHP-2 inhibitor PtpI IV (2 µM; Merck Millipore, Darmstadt, Germany) were added to the substrate solution previous to incubation with precipitated SHP-2.

Table 2.10. Antibodies used for immunoprecipitations.

Antibody	Source	Company/ Cat.Nr.
α-human SHP-2 (H-2)	Goat	Santa Cruz / sc-271550
α-Myc-Tag (71D10)	Goat	Cell Signaling Technology / 2278

→ PTP lysis buffer

150 mM	NaCl
50 mM	1 M Tris-HCl, pH 7.4 (Tris –base equilibrated with HCl)
5 mM	EDTA
1:500	Proteinase Inhibitor Cocktail (Sigma-Aldrich)
0.5%	Nonidet P-40 (NP-40)
0.1%	Deoxycholic acid (DOC)
0.1%	SDS
1mM	$NaVO_3$

PTP lysis buffer was freshly prepared in distilled water and brought to pH 7.35.

→ Phosphatase buffer

24 mM	HEPES
120 mM	NaCl

Phosphatase buffer was prepared in distilled water, brought to pH 7.4 and could be stored at 4°C for up to 2 month.

→ pNPP (p-nitrophenylphosphate) substrate solution

12.5 mM	pNPP
5 mM	DTT

pNPP was purchased as 5 mg tablet which was dissolved in 900 µl phosphatase buffer with DTT directly before use. As the substrate solution was diluted by the void volume of the separation columns (30 µl) the final concentration in the assay was 10 mM. The solution was protected from light throughout the procedure.

2.3 *In vivo* Experiments

2.3.1 Study approval and general mouse housing conditions

All animal studies were conducted in accordance with the German animal protection law and approved by the district government of upper Bavaria (Regierung von Oberbayern, approval reference number AZ55.2-1-54-2532-172-13 and AZ55.2-1-54-2532-36-2015). The investigations conformed to the Guide for the Care and Use of Laboratory Animals published by the US National Institutes of Health (NIH Publication No. 85-23, revised 1996).

The animal experiments were performed with 16-24 week old male and female C57 BL/6J wild type mice purchased from Charles River (Sulzfeld, Germany). Mice were kept in individually ventilated cages (IVC, Techniplast, Germany) under a 12 h day-night cycle with dusk/dawn imitation. Animals had free access to water and laboratory chow and were provided with mouse houses and cotton fibre nestlets as cage enrichments. Room temperature was kept between 22-23°C and humidity was 50%. Health management and general maintenance was performed by the staff of the animal facility. Due to special safety regulations and requirements regarding the conduction of S2 animal experiments and housing conditions for S2 animals, the procedures described in Section 2.3.2 to 2.3.4 were partially performed in the S2 animal facility of the Klinikum Rechts der Isar (TU Munich). Mice injected with lentiviral MMB were classified as S2 organisms until 48 h after transduction and were subsequently downgraded to S1 level as no residual or excreted lentiviral particles could be found in different body fluids (see Section 2.3.9). To ensure tight monitoring, mice were inspected daily and the condition of every mouse was reported in specific score sheets from beginning of the experiment to euthanasia of the animal. Experiments were prematurely abrogated if the score of a mouse reached a certain score level predetermined in the animal test proposal.

2.3.2 Anaesthesia, antagonisation and analgesia

All surgical procedures were performed under deep anaesthesia achieved by intraperitoneal (i.p.) injection of Midazolam (5 mg/kg body weight), Medetomidin (0.5 mg/kg body weight) and Fentanyl (0.05 mg/kg body weight) in 0.9% NaCl. After reaching surgical tolerance, as verified by loss of the conjunctival and pedal withdrawal reflexes, experimental procedures were started. Bepanthen salve (Bayer, Leverkusen, Germany) was applied to the eyes to avoid eye damages through desiccation. To achieve fast awakening after surgeries, antagonisation of anaesthesia was performed by subcutaneous (s.c.) injection of Flumazenil (0.5 mg/kg body weight) and Atipamezol (2.5 mg/kg body weight) in 0.9 % NaCl. Postsurgical analgesia was provided by s.c. injection of 0.065 mg/kg body weight Buprenorphin with the first injection 10 min before injection of the antagonisation following administration in a 12 hour-cycle until 3 days after lentiviral MMB application. Additionally, mice were provided with 300 µl NaCl by s.c. injection to ensure sufficient rehydration. Throughout the procedures mice were placed on a 40°C heating plate to prevent cooling until complete recovery and were subsequently transferred back to their cages.

2.3.3 Preparation of the dorsal skin

The implantation of a dorsal skinfold chamber (DSFC) is an established animal model enabling long-term follow up of the dorsal vascular bed in living animals via intravital microscopy [90]. One major advantage is given by the fact that the implanted observation chamber allows for repeated microscopic access in restrained animal without anaesthesia. As fixture for the dorsal skinfold serves a pair of inverse titanium frames (Figure 2.5.a). The front frame comprises a circular observation window in which a coverslip (ø 11.8 mm, Menzel, Braunschweig, Germany) is inserted. The back frame comprises three screws for fixation of the frame sandwich. To implant the DSFC, mice were anesthetized (see Section 2.3.2), the hair on the back area was trimmed (Aesculap, Braun) and the skin was depilated using a chemical depilation creme (Pilcamed, Schwarzkopf). Loose fur and depilation creme were completely removed with warm water and the skin was disinfected with 70% ethanol. The back skin was strained and the back frame was attached by non-absorbable suture (silk, 5/0; FST). The lower screws of the back frame were passed through the skin

via two holes pierced with a cannula. Using an operation microscope (Stemi 2000-CS, Zeiss) and sterile surgical instruments (FST) the skin layer on the front side was removed in a circular area matching the window area of the front frame (ø 14 mm). Connective tissue was removed from the exposed subcutaneous vascular bed to achieve maximal microscopic resolution. The front frame was then attached to the screws of the back frame whereby complete closure of the opened skin area and adhesion to the coverslip had to occur. Both frames were fixed by suture. Representative pictures of the completely implanted DSFC and the resulting exposed microcirculation are shown in Figure 2.5.b. Antagonisation, analgesia and follow-up care were done as described in Section 2.3.2. Maximal two mice with DSFC were maintained in one cage without houses and moisturized chow was provided in a petri dish placed on the ground. Catheterization and lentiviral MMB mediated transduction were performed 24 h after DSFC implantation to allow for proper equilibration of blood flow in the window area.

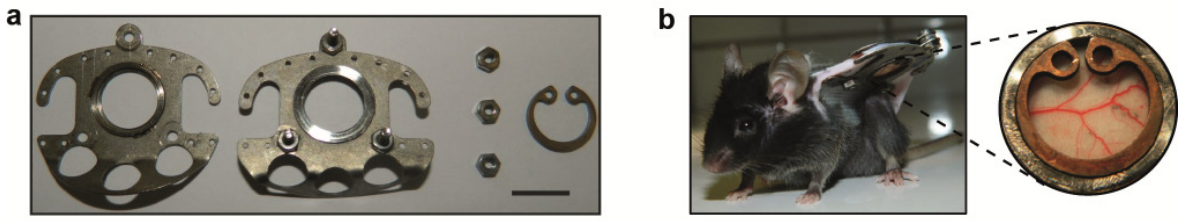

Figure 2.5. The dorsal skinfold chamber (DSFC) model in mice.
(a) From left: Titanium frames, screws and circlip used for the implantation of the DSFC. Scale bar indicates 1 cm. **(b)** A mouse implanted with a DSFC. The resulting observation window (ø 14 mm) allows for macro- and microscopic visualization of vessels of the dorsal skin.

2.3.4 Catheterization of the Arteria carotis

To assure that a large quantity of lentiviral MMB reaches the vessels of the dorsal skin within the first round of circulation, the Arteria carotis was chosen as site of injection. To place the catheter, the mouse was anesthetized and placed in dorsal position on a special operation table featuring a slot for the implanted DSFC. The throat area was amply disinfected and the skin was cleanly opened by a single cut (15-20 mm). The right Arteria carotis communis was freed from surrounding tissue and the vagus nerve and blood flow was disabled by application of a cardial clamp and cranial ligation by suture. The vessel

was opened with a microscissor and the catheter (D_i=0.28 mm, D_o=0.61 mm; SIMS Portex) connected to a 1 ml syringe filled with NaCl was inserted in cardial direction and fixed with three suture straps. The cardial clamp was removed and injection of lentiviral MMB could be performed as described in Section 2.3.5. After conduction of the transduction procedure, the Arteria carotis was cardially ligated by suture and the catheter was removed. The skin incision was closed by suture and antagonisation, analgesia and follow-up care were done as described in Section 2.3.2. Upon recovery, mice were carefully monitored to exclude any neuromuscular dysfunctions resulting from the ligation of the Arteria carotis or the injection procedure.

2.3.5 Injection of lentiviral MMB via the Arteria carotis catheter

The experimental aim was to target the lentiviral MMB injected via the Arteria carotis to the vascular endothelium of the dorsal skin by simultaneous application of a strong magnetic field (MF) and ultrasound (US). To do so, the anaesthetized mouse implanted with the DSFC and catheterized as described in the Sections 2.3.3 and 2.3.4 was placed on a stage on top of an electromagnet in left lateral position (2.6.a and b). The magnetic tip was thereby directly pointing to the middle of the DSFC window with a distance of 2-3 mm. A droplet of NaCl was applied onto the closed observation window to allow for efficient transduction of the ultrasonic waves to the vessels of the dorsal skin. 100 µl of SO-Mag MMB were incubated with veffLuc LV ($8.3*10^7$ VP/ml, respectively) for 10 min and drawn up into a 1 ml syringe. The electromagnet (1039 mT) was switched on, lentiviral MMB were slowly injected (20 s) and US was applied for 30 s (2 W/cm², 1 MHz, 50% duty cycle). The MF was applied for further 5 min before the mouse was transferred back to the surgical stage to remove the catheter as described in Section 2.3.4.

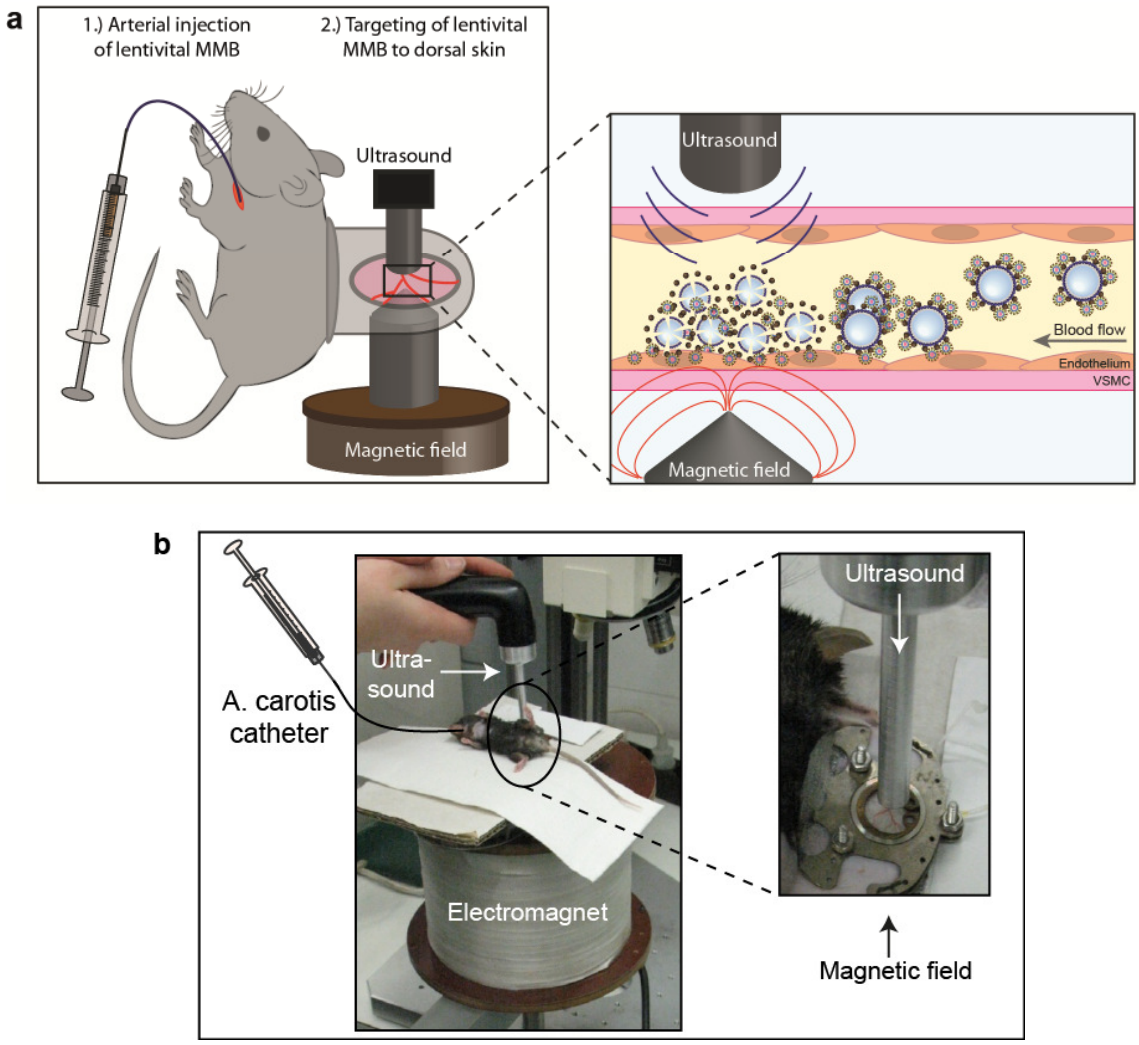

Figure 2.6. Experimental setting applied for targeted transduction using lentiviral MMB. **(a)** Schematic illustration of the setup implemented for lentiviral MMB targeting *in vivo*. The observation window of the DSFC was centred between the tip of an electromagnet and the US transducer. During injection of the lentiviral MMB via the Arteria carotis catheter, MF and US were simultaneously applied to achieve localized transduction of vascular endothelial cells. **(b)** Actual experimental setting of the lentiviral MMB technique *in vivo*. Modified from Mannell et al.[40].

2.3.6 Bioluminescence imaging

To assess the systemic distribution of transgene expression resulting from veffLuc LV-MMB transduction, luciferase activity was detected 7-10 days after the procedure. The mouse was anaesthetized and luciferin was applied via i.p. injection (100 µl, 3 mg/ml in 0.9% NaCl). After placing the mouse in the preheated acquisition chamber (37°C) bioluminescence was detected at different exposure times using an IVIS imaging system from PerkinElmer (Waltham, MA, USA). Afterwards, mice were euthanized by cervical dislocation under existing anaesthesia and bioluminescence of isolated organs was assessed by placing these in a petri dish.

2.3.7 DNA isolation from mouse tissue and quantification of proviral genome copy numbers

Genomic DNA was extracted from mechanically homogenized tissues (dorsal skin tissue, livers and lungs) of mice receiving lentiviral MMB with or without MF and US targeting using the NucleoSpin® Tissue gDNA Kit (Macherey-Nagel). The provirus genome copy numbers per cell were assessed by using the Lenti-X™ Provirus Quantitation Kit (Macherey-Nagel) following the manufacturer's instructions.

2.3.8 MNP detection in organs

The systemic distribution of MNP in lentiviral MMB treated mice was assessed by magnetic particle spectroscopy (MPS) in cooperation with Dr. Dietmar Eberbeck from the Physikalisch-Technische Bundesanstalt (PTB), Berlin. Organs were isolated, minced and added to 0.5 ml tubes (Applied Biosystems). Only non-metallic (iron-free) instruments were used for these preparations to avoid any sample contamination. MPS measurements were performed as described before [91].

2.3.9 p24 core protein ELISA

To analyse if any lentiviral particles remain or are secreted 48 h after lentiviral MMB mediated transduction, a LentiX™ p24 Rapid Titer Kit (Clontech, California, USA) was performed according to the manufacturer's instructions. The ELISA kit allows for sensitive detection of HIV-1 p24 core protein in sample supernatants. Saliva smears and smears of the catheter wound were collected with moist cotton swabs. Urine was collected with a pipette, faeces were collected from the cage and whole blood was drawn from the Vena cava to gain plasma. Cotton swabs and faeces were soaked and vortexed in 300 µl PBS following centrifugation (14.000 g, 10 min) to gain a clean supernatant. Each sample (100 µl) was exposed in duplicates to the p24 ELISA. PBS containing $2.3*10^2$ VP of GFP LV was measured alongside as positive control.

2.4 Statistical analysis

Statistical analyses were performed using Sigma Stat version 3.5. For multiple comparisons of normal distributed data sets the one-way analysis of variance (1-way ANOVA), followed by Student-Newman-Keuls post-hoc test was performed. The unpaired Student's t-test was used for the comparison of two normal distributed independent groups. For comparison of two not normally distributed independent data sets the Mann-Whitney Rank Sum Test was performed. Differences were considered significant at an error probability level of $*p \leq 0.05$. All data are presented as means ± standard error of the mean (SEM).

3 Results

3.1 Characterisation and comparison of SO-Mag and PEI-Mag MMB *in vitro*

3.1.1 Integration of SO-Mag and PEI-Mag magnetic nanoparticles into MMB

An important prerequisite for the successful generation of a multi component carrier system is the complete cooperation of the single components with each other. In case of the MMB, the stable and evenly uptake of magnetic nanoparticles (MNP) into the MB lipid shell is essential to create an effective targeting system. This might be influenced by different factors, including composition of the phospholipid solution, surface charge of the nanoparticles or ionic strength of the surrounding medium. The phospholipid solution containing DPPE and DPPC used in this study has been established and verified before [40, 41] as has been its combination with the positively charged PEI-Mag MNP (PEI-Mag MMB). In this study a new type of MMB coupled to SO-Mag MNP (SO-Mag MMB) was generated. To allow for a rational comparison, MMB containing equimolar concentrations of iron (150 µg Fe/ml lipid solution) were prepared. Both MMB types displayed the typical feature of floating to the surface within 1-5 min indicating that gas filled bubbles were formed (Figure 3.1.a; n=3). In case of the SO-Mag MMB this floating process occurred more rapidly (1 min). The PEI-Mag MMB floated slower and the solution remaining below did not clear off completely within 5 min as was the case with SO-Mag MMB. Importantly, after floating to the surface, SO-Mag and PEI-Mag MMB could be easily redistributed into the solutions by gentle agitation. To test the magnetic responsiveness of both MMB types, they were exposed to a sideward magnetic field (MF). SO-Mag and PEI-Mag MMB were both attracted towards the MF, whereby SO-Mag MMB were attracted more rapidly (1 min) leaving a clear microbubble-free solution (Figure 3.1.b; n=3). PEI-Mag MMB in contrast, accumulated only slowly and incompletely at the site of MF within 5 min of exposure (Figure 3.1.b; n=3).

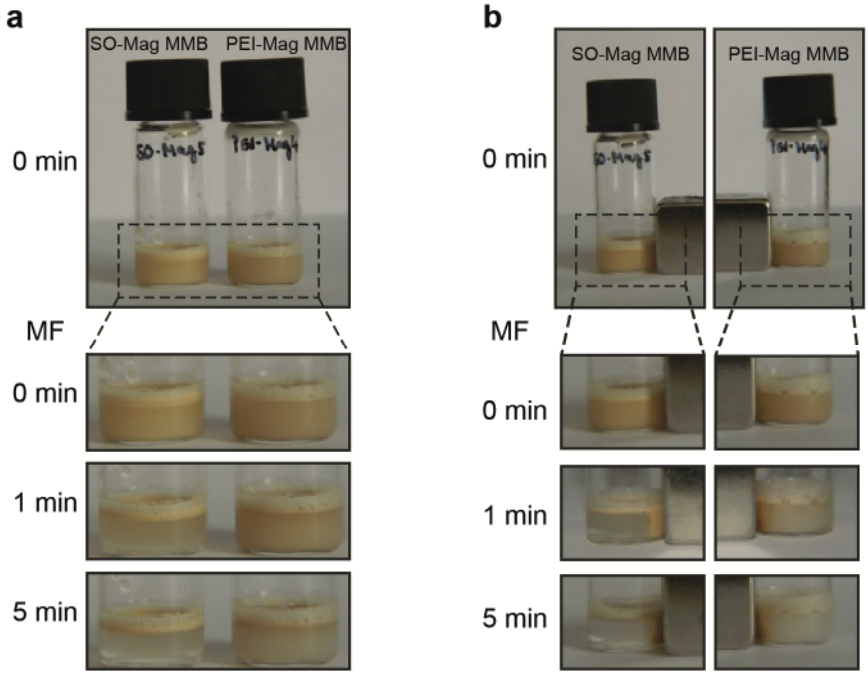

Figure 3.1. SO-Mag MNP show a better MMB association than PEI-Mag MNP.
(a) After preparation, MMB in both solutions rose to the surface, whereby this process was faster and more complete with SO-Mag MMB compared to PEI-Mag MMB. n=3. **(b)** When exposed to a sideward magnetic field, SO-Mag MMB were quickly attracted whereby the remaining solution was optically free of bubbles or MNP. PEI-Mag MMB, in contrast, responded slower to MF application and did not completely accumulate at the site of MF within 5 min. n=3.

3.1.2 General physico-chemical characteristics of MMB

The size of a single carrier component can be decisively for successful gene delivery, especially if applied *in vivo* via the circulatory system. In case of MMB, too large bubbles may cause obstructions within the smallest vessels leading to severe ischemic complications. Too small bubbles, in contrast, may incorporate too little amounts of MNP whereby their magnetic moment might be significantly reduced. Also the recognition and clearance by natural mechanisms, such as the reticuloendothelial system, is strongly depending on matters of size. Therefore, we assessed important physico-chemical parameters of the SO-Mag and PEI-Mag MMB listed in Table 3.1. After integration of SO-Mag and PEI-Mag MNP, the mean diameter of the MMB increased by 20.80 ± 0.56% and 12.09 ± 1.91%, respectively, compared to naked MB (*$p \leq 0.05$, n=3). By association of lentiviruses, however, diameter of both MMB types was decreased again, whereby no difference in mean diameter between PEI-Mag and SO-Mag MMB could be detected (Table 3.1; *$p \leq 0.05$, n=3). Despite the fact that SO-Mag and PEI-Mag MNP possessed

completely opposed ζ potentials (-16.1 ± 0.6 mV and 14.7 ± 1.2 mV, respectively) the resulting MMB complexes both exhibited a positive ζ potential as assessed in HBSS. Therefore, interactions between both MMB types and the negatively charged lentiviruses (-8.8 ± 0.6 mV) might predominantly occur via electrostatic interactions. Calculations of the average number of MNP embedded in one MMB revealed that one single SO-Mag MMB contained significantly higher amounts of MNP than PEI-Mag MMB (Table 3.1; *p≤0.05, n=3).

Table 3.1. Physico-chemical properties of MB with and without associated MNP (150 µg Fe/ml) and lentiviruses (5*10^8 VP/ml MMB).

	LV	Diameter [µm][a, b]	µg Fe/MMB[b]	MNP/MMB[b, c]	ζ Potential [mV][b]
naked MB	-	5.0 ± 0.2	-	-	6.2 ± 0.3
pCHIV.eGFP	+	1.9 *10^{-1} ± 0.8 *10^{-2}	-	-	-8.8 ± 0.6
SO-Mag MNP	-	4.0*10^{-2} ± 1.4*10^{-3} [d]			-16.1 ± 0.6
SO-Mag MMB	-	6.1 ± 0.1	2.0*10^{-8} ± 8.1*10^{-11}	3.6*10^6 ± 2.5*10^{-4}	3.9 ± 0.5
	+	4.9 ± 0.5	4.4*10^{-8} ± 8.1*10^{-9}	6.2*10^6 ± 1.2*10^{-6}	5.0 ± 0.2
PEI-Mag MNP	-	2.8*10^{-2} ± 0.2*10^{-2} [d]	-	-	14.7 ± 1.2
PEI-Mag MMB	-	5.6 ± 0.2	2.5*10^{-8} ± 1.5*10^{-9}	1.7*10^6 ± 4.6*10^{-4}	9.6 ± 0.5
	+	4.7 ± 0.2	6.8*10^{-8} ± 7.4*10^{-9}	3.4*10^6 ± 2.4*10^{-5}	9.4 ± 0.5

[a] Particle diameter for MMB and lentivirus-MMB complexes, hydrodynamic diameter for sole pCHIV.eGFP LV; [b] mean ± SEM; *p≤0.05 vs. naked MB, #p≤0.05 vs. MB+MNP, n=3 in duplicates; [c] MNP iron/particle content: 6.2*10^{-13}µg Fe/SO-Mag MNP and 1.4*10^{-12}µg Fe/PEI-Mag MNP; [d] adapted from Almstätter et al. [36]

MNP: magnetic nanoparticles; MMB: magnetic microbubble; MB: microbubble; LV: lentivirus; Fe: iron.

3.1.3 Verification of lentivirus binding to MMB

There are manifold options for genetic vectors to be used for gene therapy purposes. In this study we decided to use lentiviruses in combination with our MMB system, due to their unique infectious capacity and related high gene transfer efficiency. The capacity of PEI-Mag MMB to complex lentiviruses has been shown before [41]. To assess if the new SO-Mag MMB are equally or even more efficient in binding lentiviruses, we incubated both MMB solutions with fluorescence-labelled lentiviral particles (pCHIV.eGFP LV) allowing the visualization by fluorescence microscopy and quantification using flow cytometry. As shown in Figure 3.2.a, SO-Mag and PEI-Mag MMB successfully associated the added pCHIV.eGFP LV to their outer shell (n=3). No lentiviral particles were thereby found within the MMB gas core. Flow cytometry analysis revealed a substantial increase in fluorescence of the MMB upon addition of pCHIV.eGFP LV. The quantitative analysis of these signals resulted in no difference between the MMB types indicating that the single SO-Mag and PEI-Mag MMB associate approximately the same amount of lentiviruses to their shell (3.2.b and c; *p≤0.05, n=4).

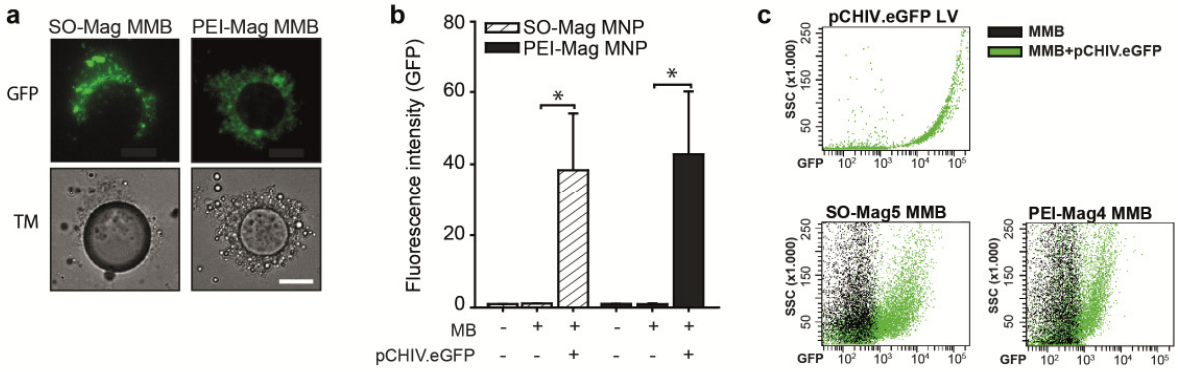

Figure 3.2. Visualization of pCHIV.eGFP LV binding to SO-Mag and PEI-Mag MMB
(a) Both MMB types were capable to associate the added lentiviral particles to their outer shell as visualized by fluorescence microscopy. n=3. **(b)** The quantitative analysis of this complex formation by flow cytometry showed that SO-Mag and PEI-Mag MMB were equally efficient in binding lentiviruses. *p≤0.05, n=4, 1-way ANOVA. **(c)** Representative dot plot overlays of MMB without and with incubated pCHIV.eGFP LV as well as the lentivirus alone.

3.1.4 Lentivirus binding capacity of the MMB

After the general ability of MMB to bind lentiviruses was verified we sought to test if the added lentiviral particles are completely complexed by the MMB. This is important, as no free lentiviral particles should remain within the solution which may otherwise cause unspecific gene expression. To verify that SO-Mag and PEI-Mag MMB possess the capacity to indeed bind the optimal lentivirus amounts determined before ($5*10^6$ IP/ml MMB), MMB and lentiviruses were incubated for 10 min. MMB solutions were then magnetically separated by exposure to an external MF for 15 min following separate application of the resulting MB free supernatant and MMB concentrate to cells. HUVEC treated with the supernatants from both MMB types exposed very low GFP expression indicating only marginal lentiviral particles remaining unbound by the MMB (Figure 3.3.a and b). In contrast MMB concentrates achieved very high transduction rates. Interestingly, lentiviral SO-Mag MMB achieved a higher transduction rate than lentiviral PEI-Mag MMB (*p≤0.05, n=6). As the absolute number of lentiviral particles bound to the MMB was the same for both MMB types (as shown in Section 3.1.3), this difference in transduction efficiency can only be explained by a better magnetic sedimentation of the SO-Mag MMB in the cell culture dish and therefore enhanced delivery of lentiviruses to cells compared to PEI-Mag MMB.

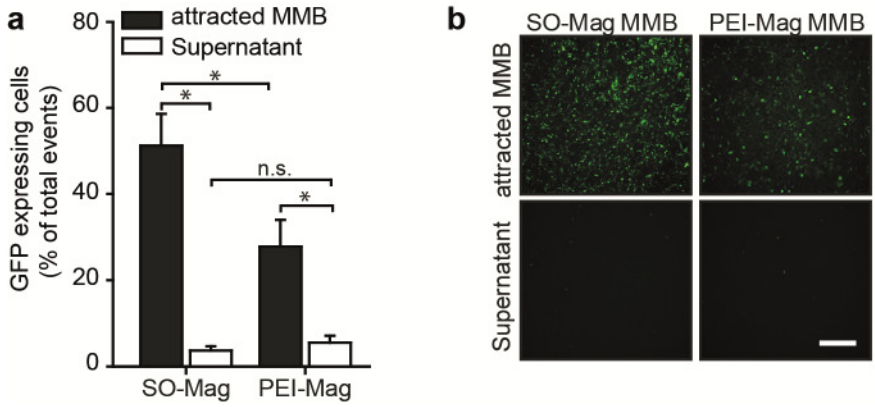

Figure 3.3. Lentivirus uptake capacity of SO-Mag and PEI-Mag MMB.
(a) GFP LV given to the MMB solution was nearly completely complexed by both MMB types as can be seen by the low GFP signal of cells incubated with the magnetically separated supernatants. Cells treated with the magnetically concentrated MMB portions exposed a strong GFP expression signal. This signal was significantly higher when SO-Mag MMB were used. *p≤0.05, n=6, 1-way ANOVA. **(a)** Representative fluorescence pictures of GFP expression in cells. Scale bar indicates 500 µm.

3.1.5 Measurements of magnetic velocities and magnetic moments

As described in the former section, SO-Mag MMB were found to deliver their lentiviral cargo to endothelial cells with higher efficiency than PEI-Mag MMB. To test if this effect might be due to superior magnetic properties of the SO-Mag MMB, velocities and magnetic moments of both MMB compositions (150 µg Fe/ml) were assessed by application of a magnetic field gradient. As depicted in Figure 3.4.a, SO-Mag MMB exposed a 1.6-fold higher velocity (peak at 19.10 ± 0.69 µm/s) compared to PEI-Mag MMB (peak at 11.40 ± 0.22 µm/s). This difference in magnetic potency became even more striking by calculation of the magnetic moments of the two MMB types, with SO-Mag MMB possessing an about three-fold higher magnetic moment than the PEI-Mag MMB (94.74 ± 0.47 fA m^2 vs. 32.14 ± 0.12 fA m^2, respectively; Figure 3.4.b).

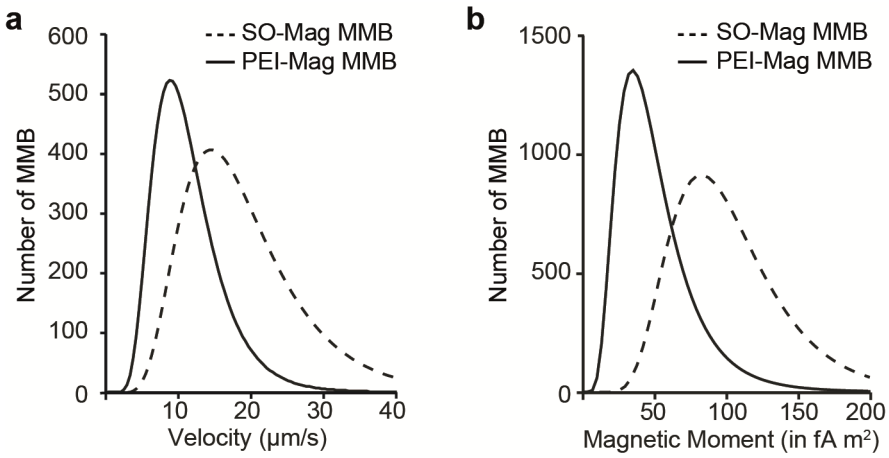

Figure 3.4. Velocity and magnetic moments of SO-Mag and PEI-Mag MMB under a magnetic field gradient.
(a) SO-Mag MMB were found to exhibit an 1.6-fold higher velocity under a magnetic field gradient compared to PEI-Mag MMB. **(b)** This resulted in a nearly 3-fold higher magnetic moment of SO-Mag MMB. n=3.

3.1.6 Cytotoxicity of MMB and technical parameters

We furthermore evaluated potential cytotoxicity of each method parameter applied during lentiviral MMB mediated gene delivery (GFP LV ± PEI-Mag/SO-Mag MMB ± MF ± US). Therefore, cell viability was assessed 72h after the respective treatment combination using the MTT assay. Application of lentivirus, MMB or MF alone did not change cell viability, indicating low cytotoxic effects of these components (Figure 3.5). Only the application of US induced slight cell toxicity by about 20% compared to untreated cells, regardless of the MNP type used (*p≤0.05, n=4 in triplicates).

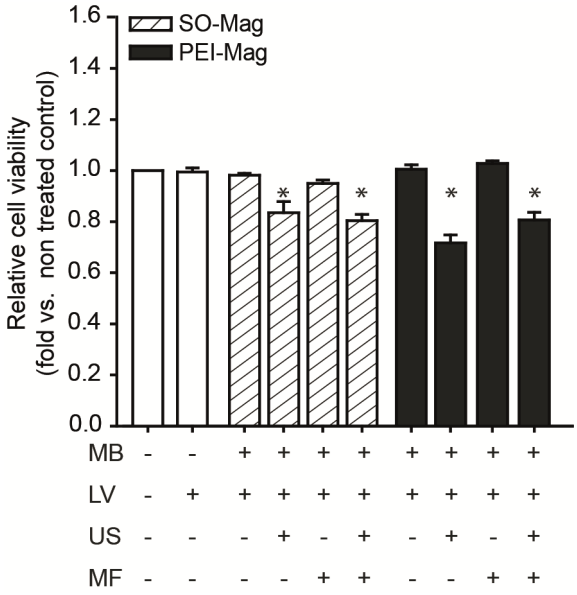

Figure 3.5. Detection of cytotoxic effects of the components of the lentiviral MMB technique using the MTT Assay.
Application of SO-Mag and PEI-Mag MMB alone or with additional exposure to MF did not cause any cytotoxicity in endothelial cells. However, direct exposure to US reduced cell viability by around 20%. *p≤0.05, n=4 in triplicates, 1-way ANOVA.

3.1.7 Endocytic uptake mechanism accounting for lentiviral MMB mediated transduction

We were furthermore interested to identify the responsible mechanism of uptake relevant for lentiviral MMB-mediated gene delivery to endothelial cells. Therefore, cells were treated with inhibitors of different endocytic pathways previous to MF and US assisted transduction using SO-Mag MMB complexed with GFP LV. Lentiviral uptake was measured by detection of the percentage of GFP expressing cells using flow cytometry 72 h later. As shown in Figure 3.6, inhibition of caveolae-mediated endocytosis by methyl-β-cyclodextrin (MβCD), significantly decreased lentivirus uptake compared to cells without inhibitor treatment (*p≤0.05, n=5 in duplicates). In contrast, inhibition of phagosome-lysosome fusion by ammoniumchloride (NH_4Cl) or inhibition of the clathrin-mediated endocytic pathway by Cytochalasin B (CytoB) did not influence lentiviral MMB mediated transduction.

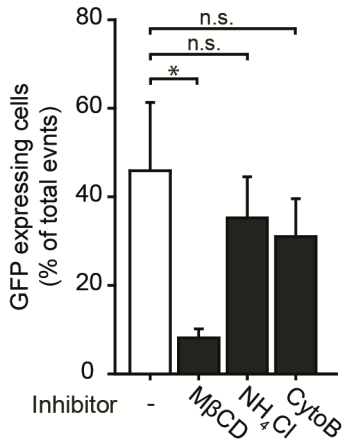

Figure 3.6. Identification of the cellular uptake mechanism relevant for MMB-mediated transduction.
Inhibition of caveolin-dependent endocytosis with methyl-β-cyclodextrin (MβCD; 10 mM) resulted in severe impairment of lentiviral MMB mediated transduction efficiency (SO-Mag MMB with GFP LV). In contrast, inhibition of endosome-lysosome fusion by ammoniumchloride (NH_4Cl; 10 nM) or clathrin-dependent endocytosis by Cytochalasin B (CytoB; 10 µM) did not change GFP expression compared to the untreated controls. *p≤0.05, n=4, 1-way ANOVA.

3.1.8 Gene transfer efficiency of lentiviral MMB under static conditions in vitro

To compare the gene transfer efficiencies of both MMB compositions, GFP LV coupled MMB were added to endothelial cell cultures following combined or separate application of MF (30 min) and US (30 s, 2 W/cm², 1 MHz, 50% DC). As control, cells were incubated with only GFP LV for 30 min. Flow cytometry analysis of GFP expressing cells revealed that application of lentivirus alone yielded only very low transduction rates (1.8% ± 0.3%; Figure 3.7). Also application of lentiviral MMB without MF and US targeting did not enhance gene transfer substantially. Interestingly, even if US was applied in combination with lentiviral MMB no noteworthy increase in transduction efficiency was detected either. In contrast, lentiviral MMB with MF exposure resulted in a strong increase in transduction efficiency of both, SO-Mag MMB and PEI-Mag MMB coupled to GFP LV (26.0% ± 2.9% and 14.9% ± 2.3%, respectively; *$p \leq 0.05$, n=4). Importantly, a cumulative effect of combined MF and US exposure in addition to lentiviral MMB application on transduction efficiency could be observed for both MMB types (32.0% ± 0.8% and 23.0% ± 3.0%, respectively; *$p \leq 0.05$, n=4). However, if comparing the transduction efficiencies of fully targeted lentiviral SO-Mag and PEI-Mag MMB with each other, SO-Mag MMB yielded an approximately 25% higher gene transfer (*$p \leq 0.05$, n=4).

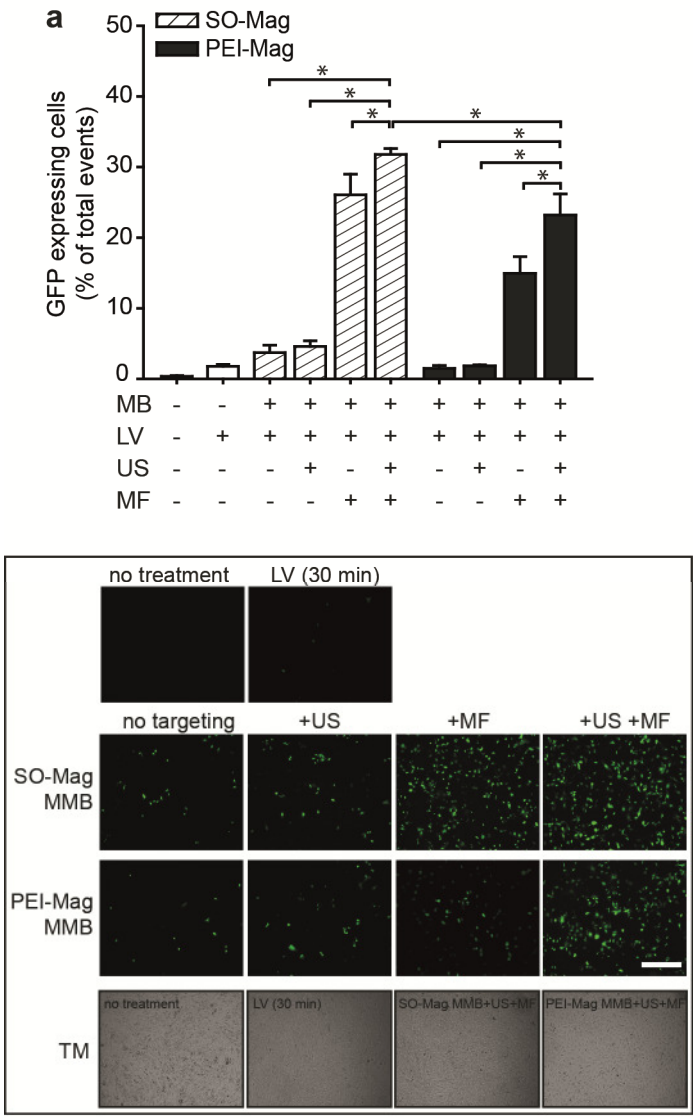

Figure 3.7. Determination of transduction efficiencies of SO-Mag and PEI-Mag MMB as well as the single methodical parameters on endothelial cells under static conditions.
(a) Full gene transfer efficiency could only be achieved by completely targeting the lentiviral MMB with MF and US. The omission of MF or US from the procedure resulted in significant reduction of GFP positive cells. In direct comparison, lentiviral SO-Mag MMB exhibited enhanced transduction capacity compared to lentiviral PEI-Mag MMB, with full targeting, respectively. *$p \leq 0.05$, n=4 in duplicates, 1-way ANOVA. **(b)** Representative fluorescence images of GFP expression in cells. Lower panels: representative transmission light pictures showing that the endothelial cell layers remained intact after incubation with lentivirus alone as well as US and MF targeting of lentiviral MMB. Scale bar indicates 500 µm.

3.1.9 Gene transfer efficiency of lentiviral MMB under flow conditions in vitro

To evaluate the performance of the lentivirus-MMB complexes under flow conditions, endothelial cells cultured in channel slides were perfused with MMB complexed to lentivirus containing a luciferase reporter gene (veffLuc LV) and targeted by simultaneous application of MF and US. As seen in Figure 3.8.a, detected luciferase activity strongly co-localized with the area of MNP accumulation, perceptible as brownish sediments. The lentiviral MMB-mediated gene transfer under a shear rate of 1 dyn/cm^2 resulted in a strong and local luciferase expression regardless of the MNP type used. Under increased shear rates of 5 and 7.5 dyn/cm², the lentiviral SO-Mag MMB mediated transgene expression remained high. In contrast, lentiviral PEI-Mag MMB showed reduced transduction efficiencies under these enhanced shear conditions (Figure 3.8.b; *p≤0.05, **p≤0.01, n=4). As the SO-Mag MMB were repeatedly found to possess functional advantages under static as well as under flow conditions compared to PEI-Mag MMB, only the former were used in further experiments.

In Section 3.1.8 it was demonstrated that the targeting of lentiviral MMB by MF and US under static conditions is essential to allow for maximal gene delivery (see Figure 3.7). To assess if this is also the case under flow conditions, we omitted either MF or US from the procedure while perfusing the lentiviral MMB with shear rates of 1 and 7.5 dyn/cm². As can be seen in Figure 3.8.c, luciferase expression was significantly decreased if MF exposure was omitted from the procedure compared to full treatment (**p≤0.01, n=4). Importantly, if only US without MF exposure was applied, transgene expression was minimal, emphasizing the importance of magnetic attraction under flow conditions for successful gene delivery (**p≤0.01, n=4).

To verify the advantage of fully assembled lentiviral MMB over sole lentivirus-MNP complexes, we assessed the luciferase activities resulting from perfusion and targeting of these two solutions under shear rates of 1 and 7.5 dyn/cm² (SO-Mag MNP and MMB). As expected, application of lentivirus-MNP complexes resulted in significantly reduced gene transfer efficiency under both shear rates compared to lentiviral MMB application (Figure 3.8.d; *p≤0.05, **p≤0.01, n=4).

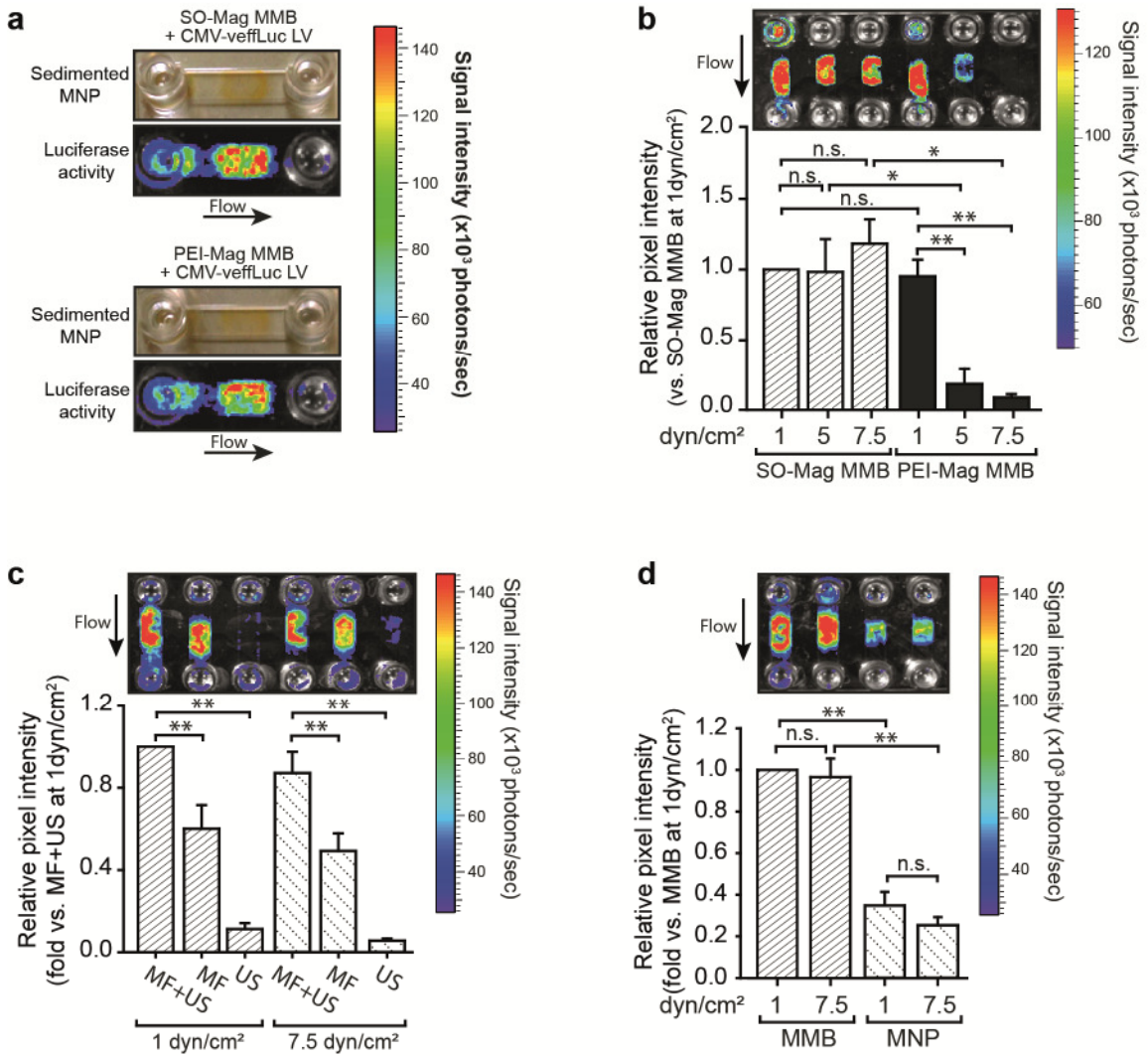

Figure 3.8. Transduction efficiency of SO-Mag and PEI-Mag MMB under different shear rates and contribution of single method parameters to gene transfer efficiency under flow conditions.

To study the performance of lentiviral MMB under flow conditions, HUVEC were cultured in flow channels and MMB were targeted by US and MF under constant perfusion with different shear rates. **(a)** MNP released from MMB mainly sedimented in the area of MF application. The resulting luciferase activity (detected 72 h after transduction) strongly co-localized with these MNP sediments. n=3. **(b)** Gene targeting efficiencies of lentiviral SO-Mag and PEI-Mag MMB with simultaneous MF and US application were similar under low shear of 1 dyn/cm². However, when increasing the shear (5 and 7.5 dyn/cm²) transduction efficiency of PEI-Mag MMB was strongly reduced while SO-Mag MMB delivered the genetic material with constant efficiency. *p≤0.05, **p≤0.01, n=4, 1-way ANOVA. **(c)** Gene transfer efficiency of SO-Mag MMB was significantly diminished if either MF or US were omitted from the targeting procedure independent from the applied shear rate (1 or 7.5 dyn/cm²). **p≤0.01, n=4, 1-way ANOVA. **(d)** The use of fully assembles MMB is essential for efficient gene delivery as targeting of sole lentiviral SO-Mag MNP did only yield weak luciferase expression. **p≤0.01, n=4, 1-way ANOVA.

3.2 Targeted gene expression in the aortic endothelium *ex vivo* using lentiviral SO-Mag MMB

3.2.1 Localized GFP expression by targeting lentiviral SO-Mag MMB to the endothelium in mouse aortas

As the lentiviral SO-Mag MMB were capable to achieve a local gene delivery under flow *in vitro*, we were furthermore interested to test their functionality *ex vivo* in isolated mouse aortas. To create conditions similar to *in vivo* conditions, we carried out the MMB targeting procedure under flow conditions using the recirculation setting as depicted in Section 2.1.16. Depending on the aortic diameter, a shear rate of around 7-8 dyn/cm^2 was applied. GFP LV-SO-Mag MMB were targeted at the central section of the aorta by application of MF and US. The resulting GFP expression was essentially localized in the region of MF and US application, as visualized by fluorescence microscopy of the whole aorta 72 h after transduction (Figure 3.9.a; n=3). In aortas without MF and US targeting no transgene expression could be detected. Specific targeting of the endothelial cell layer was verified by PECAM-1 co-staining of GFP expressing cells in cross sections of the treated aortas (Figure 3.9.b; n=3). GFP expression was thereby uniquely found in endothelial cells and not in other cell types, such as vascular smooth muscle cells.

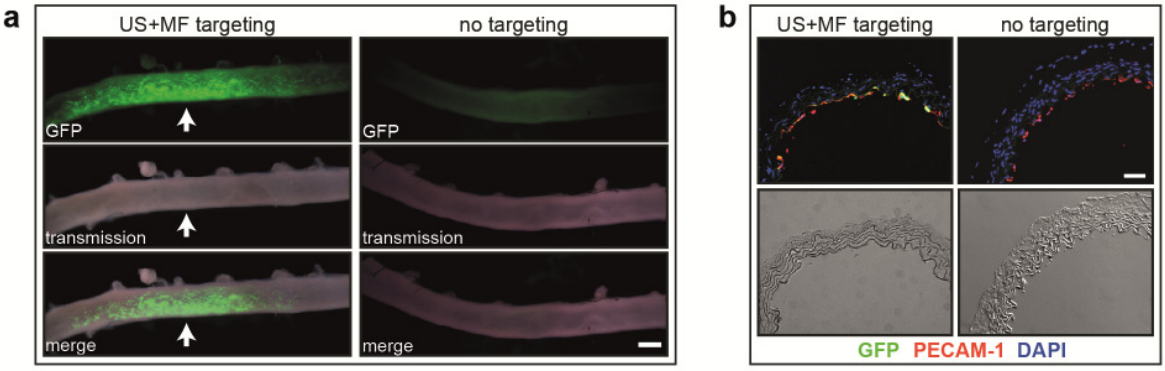

Figure 3.9. Targeted delivery of GFP LV to aortic endothelium using SO-Mag MMB.
(a) GFP LV complexed to SO-Mag MMB was locally delivered to mouse aortas (left panels) as visualized by fluorescence microscopy of the whole aortas. n=3. In contrast, aortas which were perfused with lentiviral MMB without targeting completely lacked transgene expression (right panels). The arrow indicates the site of MF and US application. Scale bar indicates 1 mm. **(b)** GFP expression was specifically found in aortic endothelial cells which were co-stained with the endothelial cell marker PECAM-1. Scale bar indicates 10 µm. n=3.

3.2.2 Targeted over-expression of VEGF in aortic endothelium for the enhancement of angiogenic responses

To assess if the SO-Mag MMB mediated gene transfer is indeed capable to achieve functional alterations in the vascular endothelium, we applied a lentiviral construct harbouring an over-expression cassette for human vascular endothelial growth factor (VEGF). VEGF is a growth factor produced and secreted by different cells types upon stimulation by i.e. hypoxia. Upon binding of VEGF to VEGF receptors on endothelial cells angiogenic responses are elicited. To achieve over-expression in aortic endothelium, VEGF LV was complexed to SO-Mag MMB and targeted as described in Section 2.1.16. As control, aortas treated with GFP LV-SO-Mag MMB were prepared. Indeed, VEGF LV-treated aortas expressed significantly higher levels of VEGF compared to GFP control aortas, as detected by qRT-PCR (Figure 3.10.a; $^{**}p \leq 0.01$, n=5). Thereupon, it was assessed if this VEGF over-expression in endothelial cells also results in enhanced VEGF secretion and subsequent stimulation of vessel sprouting. Levels of secreted VEGF detected in medium supernatants 72 h after transduction were indeed significantly higher compared to levels in medium of GFP control aortas (Figure 3.10.b; $^{**}p \leq 0.01$, n=5). In accordance with this, VEGF-transduced aortas generated significantly more sprouting tips resulting in a larger vascularization area compared to controls, as assessed by the aortic ring sprouting assay (Figure 3.10.c-e; $^{*}p \leq 0.05$, n=3).

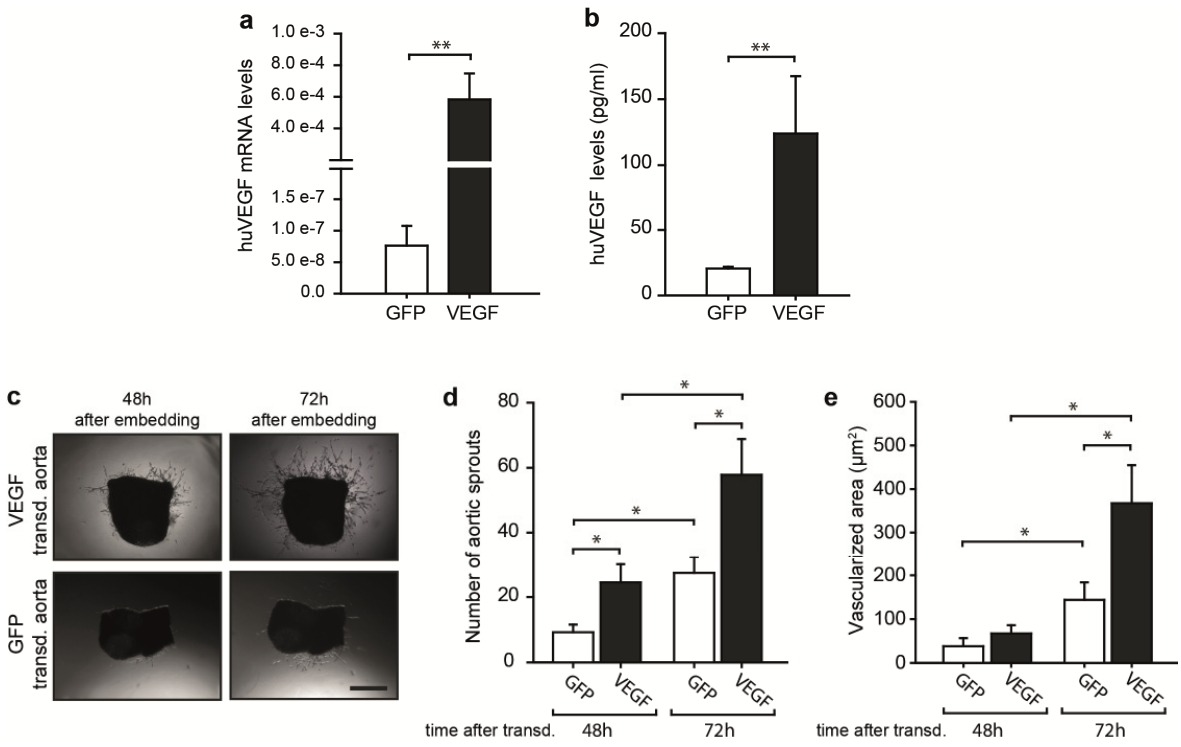

Figure 3.10. SO-Mag MMB mediated over-expression of VEGF in aortic endothelium results in enhanced angiogenic responses.

(a) Successful over-expression of VEGF in isolated aortas achieved by SO-Mag MMB mediated transduction was detected by qRT-PCR with GFP-treated aortas as negative control. **$p \leq 0.01$, n=5, t-test. **(b)** VEGF expression in aortas resulted in 6-fold higher levels of secreted VEGF into the medium compared to levels secreted by GFP control aortas. **$p \leq 0.01$, n=5, t-test. **(c)** Strong angiogenic activation was observed in VEGF over-expressing aortic rings resulting in significantly higher numbers of sprouting tips and a larger vascularized area compared to rings from GFP control aortas. Scale bar indicates 200 µm. *$p \leq 0.05$, n=3 aortas with 6-8 rings each, 1-way ANOVA.

3.2.3 Functional analysis of SHP-2's role during insulin resistance ex vivo

3.2.3.1 Chronic exposure of endothelial cells to high insulin and glucose concentrations induces insulin resistance and a pro-inflammatory phenotype

The successful targeted expression of VEGF in aortic endothelium clearly demonstrated that the SO-Mag MMB technique has the potential to deliver therapeutic genes at an intended site of a vessel resulting in physiological responses. Based on that, we were furthermore interested to study a new potential target in endothelial inflammation under insulin resistant conditions, the protein tyrosine phosphatase SHP-2, with the objective to verify our *in vitro* findings *ex vivo* using the lentiviral MMB technique.

To study the inflammatory phenotype of endothelial cells under diabetic conditions, we generated insulin resistant endothelial cells by treatment with high insulin (100 nM) and glucose (15 mM) concentrations (high insulin/glucose: HIG) for 24 h or 48 h. Under such conditions, defective activation of central insulin-induced signaling molecules, such as PI3K and AKT, has been observed [92, 93]. In accordance with this, cells kept under HIG conditions displayed strongly diminished AKT activation in response to short term (5 min) stimulation with 1 nM insulin (Figure 3.11.a; *$p \leq 0.05$, n=3). To assess the degree of endothelial inflammation, surface expression of the adhesion molecules ICAM-1 and VCAM-1 was detected by flow cytometry. Both adhesion molecules were strongly expressed on insulin resistant cells with highest expression levels after 48 h of HIG treatment (Figure 3.11.b; *$p \leq 0.05$, n=4-6).

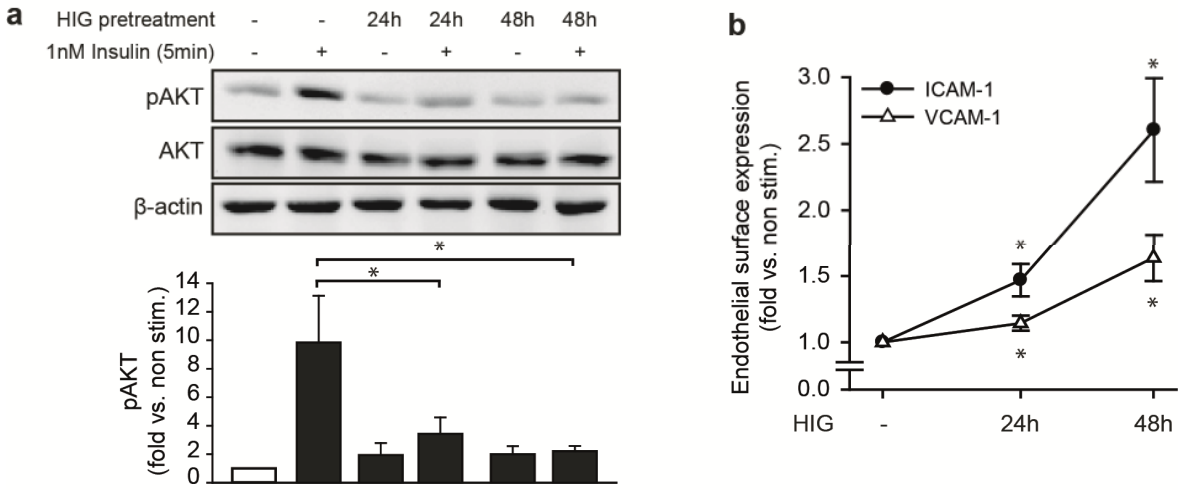

Figure 3.11. Insulin resistant endothelial cells feature a strong inflammatory phenotype.
(a) Short term stimulation of endothelial cells with 1 nm Insulin for 5 min strongly induced AKT activation. Upon chronic exposure of cells to HIG for 24 h and 48 h this activation of AKT was absent, as assessed by western blot. Total AKT levels remained unchanged under the different conditions. Graph shows quantification of pAKT band intensities normalized to β-actin. *p≤0.05, n=3, 1-way ANOVA. **(b)** ICAM-1 and VCAM-1 surface expression on endothelial cells significantly increased under chronic HIG conditions. *p≤0.05 vs. non stimulated cells, n=4-6 in duplicates, 1-way ANOVA.

3.2.3.2 SHP-2 phosphatase activity is diminished under insulin resistance in endothelial cells

To assess if SHP-2 is involved in endothelial inflammatory signaling induced during insulin resistance, its phosphatase activity was detected. Therefore, SHP-2 protein was immunoprecipitated and incubated in a pNPP substrate solution. Interestingly, basal phosphatase activity of SHP-2 under control conditions could be detected (Figure 3.12.a). By incubation of the precipitated SHP-2 with the phosphatase inhibitor Na_3VO_4 (25 mM; *p≤0.05, n=4) a significant reduction in enzymatic activity of SHP-2 by around 50% was detected. This effect was reproduced by incubation with the specific SHP-2 inhibitor PtpI IV (2 µM; *p≤0.05, n=4). As can be seen in Figure 3.12.b, chronic insulin resistance (24 h HIG) resulted in a reduction of basal phosphatase activity similar to the effects seen with the pharmacological inhibitors (**p≤0.01, n=4). Importantly, the total protein levels of SHP-2 remained constant under HIG treatment (Figure 3.12.c; n=4).

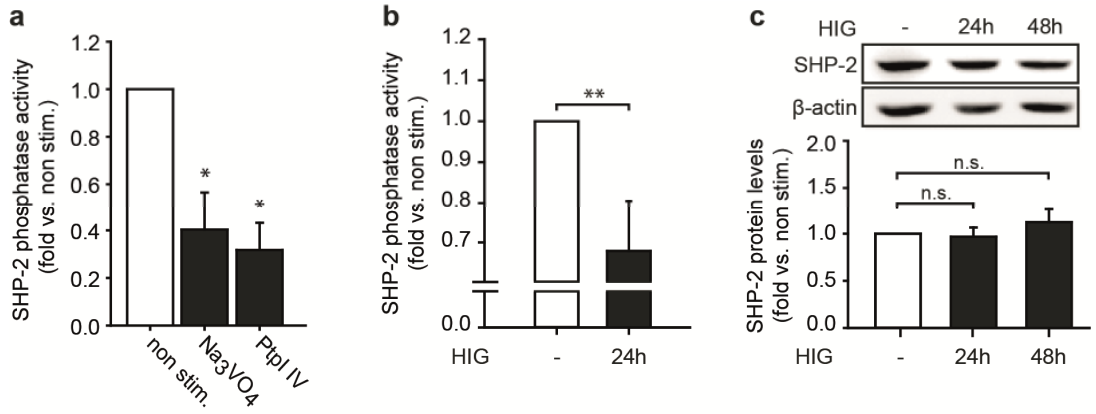

Figure 3.12. Detection of SHP-2 activity under basal and insulin resistant conditions.
(a) SHP-2 exhibits basal phosphatase activity under normal conditions in endothelial cells, which was significantly reduced upon inhibition with the general phosphatase inhibitor Na_3VO_4 (25 mM) or the specific SHP-2 inhibitor PtpI IV (2 µM). *p≤0.05, n=4, 1-way ANOVA. **(b)** Upon 24 h HIG treatment, SHP-2 exhibits a strongly diminished phosphatase activity. **p≤0.01, n=4, t-test. **(c)** SHP-2 protein expression did not change under chronic insulin resistance as assessed by western blot. Graph shows quantitative analysis of SHP-2 band intensities normalized to β-actin. n=4, 1-way ANOVA.

3.2.3.3 The phosphatase activity of SHP-2 negatively regulates endothelial adhesion molecule expression under insulin resistance

To further analyse the impact of SHP-2's phosphatase activity on inflammatory responses triggered by HIG treatment, two opposite enzyme mutants of SHP-2 (SHP-2 CS: dominant negative; SHP-2 E76A: constitutively active) were introduced to endothelial cells by lentiviral transduction. As control, cells over-expressing the wild type (WT) form of SHP-2 were always measured alongside. First of all, the actual activity state of the three SHP-2 proteins under basal conditions was checked. Therefore, proteins were precipitated from full lysates with an antibody recognizing the Myc-Tag sequence joined to the SHP-2 sequences. Isolated proteins were then exposed to the pNPP assay. As anticipated, the SHP-2 CS mutant showed reduced phosphatase activity compared to the SHP-2 WT protein (Figure 3.13.a; *$p \leq 0.05$, n=3). In contrast to this, the activity of SHP-2 E76A was enhanced compared to SHP-2 WT (*$p \leq 0.05$, n=3). After verifying the functional phenotype of the SHP-2 enzyme variants, their effects under insulin resistant conditions in endothelial cells were assessed. As shown in Figure 3.13.b and d, over-expression of dominant negative SHP-2 CS led to significantly enhanced surface expression of ICAM-1 and VCAM-1 after 24 h and 48 h HIG treatment compared to SHP-2 WT cells (*$p \leq 0.05$, **$p \leq 0.01$, n=6). In contrast to that, over-expression of the SHP-2 E76A mutant completely prevented adhesion molecule upregulation at both time points (*$p \leq 0.05$, **$p \leq 0.01$, n=6).

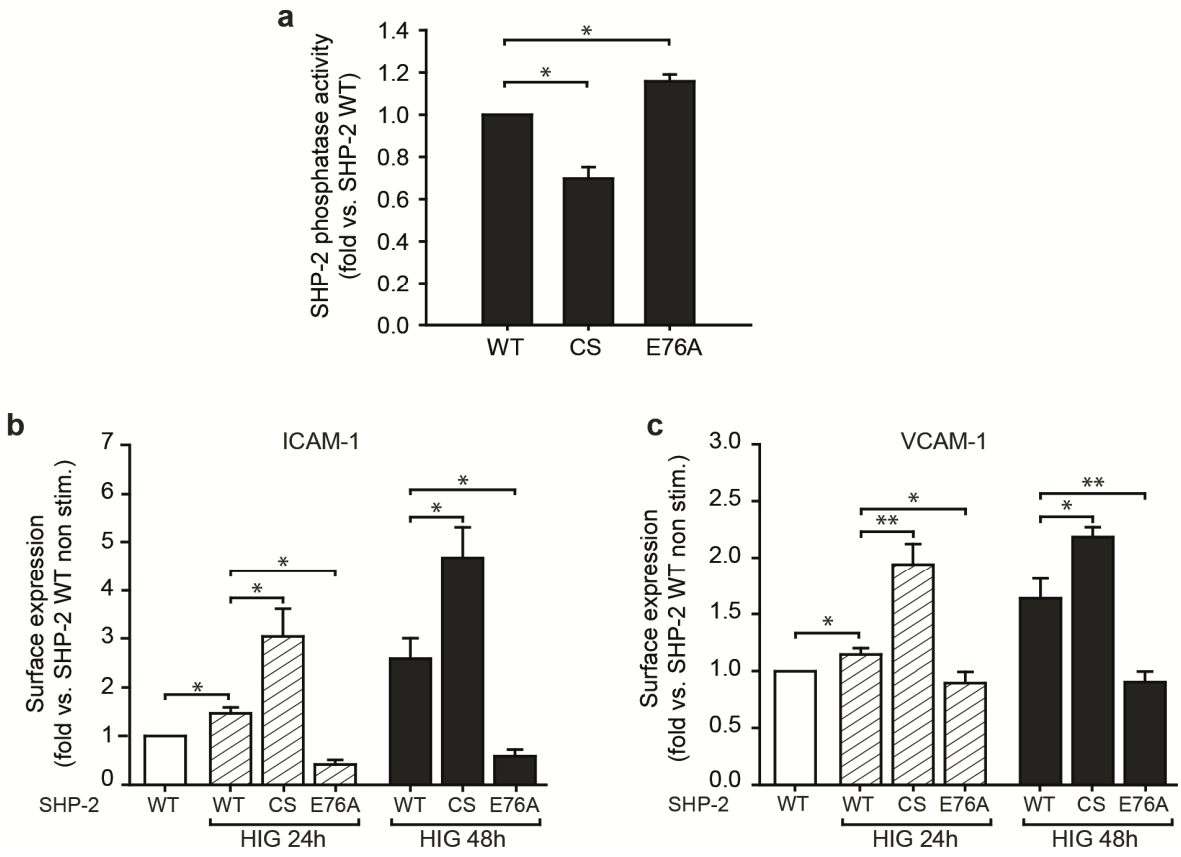

Figure 3.13. Analysis of SHP-2's role during insulin resistance by over-expression of the SHP-2 enzyme variants SHP-2 CS and E76A in endothelial cells.

(a) The two enzyme mutants of SHP-2 exhibited reduced (SHP-2 CS) or enhanced (SHP-2 E76A) phosphatase activity compared to SHP-2 WT. *p≤0.05, n=3, 1-way ANOVA. **(b)** and **(c)** Insulin resistant cells (24 h and 48 h HIG) transduced with SHP-2 CS exhibited significantly enhanced surface levels of ICAM-1 and VCAM-1 compared to SHP-2 WT cells. In contrast, cells over-expressing SHP-2 E76A showed reduced levels of these surface adhesion molecules. *p≤0.05, **p≤0.01, n=6, 1-way ANOVA.

3.2.3.4 Lentiviral SO-Mag MMB mediated expression of constitutively active SHP-2 represses the pro-adhesive switch in vascular endothelium ex vivo.

To investigate if a targeted SO-Mag MMB assisted lentiviral gene delivery of the functional SHP-2 mutants is capable to modulate the pro-adhesive phenotype in insulin resistant endothelial cells, we applied this technique to isolated vessels. Therefore, the endothelium of mouse aortas was targeted under flow using SO-Mag MMB coupled to the respective lentiviral SHP-2 constructs (WT, CS or E76A) by simultaneous application of a MF and US as depicted in Section 2.1.16. Under insulin resistant conditions, increased ICAM-1 and VCAM-1 mRNA expression levels were detected in vessels expressing SHP-2 WT (Figure 3.14; *p≤0.05, n=3). In accordance with the effects observed *in vitro*, over-expression of SHP-2 CS significantly further increased ICAM-1 and VCAM-1 expression in aortas induced by chronic HIG treatment compared to SHP-2 WT expressing vessels (*p≤0.05, n=3). Importantly, over-expression of SHP-2 E76A in vascular endothelial cells *ex vivo* completely prevented the induction of adhesion molecule expression seen under insulin resistance (*p≤0.05, n=3).

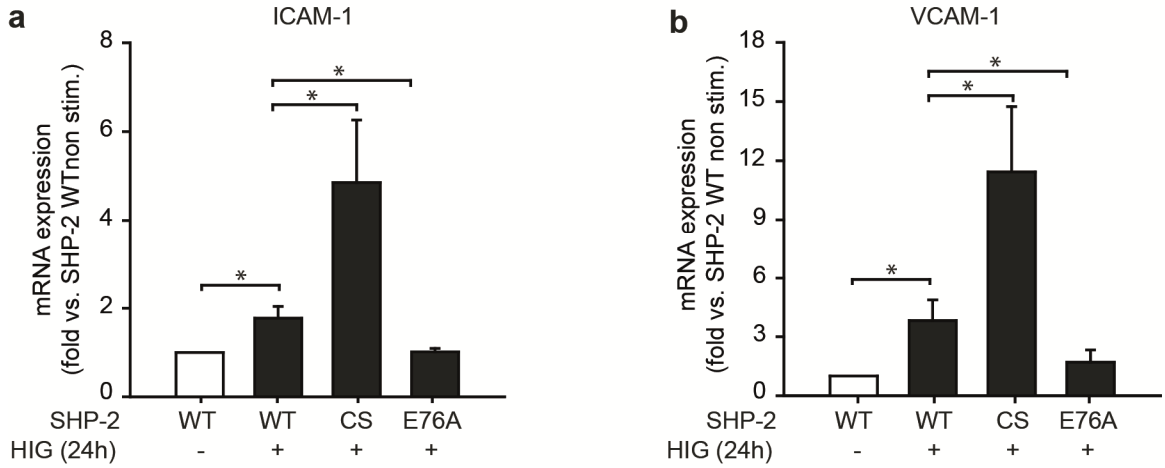

Figure 3.14. SO-Mag MMB mediated expression of the enzymatic SHP-2 mutants (CS and E76A) to aortic endothelium substantially modulates the expression of adhesion molecules under insulin resistance.
(a) and **(b)** Upon HIG treatment, mRNA expression of ICAM-1 and VCAM-1 was strongly induced in SHP-2 WT expressing aortas compared to non stimulated WT aortas. This induced adhesion molecule expression was significantly further enhanced in aortas expressing dominant negative SHP-2 (CS). In SHP-2 E76A expressing aortas, in contrast, adhesion molecule mRNA levels were similar to levels detected in non stimulated aortas. *p≤0.05, n=3, 1-way ANOVA.

3.3 Targeted gene delivery *in vivo* using the lentiviral SO-Mag MMB technique

Since the lentiviral SO-Mag MMB technique has been shown to yield a significantly improved gene delivery *in vitro* as well as *ex vivo*, the next step to take was its application *in vivo*. However, the successful intravascular application of a gene carrier system in a whole organism strongly depends on its capacity to withstand several challenging conditions. To test the functionality of the SO-Mag MMB technique to specifically deliver the complexed lentiviruses to a desired vascular bed, the murine dorsal skinfold chamber (DSFC) model was used (for details see Sections 2.3.3 - 2.3.5).

3.3.1 Biodistribution of MNP after intravascular application of lentiviral MMB

If an injected nanomaterial is accumulated, biotransformed or degraded within an organism strongly depends on different physico-chemical and biological properties such as size, surface charge and core material. In case of the MMB, two components have to be considered for biocompatibility: the phospholipids DPPE and DPPC and the iron-oxide MNP. As DPPE and DPPC are both found in biological membranes, their *in vivo* application can be considered as unproblematic. The contained MNP, however, are foreign components. Therefore, the fate of the applied MNP was analyzed by magnetic particle spectroscopy (MPS). Importantly, this method specifically detects non-heme iron, thereby allowing for distinction of MNP-derived (exogenous) iron from endogenous iron contained in haemoglobin or ferritin. MPS was performed with homogenates of the main organs (heart, lung, liver, kidney, spleen, brain), which were isolated from mice 1 h as well as 96 h after lentiviral SO-Mag MMB treatment. As shown in Figure 3.15, high amounts of exogenous iron were detected 1 h after treatment in all analyzed organs (n=4-5). The highest iron accumulation was thereby found in the liver (41.3% ± 9.4% of applied dose (o.a.d.)) followed by lung (19.1% ± 4.0% o.a.d.) and spleen (8.4% ± 2.0% o.a.d.). In the remaining organs (heart, kidney and brain) 4-5% o.a.d. were detected, respectively. The remaining 20-25% of applied MNP were probably taken up by organs and body compartments which have not been analyzed here. Surprisingly, only traces (between 0.1-0.3% o.a.d.) of MNP-derived iron could be detected in all of the analyzed organs 96 h after treatment.

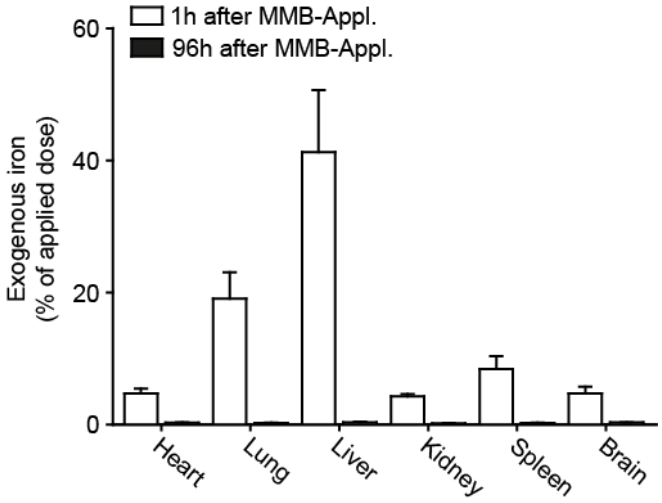

Figure 3.15. Systemic distribution of exogenous iron 1 h and 96 h after treatment.
1 h after intra-aterial injection of SO-Mag MMB, more than 60% of the MNP were detected in liver and lung. However, 96 h after treatment, only traces of exogenous iron remained in the analyzed organs. n=4-5.

3.3.2 Detection of residual lentiviral particles after in vivo *application*

The lentiviruses used in this study were chosen due to their highly effective gene transfer as well as the resulting stable transgene expression in targeted cells. Importantly, only recombinant third-generation lentiviruses incapable to replicate after infection were used for all experiments. However, lentiviral particles which did not enter cells or have not been eliminated after treatment, represent a hazardous risk for the environment. To analyse potential sources of contamination of residual lentiviral particles, p24 core protein, a component of the lentiviral capsid, was detected in plasma, saliva, faeces, urine and smears from the skin area of the catheter surgery (injection site) sampled 48 h after lentiviral MMB treatment. As positive control a sample containing $2*10^5$ VP was measured. Except for the positive control, no remaining lentiviral particles were detected in the different samples indicating the complete uptake or clearance after systemic injection (Figure 3.16). Additionally, the absence of p24 core protein in the smear sample taken from the injection site proves that the lentivirus application via the Arteria carotis catheter represents a clean procedure without contamination risk.

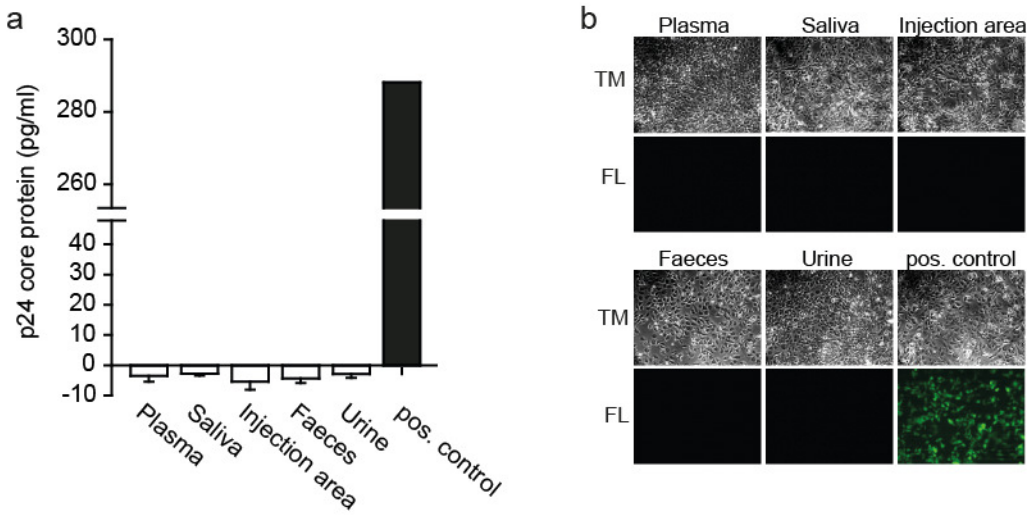

Figure 3.16. Detection of p24 core protein in different body fluids and smears of lentiviral MMB injected animals.
No residual lentiviral particles were detected in body fluids (plasma and saliva), excreta (faeces and urine) or injection area smears (throat skin) collected from mice 48 h after treatment as assessed by a p24 core protein ELISA **(a)** or direct application to HUVEC and fluorescence microscopy **(b)** (n=4 animals). In contrast, a strong signal was detected in the positive control sample containing $2*10^5$ VP.

3.3.3 Localized delivery of lentiviral vectors to the dorsal skin of mice by SO-Mag MMB targeting

The intravascular application of genetic vectors is mainly limited by its lack of efficiency and site-specificity. The application of lentivirus coated SO-Mag MMB has shown promising results in the former presented *in vitro* and *ex vivo* experiments. *In vivo*, arterial injection of MMB via the Arteria carotis has been shown to be effective for targeted gene delivery of pDNA to the dorsal skin of mice [40]. Therefore, the experimental setting for in *vivo* gene transfer using lentiviral MMB was adopted from this former study (for detailed settings see Figure 2.6). To allow for systemic analysis of transgene expression, the luciferase lentivirus was chosen. Eight days after lentiviral MMB targeting *in vivo*, mice showed a strong and local bioluminescence signal at the area of MF and US exposure indicating successful delivery of the luciferase expressing lentivirus via SO-Mag MMB targeting (Figure 3.17.a and b, right image and graph; n=3). Lentiviral MMB injection without MF and US targeting, in contrast, did not result in a luciferase activity signal in the

DSFC (Figure 3.17.a and b, left image and graph; n=3). Successful targeting was furthermore verified by quantitative analysis of absolute genome copy numbers of proviral DNA, which was significant higher in animals with MF and US targeting (Figure 3.17.c). However, the spleen and lung were identified as second expression sites in animals of both groups (Figure 3.17.d). Interestingly, whereas lentiviral MMB treatment without MF and US targeting caused strong transgene expression in the spleen and liver (Figure 3.17.d, upper images), lentiviral MMB treatment with MF and US targeting reduced the transgene expression in the liver (Figure 3.17.d, lower images). This finding was further confirmed by detecting the proviral genome copy numbers in liver homogenates. There, the livers of mice in which the lentiviral MMB were targeted to the dorsal skin exhibited significantly reduced proviral genome insertions compared to livers of mice without targeting (Figure 3.17.e). In lung tissues, in contrast, genome copy numbers remained the same regardless if MMB targeting was performed or not (Figure 3.17.f).

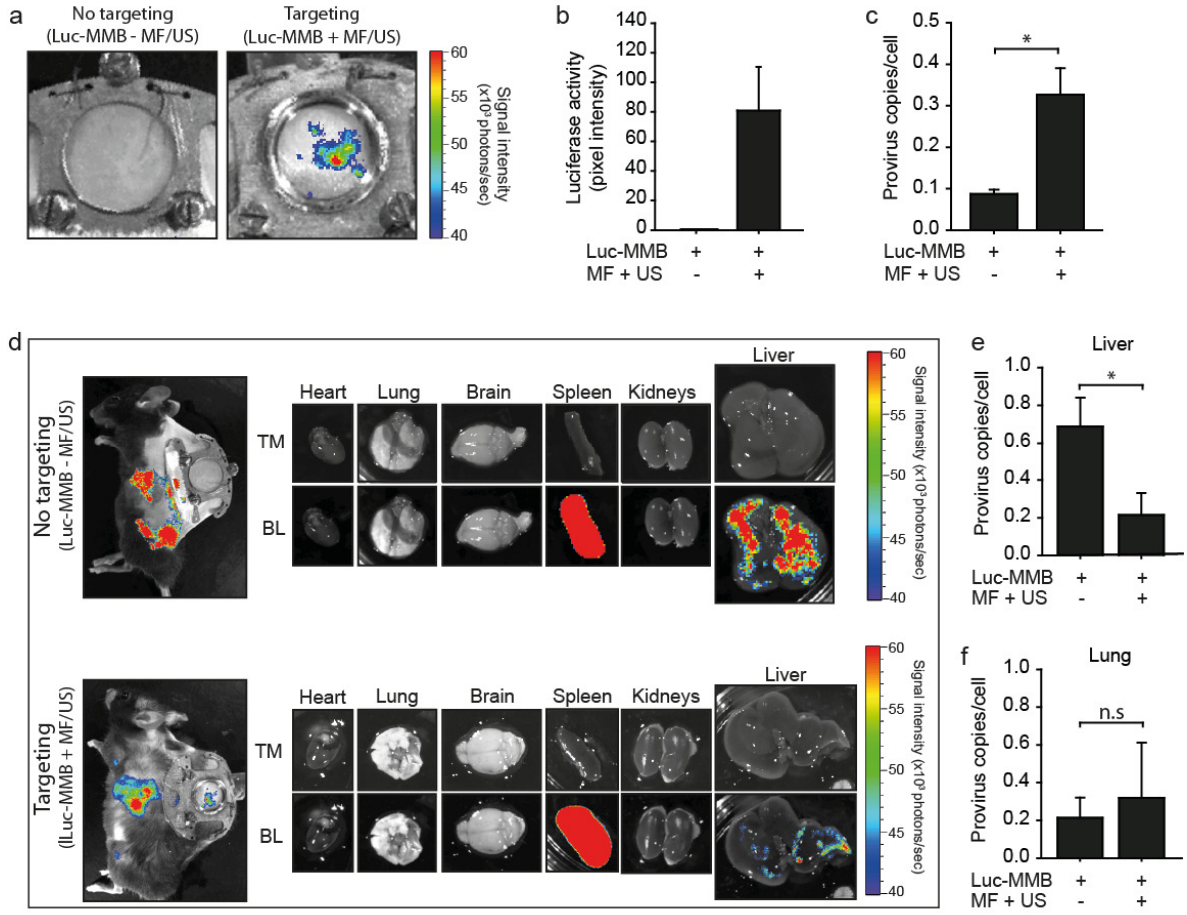

Figure 3.17. SO-Mag MMB achieve targeted lentiviral delivery after systemic injection *in vivo*.

(a) Representative bioluminescence images of the DSFC observation window in mice received 8 days after Luc-MMB application. Upon magnetic and ultrasonic targeting of Luc-MMB to the DSFC window a strong and local luciferase expression could be detected (right image). In contrast to this, injection of Luc-MMB without targeting resulted in no detectable luciferase activity in the DSFC window area (left image). n=3 animals. **(b)** Quantitative measurements of pixel densities in DSFC windows of mice +/- MF and US targeting. n=3 animals. **(c)** Numbers of proviral DNA integrations in DSFC window tissue +/- MF and US targeting. *p≤0.05, n=3 animals, t-test. **(d)** Systemic distribution of luciferase expression in Luc-MMB treated mice was assessed by whole-body bioluminescence measurements (left upper and lower images) as well as detection in isolated organs (right upper and lower images). Luciferase activity was detected in the spleen and liver in animals receiving lentiviral MMB without targeting (upper images), whereas non-specific transgene expression in mice receiving lentiviral MMB and targeting was mostly in the spleen (lower images). n=3. **(e)** Detection of proviral DNA integration numbers revealed that MF and US targeting to the DSFC reduces unspecific genome integrations in the liver. *p≤0.05, n=5 animals, t-test. **(f)** In contrast, genome copy numbers in lungs of mice +/- MF and US targeting remained unchanged. *p≤0.05, n=5 animals, t-test

Luc: Luciferase, MMB: Magnetic microbubbles, MF: Magnetic Field, US: Ultrasound, DSFC: dorsal skinfold chamber, TM: Transmission, BL: Bioluminescence.

4 Discussion

This thesis describes the establishment and verification of an advanced vascular gene targeting approach, the lentiviral magnetic microbubble (MMB) technique. Here, ultrasonic microbubble-mediated delivery and magnetic nanoparticles (MNP)-assisted transport were combined with lentiviral gene delivery resulting in a potent gene transfer system eligible for functional *in vitro* and *ex vivo* studies as well as *in vivo* applications.
Two types of MMB coated with different superparamagnetic iron-oxide nanoparticles (SO-Mag and PEI-Mag MNP) were directly compared to evaluate their functional and biological performance. The superior SO-Mag MMB were then further applied to analyse the potential of the MMB technique to also achieve physiological responses by targeted lentiviral gene transfer to the endothelium in intact isolated vessels. Moreover, site-specific gene delivery by SO-Mag MMB-mediated lentiviral transduction *in vivo* was evaluated by using the dorsal skinfold chamber (DSFC) model in mice.

4.1 Comparison of the newly established SO-Mag MMB with PEI-Mag MMB

4.1.1 Physico-chemical characteristics

The effectiveness of a gene carrier system is always the result of the successful cooperation of its single components. The different characteristics of the combined materials therefore substantially influence structural aspects such as size, charge and stability. The magnetic microbubbles (MMB) presented in this study feature a gas filled core encapsulated by a homogenous phospholipid-MNP shell. In former studies of us, microbubbles coated with PEI-Mag MNP were demonstrated to successfully bind and deliver genetic vectors, such as pDNA and lentiviruses to endothelial cells [40, 41]. However, in a study from Mykhaylyk et al., a new type of silica-coated iron-oxide MNP, named SO-Mag MNP, were found to possess improved magnetic properties (e.g. 1.5-fold higher magnetic moment) compared to the former established PEI-Mag MNP [84]. This finding was decisive for the establishment of new MMB containing SO-Mag MNP. To allow for an accurate evaluation of the SO-Mag MMB they were directly compared to PEI-Mag MMB. It has been shown that not every MNP type is adequately incorporated to the lipid shell of microbubbles [40]. However, similar to PEI-Mag MNP, SO-Mag MNP evenly distribute in the lipid layer resulting in

floating and magnetic responsive MMB. With a mean diameter below 5 µm in combination with their flexible lipid shell the generated SO-Mag MMB showed positive characteristics for later *in vivo* applications, where the ability to freely pass through the smallest capillary beds determines the success and applicability of a gene transfer method. A further essential prerequisite for MMB to be suitable as vascular gene carrier is their ability to resist blood flow upon local MF exposure. MNP alone have been implemented as gene carriers in many *in vitro* and *in vivo* studies by us [32, 94, 95] and other groups [34, 36, 82]. This so called magnetofection method not only improved gene delivery to cultured cells under static and flow conditions but also reduced cytotoxicity due to the decrease in transfection duration [32]. However, magnetofection after systemic administration *in vivo*, has proven to be difficult probably due to low magnetic moments of the single MNP, particle aggregation as well as rapid clearance from the circulation by interactions with immune cells and the glycocalix. The embedding of several MNP within the lipid monolayer of a MB has not only the advantage to reduce their biological clearance but also enormously increases the ability of site-specific targeting by withstanding the forces of blood flow in comparison to single MNP application. Indeed, a single MMB exhibited an about $2x10^5$-fold higher magnetic moment compared to the respective single MNP. Interestingly, twice the number of SO-Mag MNP were incorporated into the MMB compared to PEI-Mag MNP. This, in combination with the formerly mentioned higher magnetic moment of single SO-Mag MNP compared to PEI-Mag MNP, accounts for the enhanced magnetic velocity and magnetic moment observed with SO-Mag MMB.

4.1.2 Lentivirus-binding properties

Gene transfer efficiency and associated therapeutic success is substantially determined by the choice of the genetic vehicle with which a targeting system is combined. Lentiviruses represent ideal vectors for the delivery of therapeutic genes to vascular endothelial cells as they are capable to infect even slow or non dividing cells and enable permanent transgene expression due to stable genome integration [5, 12]. However, in clinical gene therapy lentiviruses are currently only applied as vehicles for *ex vivo* transduction of autologous hematopoietic stem cells of patients with hematopoietic disorders [14-16]. The major obstacles of systemic lentivirus application, such as immune activation and insufficient targeting, might be solved by combining lentiviral gene transfer with MMB-mediated targeting. The

association of negatively charged lentiviruses to MNP has been shown to be favoured if the MNP features a positive ζ potential thereby enabling electrostatic interactions. The here applied MNP featured opposite surface charges due to their respective coatings. While the PEI-Mag MNP exhibited a positive ζ potential of +55.4 mV, SO-Mag MNP possessed a negative surface charge of -33.7mV. Surprisingly, in this study, MMB coated with the negatively charged SO-Mag MNP were equally capable to bind the negatively charged lentiviruses (-8.8 mV) as were the positively charged PEI-Mag MNP. This is interesting as in a former study of us, it was demonstrated that MMB generated with negative palmitoyl dextran-coated MNP (PalD1-Mag4 and PalD2-Mag1) were not capable to efficiently bind lentiviral particles [41]. However, in contrast to this study, the ζ potential of the PalD-Mag MMB has not been assessed leaving the question regarding the actual surface charge of these MMB open. The here generated new SO-Mag - MB complexes actually exhibited a positive ζ potential similar to that of the PEI-Mag MMB giving a plausible explanation for the good lentivirus-binding properties of both the MMB types. As the naked MB exhibited a ζ potential of +6.2 mV it seems likely that the negative silica-groups on the surface of the SO-Mag MNP were masked resulting in the positive cumulative charge of the SO-Mag MMB. This finding is particularly meaningful regarding future choices of new MNP, as they demonstrate our system to be partially independent of the surface charge of the MNP itself, which means that attention can rather be focussed on magnetic properties. Importantly, nearly the complete amount of lentivirus added to the MMB solutions ($5*10^6$ IP/ml) was bound by both the MMB types as demonstrated by magnetic separation of the lentiviral MMB from the bubble free supernatant and subsequent MF and US targeting to endothelial cell cultures. However, the concentrated lentiviral SO-Mag MMB achieved a significantly increased transduction rate of endothelial cells compared to PEI-Mag MMB. As the lentivirus loading of SO-Mag and PEI-Mag MMB was the same, this effect can only be based on the enhanced magnetic moment of SO-Mag MMB resulting in a more effective gene transfer.

4.1.3 Cytotoxicity of the MMB technique

Biocompatibility is the major criterion for the applicability of newly established nanomaterials and chemical components in biomedicine. The MNP and lipid components used in this study did not induce cytotoxicity in primary endothelial cells, known to be

rather sensitive to external stimuli. This emphasizes the safety of the MMB system important for later *in vivo* application. However, a reduction of cell viability by around 20% was detected after US application. This cytotoxicity most probably results from the direct exposure of cultured cells to the ultrasonic waves given into the cell culture medium, which has also been observed in other studies applying a variety of US parameters [96, 97]. Interestingly, this extent of cytotoxicity was constant regardless if lentiviral MMB were abundant or not indicating that the MMB sonication itself did not contribute to the observed cell toxicity. Importantly, neither in this nor in a former study of us [40], tissue damages, inflammatory responses or haemorrhages were observed in the dorsal skin *in vivo* upon application of US. This might be due to potential insulation effects exerted by surrounding fibers and tissue, which reduce the mechanic stress caused by US thereby maintaining cell integrity.

4.1.4 In vitro *performance under static and flow conditions*

First, to clearly demonstrate the supremacy of the MMB technique over sheer MNP-mediated lentiviral gene delivery (magnetofection), both were tested on endothelial cells under flow conditions with full US and MF targeting. Despite the fact that magnetofection has been demonstrated to have advantages regarding gene transfer effectivity and rapidness *in vitro* [34, 94] it was proven to be much less effective under flow conditions compared to the lentivirus-MMB complexes. To further pursue the finding that SO-Mag MMB delivered their bound lentiviruses with significantly higher efficiency to endothelial cells than PEI-Mag MMB, further *in vitro* targeting experiments under static as well as flow conditions were performed. Therefore, the single parameters of the MMB technique (MMB, US and MF) were tested for their respective contribution to the over-all transduction efficiency of the method. Magnetic targeting of the MMB was found to be the most critical parameter accounting for around 70% or 60% of the complete transduction efficiency under static or flow conditions, respectively. Importantly, the combination of magnetic targeting with MMB sonication by US further increased the gene transfer. The importance of US application in addition to MF exposure for successful *in vivo* transduction has been shown before with pDNA-coated MMB [40]. The enhancing effect on gene transfer by sonication might be explained by the cooperation of two events triggered by US application: The release of the lentiviral cargo upon MMB destruction [98] and the simultaneous induction of

pores on cell membranes going along with enhanced cellular permeability (sonoporation) and endocytic activity [25, 99]. Therefore, magnetic accumulation and ultrasonic destruction of the lentiviral MMB may be seen as equally important for the success of the MMB technique *in vivo*. Importantly, upon magnetic and ultrasonic targeting, SO-Mag MMB delivered the bound lentiviruses with significantly higher efficiency to endothelial cell cultures than PEI-Mag MMB. This is in accordance with the previously assessed magnetic properties of the MMB types, where SO-Mag MMB were shown to possess a three-fold higher magnetic moment than PEI-Mag MMB. Considering these superior characteristics of the SO-Mag MMB over PEI-Mag MMB, only the former were further applied for the successive experiments of this study.

4.1.5 Analysis of the endocytic mechanism responsible for MMB-mediated transduction

There are numerous studies addressing the effects of microbubble sonication on cells and the associated enhanced gene delivery seen under these conditions. Sonoporation, the enhancement of permeability of cell membranes resulting from sublethal ultrasound exposure, accompanied by clathrin- or caveolae-dependent endocytosis are the most accepted explanations for these effects [25, 100, 101]. The major difference between both these endocytic mechanisms is given by the fact that clathrin-mediated endocytosis is receptor-dependent while caveolae-mediated processes occur independent from receptor signaling [102]. Due to these molecular differences, both mechanisms can be selectively inhibited and therefore discriminated. As caveolae formation is substantially dependent on the abundance of adequate amounts of cholesterol, cholesterol depletion by Methyl-β-cyclodextrins is an effective way to prevent this endocytic pathway [86]. On the other hand, endocytosis induced by clathrin-recruitment has been shown to strongly depend on F-actin dynamics and can be inhibited by actin depolimerizing substances such as Cytochalasin B [88]. A third possible pathway for viral particles to enter cells is pH-dependent phagosome-lysosome fusion. Therefore, also phagosome-lysosome fusion was inhibited by pH neutralization using ammonium chloride [87]. Using the full targeting settings in combination with the different inhibitors, we found transduction by lentiviral SO-Mag MMB to be mediated by caveolin-dependent endocytosis, potentially induced by sonication. Therefore, it might be hypothesized that the enhanced transduction efficiency of the MMB technique

is the result of magnetic approximation between lentiviral MMB and cells and subsequent sonication-dependent induction of caveolin-dependent endocytosis. However, due to the complexity of the whole targeting system the exact mechanism has to be reviewed in further studies.

4.2 The lentiviral SO-Mag MMB technique as tool to modulate physiological processes in aortic endothelium *ex vivo*

4.2.1 Verification of localized protein expression in aortic endothelium by MMB-mediated transduction

The intention to apply a gene therapy approach *in vivo* requires careful evaluation of its abilities to achieve efficient gene transfer not only under idealized cell culture conditions, but also under conditions which are similar to the actual complex *in vivo* environment. Aspects such as particular cell surface structures (e.g. cell junctions, glycocalix) as well as blood flow and blood components can substantially impair the accessibility of genetic vectors to the endothelial cell layer. Considering these factors, the newly established lentiviral SO-Mag MMB were tested for their transduction efficiency when applied to intact endothelial tissue as can be found in isolated mouse aortas. To furthermore approach *in vivo* conditions, MMB targeting was performed under flow with applied shear stress of 7-8 dyn/cm^2. Successful gene targeting to endothelial cells *ex vivo* could be visualized by the local expression of GFP in the transduced area and subsequent immunofluorescence staining. Importantly, no dissolution of the endothelial cell layer from the vessel wall could be observed in the aortic segments indicating good tolerance of the procedure. Moreover, our method did not reach deeper tissue, such as the vascular smooth muscle cell layer, proving its selectivity for endothelial gene transfer. This selectivity is desirable for many potential therapeutic applications intending endothelial gene manipulation. However, if targeting of deeper tissues from the luminal side is intended the current methodical settings need to be re-evaluated to assess gene transfer more precisely for different organs and tissues which exhibit heterogeneous endothelial phenotypes [103]. The precise modulation of the applied ultrasonic pulse might be the key component in this regard. It must be said that neither the effects of blood and blood components nor the role of the glycocalix, a

carbohydate-rich layer covering native endothelium [104], were regarded in the here employed *ex vivo* experiments as these specific environmental factors are difficult to simulate *ex vivo*. These will be discussed later in this work in the context of the actual *in vivo* applications (Section 4.3). The subsequent *ex vivo* studies were performed to further validate the therapeutic value of the lentiviral MMB approach as well as elucidate molecular and functional relations in vascular endothelial cells.

4.2.2 Induction of angiogenic responses by targeted over-expression of VEGF in isolated vessels

The modulation of angiogenic responses in endothelial cells is one of the most commonly regarded aims in therapeutic research. Vascular endothelial growth factor (VEGF) has thereby evolved as promising target since it is the most potent angiogenic factor with unique actions on vascular endothelium [53]. Depending on the pursued therapeutic purpose, genetic strategies aim at either promoting [54, 55] or inhibiting [56] angiogenesis by induction or inhibition of VEGF, respectively. Here, the applicability of the lentiviral SO-Mag MMB technique for physiological relevant gene transfer of human VEGF to aortic endothelial cells was to be evaluated. Upon lentivirus targeting, VEGF expression could be successfully detected on mRNA level which was reflected by the high levels of secreted VEGF detected in the medium supernatant of transduced aortas. Importantly, this constant secretion of VEGF from targeted endothelial cells indeed resulted in functional responses, namely strong pro-angiogenic behaviour. These results provide firm evidence for the relevance of the lentiviral MMB technique not only as scientific but also as therapeutic tool. Due to the central role of VEGF during angiogenic processes, VEGF-based therapies constitute very promising treatment strategies. However, the systemic application of drugs targeting VEGF is not feasible due to the severe complications this may cause. Especially the enhancement of VEGF activity in ischemic regions requires local treatment to prevent hypervascularization in unintended body areas. However, despite great scientific and clinical efforts, no effective VEGF-based targeting approach from the intravascular side has been successfully established so far [65]. Even direct localized injections or catheter-mediated approaches did not satisfy the expectations emerged after earlier animal studies [55, 64]. Therefore, the advancement of the here presented gene carrier approach might be a valuable step towards successful tissue-specific angiogenic therapy.

4.2.3 Functional analysis of the phosphatase activity dependent role of SHP-2 during endothelial dysfunction in vitro *and* ex vivo

4.2.3.1 Study of SHP-2's role during insulin resistance-induced inflammation in primary endothelial cells

The SH2 domain-containing protein tyrosine phosphatase-2 (SHP-2) has repeatedly been shown to play a role in inflammatory signaling and tissue responses [66, 70, 105]. In endothelial cells, SHP-2 is an important regulator of angiogenic [75, 76] and inflammatory responses [72, 77, 78]. For instance, it was found to control adhesion molecule upregulation in endothelial cells induced by chronically high concentrations of insulin [72]. These findings strongly indicate that SHP-2 may be an important player in the development of endothelial dysfunction, a major feature frequently found in patients with metabolic disorders such as diabetes mellitus [106].

Insulin is a hormone essentially involved during metabolic homeostasis and microcirculatory vasoreaction [107]. In endothelial cells, the PI3K and MAPK cascades have been elucidated as major opponent pathways responsible for insulin-dependent effects [45]. While activation of PI3K/AKT downstream signaling has been shown to result in vasodilative actions due to enhanced NO production [83, 84], MAPK signaling was shown to increase the expression of pro-thrombotic and pro-inflammatory factors such as ET-1, PAI-1 and adhesion molecules [108, 109]. A mutual regulation of both these pathways has been suggested and is assumed to sustain the physiological state of the endothelium [110]. Under insulin resistance, however, this balance is tilted due to reduced PI3K/AKT- and enhanced MAPK-dependent effects causing a pro-adhesive, pro-inflammatory and vasoconstrictive endothelial phenotype [111]. Although a multiplicity of signaling molecules participating in these key pathways have been identified some gaps still remain. Interestingly, the tyrosine phosphatase SHP-2 has been demonstrated to play a role in both the PI3K and the MAPK pathway in different cell types regulating processes including apoptosis, proliferation, angiogenesis and inflammation [66]. Therein, the three functional domains of SHP-2 (PTP, SH2 and pY domains) have been shown to enable distinct signal modulation depending on the applied stimulus [63, 66-69]. However, so far, the role of SHP-2's phosphatase domain for the development of insulin-resistant pro-inflammatory phenotype in endothelium has been investigated only insufficiently [72]. Here, insulin-resistance of primary endothelial cells was successfully induced by chronic exposure to pathological concentrations of insulin and

glucose. The actual proof of this condition was provided by the characteristic incapacity of insulin-resistant endothelial cells to activate AKT upon low level insulin stimulation [83, 84] as well as the enhanced surface expression levels of the adhesion molecules ICAM-1 and VCAM-1 also seen in patients with insulin resistance [112]. In fact, this switch towards a pro-inflammatory phenotype of the endothelium has been shown to be critically important for the recruitment of pro-inflammatory neutrophils and associated increased occurrence of cardiovascular events [113]. Interestingly, our data revealed that insulin resistant cells exhibited a 30% reduction of the basal SHP-2 phosphatase activity seen in non insulin-resistant cells. No time dependent increase of SHP-2 protein levels upon chronic insulin could be held responsible for this enhanced phosphatase activity. Therefore, SHP-2 enzyme activity is probably reduced by posttranslational modifications of the active site cystein such as S-nitrosylation or oxidation. Both these mechanisms have been shown to result in reversible inhibition of SHP-2's phosphatase activity [69, 114, 115]. Which of these two mechanisms actually accounts for the SHP-2 inhibition observed here, however, remains to be determined. Furthermore, enhanced adhesion molecule expression was observed in cells expressing a dominant negative SHP-2 CS mutant while a constitutively active SHP-2 E76A mutant prevented this pro-inflammatory switch. These findings are in direct contrast to the study of Giri et al., where SHP-2 activation and subsequent enhanced expression was shown to be responsible for the pro-inflammatory phenotype of endothelial cells chronically treated with high insulin concentrations [72]. However, these discrepancies to the here presented results may be explained by different facts. Firstly, in contrast to Giri et al. who applied high insulin concentrations to induce insulin-resistance in endothelial cells, we used a glucose/insulin-double exposure model. Furthermore, it should be noted that for some of their studies Giri et al. used the pharmacological inhibitor NSC 87877, which is non-selective for SHP-2 and its closest family member SHP-1 [110]. Unlike their statement, SHP-1 is abundant in endothelial cells and has been demonstrated to influence hypoxic signaling [116], angiogenesis [109] and apoptosis [117]. The use of NSC87877 to study SHP-2 related effects is therefore not eligible as a substantial interferences due to simultaneous SHP-1 inhibition cannot be excluded. In contrast to that, we used a highly selective and therefore more reliable SHP-2 inhibitor (Ptp I IV) to assess the basal activity of SHP-2 in endothelial cells. The use of enzyme mutants further verified the anti-inflammatory role of SHP-2 under endothelial insulin resistance found with the Ptp I IV inhibitor. In the study of Giri et al., siRNA knock down of SHP-2 and over-expression of a SHP-2 tyrosine phosphorylation site mutant were applied to validate the effects seen with the NSC87877

inhibitor. However, a collective interpretation and comparison of the results gained with these three approaches (enzyme inhibition, protein knock down and adaptor mutation) is rather difficult as they concern different functional domains of SHP-2.

4.2.3.2 Modulation of the inflammatory phenotype of insulin-resistant vascular endothelium by lentiviral MMB mediated over-expression of SHP-2 phosphatase mutants in ex vivo

To further verify the previous described phosphatase-dependent effects of SHP-2 during insulin-resistance also in intact native endothelium, the lentiviral MMB technique was used. Therefore, the same SHP-2 phosphatase mutant constructs as have been used in the *in vitro* studies were delivered to the endothelial layer of isolated mouse aortas by application of MF and US. Remarkably, the resulting over-expression was found to induce the same expression pattern of adhesion molecules as was observed in primary endothelial cells.

Our findings indicate that SHP-2 reactivation in insulin resistant endothelium, for example by SHP-2 E76A over-expression, has therapeutic potential for the treatment of endothelial inflammation in diabetic patients. Importantly, also in intact endothelium, expression of SHP-2 E76A strongly attenuated the upregulation of adhesion molecules under insulin resistant conditions again reassuring its strong anti-inflammatory potential. The completely opposed adhesion molecule pattern seen with the SHP-2 CS mutant emphasizes that the effects observed under these conditions indeed depend on SHP-2's phosphatase activity. In summary, we were able to change a patho-physiological phenotype in intact vessels using the lentiviral MMB technique demonstrating the great potential of this technique for gene therapy.

A further application of functional SHP-2 mutants in combination with the lentiviral MMB technique might be found in the area of angiogenic therapy. In a former study of us, SHP-2 phosphatase activity was demonstrated to be crucial for endothelial cell survival and vessel formation *in vivo* [76]. Thus, localized delivery and subsequent expression of SHP-2 E76A may be desired in the field of ischemic revascularization, while SHP-2 CS expression could hamper vascularisation and growth of tumours. Additionally, SHP-2 activity-related gene therapy could be useful in diabetic patients featuring insulin resistance, which are known to possess reduced wound healing capacity [49]. The application spectrum of the LV-

MMB method presented in this study are miscellaneous and go far beyond the here described delivery of functional SHP-2 mutants. However, by demonstrating its capacity to achieve efficient and physiological relevant gene transfer in whole vessels, a foundation for following *in vivo* studies was laid.

4.3 Vascular gene delivery of lentiviral vectors by magnetic and ultrasonic targeting of SO-Mag MMB *in vivo*

The methodical conjunction of microbubble mediated transport, magnetic accumulation and ultrasonic delivery is a promising concept for vascular gene delivery. The MMB technique presented in this study constitutes the realization of such a multimodal targeting approach. In two former studies of us, the PEI-Mag MMB could be shown to complex and deliver pDNA [40] and lentiviruses [41] to endothelial cells, whereby the actual *in vivo* applicability has only been demonstrated with pDNA-coupled MMB. However, vascular gene delivery using naked DNA vectors is known to result in rather low gene expression and has accordingly low physiological relevance. The combination of MMB with more effective genetic vectors, such as lentiviruses, was therefore an essential step for the advancement of the method towards its therapeutically relevant *in vivo* application. As described before, the newly established SO-Mag MMB were shown to possess functional advantages compared to formerly used PEI-Mag MMB allowing for effective gene transfer even to intact aortic endothelium. If the supremacy of lentiviral SO-Mag MMB persists under complex *in vivo* conditions was tested using the DSFC model in mice. By simultaneous MF and US application, arterial delivered lentiviral MMB were targeted to the microcirculatory bed of the dorsal skin. Indeed, local reporter gene expression (luciferase) in the dorsal skin was detected 8 days after the targeting procedure. In dorsal skins of mice without targeting, in contrast, reporter gene expression was completely absent highlighting the importance of MF and US application. The detection of absolute proviral genome insertions in the DSFC tissue confirmed this finding as lentiviral MMB targeting indeed resulted in significantly more proviral genome copies than no targeting. Except for the previous mentioned pDNA-MMB study [40], no comparable experimental strategy enabling this local delivery of genetic vectors from the systemic circulation by magnetic and ultrasonic targeting has been established so far. In other studies, relevant

vascular gene expression has only been achieved by local catheter-mediated delivery or direct tissue injection [6, 55, 64]. Furthermore, in advanced clinical studies, these methods mostly did not result in beneficial physiological effects most probably due to too low gene transfer rates [118]. Whether the lentiviral MMB technique indeed is capable to outperform these other methods in terms of gene expression and resulting physiological effects remains to be evaluated.

However, although lentiviral transduction could be successfully directed to the dorsal skin, unintended expression in other organs was also detected. Off-target reporter gene expression was thereby concentrated to the spleen and liver of mice. However, a reduced unspecific expression and proviral genome copy number in liver tissue of mice with US and MF targeting compared to mice without MMB targeting was detected. This finding may be accredited to a reduction of freely circulating MMB du to the local capturing at the site of MF and US application resulting in less unspecific liver expression. Interestingly, no luciferase activity could be detected in one of the other analyzed organs, such as lung or kidneys. The observed expression patterns after lentiviral MMB application mostly conform to results of others investigating the biodistribution of systemically injected viral particles [11, 119, 120]. However, in contrast to our study, they constantly found transgene expression to be higher in liver than in spleen. This is probably due to the chosen route of application, which was intra venous and intra peritoneal. Intra arterial injection of lentiviruses, as conducted here, may enhance the splenic off-target expression, as the MMB pass the spleen before passing the liver. Another hypothesis might be that the complexation of lentiviruses with MMB enhances the uptake of lentiviral particles by the spleen due to their erythrocyte-like structural features. However, as the main proportion of MNP shortly (1 h) after MMB administration was found to be located in liver and lung, an enhanced uptake of whole lentivirus-MMB complexes by the spleen seems rather unlikely.

Importantly, the further analysis of MNP distribution four days after MMB injection clearly revealed a fast and nearly complete clearance of administered MNP from the body. Whether this clearance occurs via hepatic or renal excretion or via biotransformation of the iron-oxide nanoparticles and subsequent uptake to the endogenous iron metabolism remains to be determined. This fast elimination as well as the low MNP cytotoxicity attested *in vitro* strongly indicates the MMB technique as a biocompatible gene delivery approach. Moreover, with an iron dose of 1 µg Fe/g body weight, the here presented MMB technique requires about 100-1000-fold less MNP amount than have been used by other groups aiming *in vivo* gene targeting by MNP [121]. In a study investigating the liver toxicity

in mice after acute injection of iron-dextran, no notable increase in lipid peroxidation was detected up to a dose of 50 µg/g body weight [122]. However, to estimate the risk of an iron overload and associated severe organ failure resulting from enhanced ROS production, more specific studies regarding hepatic iron concentrations and oxidative stress upon MMB injection need to be done. In healthy individuals, hepatic iron concentrations are approximately 36 µmol/g liver dry weight (2 mg/g). Hepatic iron overload and accordingly organ damages are estimated to occur at a threshold of > 80 µmol/g liver dry weight (4 mg/g) [123]. However, these levels may only be reached upon chronic administration of exogenous iron, as it is necessary in patients requiring long-term blood transfusions.

4.4 Therapeutic potential and future perspectives

In most cases, long-term treatment of cardiovascular diseases requires repeated and continuous drug intake by the patient to sustain the therapeutic drug level. The appearance of associated side effects not only results from systemic drug application but can also be assigned to unspecific off-target actions of the drug. Furthermore, systemic delivery oftentimes impedes the actual beneficial effects of a therapeutic agent as the necessary concentrations at the site of intervention cannot be reached.

The elucidation of molecular and genetic causes of cardiovascular diseases progresses rapidly and opens new possibilities for more specific and personalized treatment strategies. In this regard, gene therapeutic approaches gain more and more attention. However, their application is still hampered due to the lack of efficient and targetable gene delivery methods. The here presented lentiviral MMB technique represents a promising step towards such a gene targeting approach for the vascular system. The ability to direct and accumulate lentiviral vectors, which are known for their efficient gene transfer and stable transgene expression, may allow for the specific over-expression, knock out, or replacement of virtually any gene. As the method currently is restricted to endothelial gene therapy, molecular targets involved in endothelial specific pathological processes are of particular interest.

One highly interesting therapeutic molecule in this context, the vascular endothelial growth factor (VEGF), has been regarded in this work. The research field of VEGF-based therapies is highly active due to its central relevance in angiogenesis-related disorders. The

treatment of ischemic diseases, such as myocardial infarction and limb ischemia, as well as diseases associating a hyperangiogenic vasculature, such as tumours, might be revolutionized by the application of lentiviral MMB gene delivery. That the MMB in principle can be applied for VEGF-based therapy has been proven in this study where the local transduction of aortic endothelial cells indeed resulted in angiogenic responses. Reversely, the delivery of VEGF knock out constructs to tumour vasculature by the MMB technique might be especially valuable to restrict tumour progression and metastasis. Apart from this, the further spectrum of application is huge and includes localized modifications of relevant gene expression in for example atherosclerotic lesions as well as vascular regions prone to thrombotic and inflammatory complications.

However, there is still a long way to go before the lentiviral MMB technique might be considered for actual clinical application. Technical limitations, including the set up of strong magnetic fields capable to specifically focus on a desired site of exposure and reach deeper tissue regions, need to be overcome. Furthermore, more data concerning actual transgene expression over several months need to be provided to prove the actual long-term efficiency of the method. And also off-target expression and related potential complications need to be addressed in more detail.

Altogether, the here presented study provides a first fundament for the further optimization of the lentiviral MMB technique towards various possible applications in clinical gene therapy.

4.5 Limitations of the study and outlook

Lentiviral MMB were successfully applied *in vivo* to achieve local gene expression by combined magnetic and ultrasonic targeting. However, the study involved also certain technical limitations, which need to be considered for the accurate interpretation of the obtained results.

The microvascular bed of the dorsal skin of mice, which was exposed by implantation of the DSFC, was the region of interest to which the lentiviral gene delivery was directed. This model was chosen due to several reasons: (1) the possibility to allow for long-term microscopic imaging of the vasculature in living animals, (2) its good accessibility from

both sides during the transduction procedure and (3) its thin structure which allows for highest magnetic and ultrasonic penetrance. These factors make the DSFC an ideal model for the purpose to validate the method and conduct first experimental studies of certain molecules of interest. However, the actual tissue penetrance and applicability in deeper and larger vessels cannot be addressed by this model. To allow for effective gene transfer also in a deeper vascular network to treat for example hindlimb ischemia, a different magnet and ultrasound set up might be necessary. Furthermore, the DSFC model allows a follow up of gene expression only over 12-14 days as the resolution quality in the observation window decreases over time due to tissue remodelling and inflammatory processes. Also the welfare of mice cannot be guaranteed for a longer time period as the implanted chamber may cause skin lesions. For studies involving the assessment of gene expression over weeks to month another model has to be chosen. Interesting in this regard would be for example the non invasive targeting of the hindlimb vasculature also in view of later revascularization studies.

In line with this latter point comes the problem of magnetically attracting lentiviral MMB also in vessels of deeper body regions, such as coronary arteries or limbs. The strength of a magnetic field, the so called magnetic flux density, strongly decreases with increasing distance to the magnet tip [124]. While the magnetic attraction of lentiviral MMB to superficial vascular beds *in vivo* in principle should be no problem, deeper regions may be more complicated. First trials to circumvent this problem included the implantation of magnets [125] and magnetic field enhancing elements (FEE) [126] close to the intended site of gene transfer. Latter might be of particular interest for the treatment or prevention of stent restenosis, as such FEE can be designed in form of stents. The invasive implantation procedure may be easily performed in patients requiring a stent implantation anyway. The applicability is, however, very restricted to these patients with risk for stent restenosis. In a similar manner magnetisable orthopaedic implants could be used to specifically attract MNP-coupled genes or drugs to the sites of implantation resulting in improved engraftment. However, in general a more reasonable alternative to this invasive procedure can only be created by the technical advancements of magnetic fields by close interdisciplinary collaboration of physicists and biophysicians.

Due to time limitations, the effects of modifications of the lentiviral vectors on gene targeting efficiency and circulation time have not been addressed in this study. Others

showed that the chemical coating of viral particles can yield so called shielding effects resulting in less interactions with antibodies and accordingly higher circulation times [127, 128]. In combination with the MMB technique it would be interesting to see if lentivirus shielding may result in a higher targeting efficiency or an altered off-target expression pattern. However, such surface modifications also require the careful re-evaluation of lentivirus-MMB complexation and *in vitro* performance, which will be object of future studies. Another interesting point would be to test if the unspecific expression observed in spleen and liver could be reduced using an endothelial specific promoter instead of the CMV promoter. We assume that the strong luciferase signal observed in the spleen rather results from resident immune cells than from endothelial cells. Endothelium specific promoters, such as the VE-cadherin promoter [129], could yield a higher specificity and reduce ectopic transgene expression thereby substantially reducing potential side effects. However, it has also been shown that transgene expression driven by tissue-specific promoters is oftentimes strongly reduced compared to the original viral promoters [2]. Therefore, the actual pros and cons of such vector modifications need to be considered carefully.

The effective and solid transgene expression of lentiviruses represents one of the major advantages of these vectors in experimental gene delivery. However, for most gene therapeutic applications only a temporary transgene expression is required. Over-expression of VEGF, for example, may initially have beneficial effects for the revascularization and tissue regeneration in ischemic regions. However, long-term over-expression of VEGF have been shown to result in myocardial failure and even tumour development [130, 131]. To eliminate such risks, the use of lentiviral vectors with inducible transgene expression would be desirable. One promising approach in this regard is the Tet-dependent expression system which is already widely applied as genetic tool in scientific research [132, 133]. In combination with MMB-mediated gene targeting, such inducible gene expression vectors may have an enormous potential for clinical gene therapy enabling spatial as well as temporal control of gene expression.

In terms of biocompatibility and safety of the lentiviral MMB technique further long-term studies need to be performed. The exact mechanism of excretion for the applied MNP has not been investigated in this study. Therefore, it is not clear if the MNP are eliminated by liver and kidney or if biotransformation resulted in complete uptake of the iron-oxide

components to the endogenous iron metabolism of the mice. Also the long-term profile of transgene expression has not been assessed so far. Expression in the dorsal skin as well as the other organs has been monitored 8 days after the transduction procedure. Although lentiviral expression is assumed to sustain over time due to stable genome integration it would be very interesting to see if the systemic expression profile changes over several month, especially in immunological active organs such as the spleen. Furthermore, the analysis of genome copy numbers integrated to the vasculature of the dorsal skin tissue could give more detailed information about the actual effectivity of the lentiviral MMB targeting approach and may help to improve the procedure.

The therapeutic applicability of the lentiviral MMB technique was demonstrated by targeted delivery of VEGF and SHP-2 over-expression constructs *ex vivo*. By modulating the expression of both these proteins in the endothelium of isolated mouse aortas physiologically relevant effects could be detected. However, to completely verify the scientific and clinical potential of the MMB technique, *in vivo* experiments aiming at the modulation of therapeutically interesting molecules, such as the addressed VEGF or SHP-2, need to be done. The DSFC model is well suited for these purposes as its microvascular bed offers microscopic access over several days. By this, angiogenesis-related studies can be excellently performed using the so called wound healing assay. Thereby, wound closure in the dorsal skin is monitored over several days by repeated injection of the fluorescent dye FITC-dextran allowing for visualization of the vascular network in the observation window of the DSFC. Also for the analysis of inflammatory processes, such as leukocyte adhesion and extravasation as well as vascular permeability, the DSFC model can be used. Furthermore, the use of transgenic animals in combination with the MMB technique may be highly interesting. For example, the observed anti-inflammatory properties of constitutively active SHP-2 E76A could be nicely verified in a diabetic mouse model, such as the established Lep^{ob} mouse strain. Furthermore, such a diabetic mouse model would be highly interesting in terms of gene therapeutic treatment of impaired diabetic wound healing, for example by targeted VEGF over-expression.

5 Summary

In the clinical field of gene therapy, intravascularly applied targeting systems are promising advancements to improve specificity of a gene transfer. Magnetic microbubbles (MMB) combine the beneficial properties of magnetic nanoparticles (MNP) with those of ultrasound-sensitive lipid microbubbles and have been shown to effectively bind different genetic vectors, including lentiviruses. The magnetic characteristics of these MMB are thereby determined by the choice of MNP embedded in the lipid shell. Furthermore, size, binding capacity and toxicity are decisive factors for the applicability and effectiveness of this gene delivery system.

In this study, we characterized and compared different physico-chemical as well as biological properties of MMB coupled to silicon-oxide coated MNP (SO-Mag MMB) or polyethylenimine coated MNP (PEI-Mag MMB). While no differences between both MMB types were found concerning size, lentivirus binding, and toxicity, SO-Mag MMB exhibited superior characteristics regarding magnetic moment, magnetizability as well as transduction efficiency under static and flow conditions *in vitro*.

By evaluating the contribution of the single technical parameter of the MMB technique we found MF exposure to be most critical under static conditions as well as under flow. Despite the observation that sole US exposure to lentiviral MMB did not enhance gene transfer to endothelial cells, we could demonstrate it to considerably contribute to the complete transduction efficiency of the whole MMB technique.

By using lentiviral SO-Mag MMB, we achieved localized gene delivery to endothelial cells in an *ex vivo* perfusion model of murine aortas. Thus, we were able to utilize the new lentiviral SO-Mag MMB *ex vivo* to achieve site-directed over-expression of a lentiviral human VEGF construct resulting in actual VEGF secretion and induction of a proangiogenic phenotype in these vessels.

With the same *ex vivo* model we were furthermore able to verify new compelling *in vitro* data concerning the role of the tyrosine phosphatase SHP-2 during vascular inflammation in insulin resistant endothelium. There, we could show that in untreated endothelial cells, SHP-2 exhibits a basal phosphatase activity, which is lacking under insulin resistance conditions. The resulting hypothesis that SHP-2 phosphatase activity may negatively regulate endothelial inflammation was further supported by the finding that over-expression of a dominant negative SHP-2 mutant (CS) resulted in enhanced expression of the adhesion molecules ICAM-1 and VCAM-1 in insulin resistant endothelial cells. Accordingly, cells over-

expressing a constitutively active SHP-2 mutant (E76A) showed a less inflammatory phenotype. Finally, we were able to confirm these findings *ex vivo* by using the lentiviral MMB technique to over-express the SHP-2 phosphatase mutants in the endothelial layer of isolated mouse aortas. In accordance with the *in vitro* data, ICAM-1 and VCAM-1 expression in these vessels was either enhanced or reduced under SHP-2 CS or E76A over-expression, respectively. These findings not only demonstrate SHP-2 to be a negative regulator of endothelial inflammation evolving under diabetic conditions, but also suggest SHP-2 as a new potential therapeutic target in this pathologic context.

Lastly, we were able to prove the actual functionality of our MMB technique *in vivo*. After systemic injection of lentiviral SO-Mag MMB site-specific gene transfer was realized by local application of MF and US to the microvascular bed of the mouse dorsal skin. Interestingly, the contained MNP were nearly completely cleared from the body within four days indicating good compatibility of the method. In summary these achievements demonstrate that the lentiviral MMB technique as a valuable method for scientific applications and may be of substantial interest for future gene therapies.

6 References

1. Webster DM, Sundaram P, Byrne ME. Injectable nanomaterials for drug delivery: Carriers, targeting moieties, and therapeutics. *European journal of pharmaceutics and biopharmaceutics : official journal of Arbeitsgemeinschaft fur Pharmazeutische Verfahrenstechnik e.V*. 2013;84:1-20
2. Rincon MY, VandenDriessche T, Chuah MK. Gene therapy for cardiovascular disease: Advances in vector development, targeting, and delivery for clinical translation. *Cardiovasc Res*. 2015;108:4-20
3. Yin H, Kanasty RL, Eltoukhy AA, Vegas AJ, Dorkin JR, Anderson DG. Non-viral vectors for gene-based therapy. *Nature reviews. Genetics*. 2014;15:541-555
4. Laakkonen JP, Yla-Herttuala S. Recent advancements in cardiovascular gene therapy and vascular biology. *Hum Gene Ther*. 2015;26:518-524
5. Buchschacher GL, Jr., Wong-Staal F. Development of lentiviral vectors for gene therapy for human diseases. *Blood*. 2000;95:2499-2504
6. Giacca M, Zacchigna S. Virus-mediated gene delivery for human gene therapy. *Journal of controlled release : official journal of the Controlled Release Society*. 2012;161:377-388
7. Kotterman MA, Chalberg TW, Schaffer DV. Viral vectors for gene therapy: Translational and clinical outlook. *Annual review of biomedical engineering*. 2015;17:63-89
8. Vassalli G, Bueler H, Dudler J, von Segesser LK, Kappenberger L. Adeno-associated virus (aav) vectors achieve prolonged transgene expression in mouse myocardium and arteries in vivo: A comparative study with adenovirus vectors. *Int J Cardiol*. 2003;90:229-238
9. Hammoudi N, Ishikawa K, Hajjar RJ. Adeno-associated virus-mediated gene therapy in cardiovascular disease. *Current opinion in cardiology*. 2015;30:228-234
10. Chu D, Sullivan CC, Weitzman MD, Du L, Wolf PL, Jamieson SW, Thistlethwaite PA. Direct comparison of efficiency and stability of gene transfer into the mammalian heart using adeno-associated virus versus adenovirus vectors. *J Thorac Cardiovasc Surg*. 2003;126:671-679
11. Gonin P, Gaillard C. Gene transfer vector biodistribution: Pivotal safety studies in clinical gene therapy development. *Gene therapy*. 2004;11 Suppl 1:S98-s108
12. Vigna E, Naldini L. Lentiviral vectors: Excellent tools for experimental gene transfer and promising candidates for gene therapy. *The journal of gene medicine*. 2000;2:308-316
13. Escors D, Breckpot K. Lentiviral vectors in gene therapy: Their current status and future potential. *Archivum immunologiae et therapiae experimentalis*. 2010;58:107-119
14. Cavazzana-Calvo M, Payen E, Negre O, Wang G, Hehir K, Fusil F, Down J, Denaro M, Brady T, Westerman K, Cavallesco R, Gillet-Legrand B, Caccavelli L, Sgarra R, Maouche-Chretien L, Bernaudin F, Girot R, Dorazio R, Mulder GJ, Polack A, Bank A, Soulier J, Larghero J, Kabbara N, Dalle B, Gourmel B, Socie G, Chretien S, Cartier N, Aubourg P, Fischer A, Cornetta K, Galacteros F, Beuzard Y, Gluckman E, Bushman F, Hacein-Bey-Abina S, Leboulch P. Transfusion independence and hmga2 activation after gene therapy of human beta-thalassaemia. *Nature*. 2010;467:318-322
15. Cartier N, Aubourg P. Hematopoietic stem cell transplantation and hematopoietic stem cell gene therapy in x-linked adrenoleukodystrophy. *Brain pathology (Zurich, Switzerland)*. 2010;20:857-862
16. Aiuti A, Biasco L, Scaramuzza S, Ferrua F, Cicalese MP, Baricordi C, Dionisio F,

Calabria A, Giannelli S, Castiello MC, Bosticardo M, Evangelio C, Assanelli A, Casiraghi M, Di Nunzio S, Callegaro L, Benati C, Rizzardi P, Pellin D, Di Serio C, Schmidt M, Von Kalle C, Gardner J, Mehta N, Neduva V, Dow DJ, Galy A, Miniero R, Finocchi A, Metin A, Banerjee PP, Orange JS, Galimberti S, Valsecchi MG, Biffi A, Montini E, Villa A, Ciceri F, Roncarolo MG, Naldini L. Lentiviral hematopoietic stem cell gene therapy in patients with wiskott-aldrich syndrome. *Science (New York, N.Y.)*. 2013;341:1233151

17. Jazwa A, Florczyk U, Jozkowicz A, Dulak J. Gene therapy on demand: Site specific regulation of gene therapy. *Gene*. 2013;525:229-238
18. Lawrie A, Brisken AF, Francis SE, Cumberland DC, Crossman DC, Newman CM. Microbubble-enhanced ultrasound for vascular gene delivery. *Gene therapy*. 2000;7:2023-2027
19. Laurent S, Saei AA, Behzadi S, Panahifar A, Mahmoudi M. Superparamagnetic iron oxide nanoparticles for delivery of therapeutic agents: Opportunities and challenges. *Expert opinion on drug delivery*. 2014;11:1449-1470
20. Feinstein SB. The powerful microbubble: From bench to bedside, from intravascular indicator to therapeutic delivery system, and beyond. *American journal of physiology. Heart and circulatory physiology*. 2004;287:H450-457
21. Lindner JR, Kaul S. Delivery of drugs with ultrasound. *Echocardiography (Mount Kisco, N.Y.)*. 2001;18:329-337
22. Sirsi S, Borden M. Microbubble compositions, properties and biomedical applications. *Bubble Sci Eng Technol*. 2009;1:3-17
23. Qin S, Caskey CF, Ferrara KW. Ultrasound contrast microbubbles in imaging and therapy: Physical principles and engineering. *Physics in medicine and biology*. 2009;54:R27-57
24. Bekeredjian R, Grayburn PA, Shohet RV. Use of ultrasound contrast agents for gene or drug delivery in cardiovascular medicine. *Journal of the American College of Cardiology*. 2005;45:329-335
25. Meijering BD, Juffermans LJ, van Wamel A, Henning RH, Zuhorn IS, Emmer M, Versteilen AM, Paulus WJ, van Gilst WH, Kooiman K, de Jong N, Musters RJ, Deelman LE, Kamp O. Ultrasound and microbubble-targeted delivery of macromolecules is regulated by induction of endocytosis and pore formation. *Circulation research*. 2009;104:679-687
26. Lammers T, Kiessling F, Hennink WE, Storm G. Drug targeting to tumors: Principles, pitfalls and (pre-) clinical progress. *Journal of controlled release : official journal of the Controlled Release Society*. 2012;161:175-187
27. Laurent S, Forge D, Port M, Roch A, Robic C, Vander Elst L, Muller RN. Magnetic iron oxide nanoparticles: Synthesis, stabilization, vectorization, physicochemical characterizations, and biological applications. *Chemical reviews*. 2008;108:2064-2110
28. Silva AC, Oliveira TR, Mamani JB, Malheiros SM, Malavolta L, Pavon LF, Sibov TT, Amaro E, Jr., Tannus A, Vidoto EL, Martins MJ, Santos RS, Gamarra LF. Application of hyperthermia induced by superparamagnetic iron oxide nanoparticles in glioma treatment. *International journal of nanomedicine*. 2011;6:591-603
29. Anzai Y, Piccoli CW, Outwater EK, Stanford W, Bluemke DA, Nurenberg P, Saini S, Maravilla KR, Feldman DE, Schmiedl UP, Brunberg JA, Francis IR, Harms SE, Som PM, Tempany CM. Evaluation of neck and body metastases to nodes with ferumoxtran 10-enhanced mr imaging: Phase iii safety and efficacy study. *Radiology*. 2003;228:777-788
30. Thoeny HC, Triantafyllou M, Birkhaeuser FD, Froehlich JM, Tshering DW, Binser T, Fleischmann A, Vermathen P, Studer UE. Combined ultrasmall superparamagnetic particles of iron oxide-enhanced and diffusion-weighted magnetic resonance imaging

reliably detect pelvic lymph node metastases in normal-sized nodes of bladder and prostate cancer patients. *European urology*. 2009;55:761-769
31. He X, Nie H, Wang K, Tan W, Wu X, Zhang P. In vivo study of biodistribution and urinary excretion of surface-modified silica nanoparticles. *Anal Chem*. 2008;80:9597-9603
32. Krotz F, de Wit C, Sohn HY, Zahler S, Gloe T, Pohl U, Plank C. Magnetofection--a highly efficient tool for antisense oligonucleotide delivery in vitro and in vivo. *Molecular therapy : the journal of the American Society of Gene Therapy*. 2003;7:700-710
33. Huth S, Lausier J, Gersting SW, Rudolph C, Plank C, Welsch U, Rosenecker J. Insights into the mechanism of magnetofection using pei-based magnetofectins for gene transfer. *The journal of gene medicine*. 2004;6:923-936
34. Mykhaylyk O, Antequera YS, Vlaskou D, Plank C. Generation of magnetic nonviral gene transfer agents and magnetofection in vitro. *Nature protocols*. 2007;2:2391-2411
35. Rieck S, Zimmermann K, Wenzel D. Transduction of murine embryonic stem cells by magnetic nanoparticle-assisted lentiviral gene transfer. *Methods in molecular biology (Clifton, N.J.)*. 2013;1058:89-96
36. Almstatter I, Mykhaylyk O, Settles M, Altomonte J, Aichler M, Walch A, Rummeny EJ, Ebert O, Plank C, Braren R. Characterization of magnetic viral complexes for targeted delivery in oncology. *Theranostics*. 2015;5:667-685
37. Wang K, Kievit FM, Sham JG, Jeon M, Stephen ZR, Bakthavatsalam A, Park JO, Zhang M. Iron-oxide-based nanovector for tumor targeted sirna delivery in an orthotopic hepatocellular carcinoma xenograft mouse model. *Small (Weinheim an der Bergstrasse, Germany)*. 2016;12:477-487
38. Yang F, Li Y, Chen Z, Zhang Y, Wu J, Gu N. Superparamagnetic iron oxide nanoparticle-embedded encapsulated microbubbles as dual contrast agents of magnetic resonance and ultrasound imaging. *Biomaterials*. 2009;30:3882-3890
39. Song S, Guo H, Jiang Z, Jin Y, Wu Y, An X, Zhang Z, Sun K, Dou H. Self-assembled microbubbles as contrast agents for ultrasound/magnetic resonance dual-modality imaging. *Acta Biomater*. 2015;24:266-278
40. Mannell H, Pircher J, Fochler F, Stampnik Y, Rathel T, Gleich B, Plank C, Mykhaylyk O, Dahmani C, Wornle M, Ribeiro A, Pohl U, Krotz F. Site directed vascular gene delivery in vivo by ultrasonic destruction of magnetic nanoparticle coated microbubbles. *Nanomedicine : nanotechnology, biology, and medicine*. 2012;8:1309-1318
41. Mannell H, Pircher J, Rathel T, Schilberg K, Zimmermann K, Pfeifer A, Mykhaylyk O, Gleich B, Pohl U, Krotz F. Targeted endothelial gene delivery by ultrasonic destruction of magnetic microbubbles carrying lentiviral vectors. *Pharmaceutical research*. 2012;29:1282-1294
42. Owen J, Rademeyer P, Chung D, Cheng Q, Holroyd D, Coussios C, Friend P, Pankhurst QA, Stride E. Magnetic targeting of microbubbles against physiologically relevant flow conditions. *Interface focus*. 2015;5:20150001
43. Cines DB, Pollak ES, Buck CA, Loscalzo J, Zimmerman GA, McEver RP, Pober JS, Wick TM, Konkle BA, Schwartz BS, Barnathan ES, McCrae KR, Hug BA, Schmidt AM, Stern DM. Endothelial cells in physiology and in the pathophysiology of vascular disorders. *Blood*. 1998;91:3527-3561
44. Galley HF, Webster NR. Physiology of the endothelium. *British journal of anaesthesia*. 2004;93:105-113
45. Muniyappa R, Sowers JR. Role of insulin resistance in endothelial dysfunction. *Rev Endocr Metab Disord*. 2013;14:5-12
46. Johnson Andrew MF, Olefsky Jerrold M. The origins and drivers of insulin resistance.

Cell. 2013;152:673-684
47. Vazzana N, Ranalli P, Cuccurullo C, Davi G. Diabetes mellitus and thrombosis. *Thrombosis research*. 2012;129:371-377
48. Rosenberg CS. Wound healing in the patient with diabetes mellitus. *The Nursing clinics of North America*. 1990;25:247-261
49. Brem H, Tomic-Canic M. Cellular and molecular basis of wound healing in diabetes. *The Journal of clinical investigation*. 2007;117:1219-1222
50. Carmeliet P, Jain RK. Molecular mechanisms and clinical applications of angiogenesis. *Nature*. 2011;473:298-307
51. Carmeliet P. Angiogenesis in life, disease and medicine. *Nature*. 2005;438:932-936
52. Ferrara N, Kerbel RS. Angiogenesis as a therapeutic target. *Nature*. 2005;438:967-974
53. Ferrara N, Gerber HP, LeCouter J. The biology of vegf and its receptors. *Nature medicine*. 2003;9:669-676
54. Grochot-Przeczek A, Dulak J, Jozkowicz A. Therapeutic angiogenesis for revascularization in peripheral artery disease. *Gene*. 2013;525:220-228
55. Yla-Herttuala S. Cardiovascular gene therapy with vascular endothelial growth factors. *Gene*. 2013;525:217-219
56. Ellis LM, Hicklin DJ. Vegf-targeted therapy: Mechanisms of anti-tumour activity. *Nature reviews. Cancer*. 2008;8:579-591
57. Dai Q, Huang J, Klitzman B, Dong C, Goldschmidt-Clermont PJ, March KL, Rokovich J, Johnstone B, Rebar EJ, Spratt SK, Case CC, Kontos CD, Annex BH. Engineered zinc finger-activating vascular endothelial growth factor transcription factor plasmid DNA induces therapeutic angiogenesis in rabbits with hindlimb ischemia. *Circulation*. 2004;110:2467-2475
58. Lahteenvuo JE, Lahteenvuo MT, Kivela A, Rosenlew C, Falkevall A, Klar J, Heikura T, Rissanen TT, Vahakangas E, Korpisalo P, Enholm B, Carmeliet P, Alitalo K, Eriksson U, Yla-Herttuala S. Vascular endothelial growth factor-b induces myocardium-specific angiogenesis and arteriogenesis via vascular endothelial growth factor receptor-1- and neuropilin receptor-1-dependent mechanisms. *Circulation*. 2009;119:845-856
59. Kastrup J, Jorgensen E, Ruck A, Tagil K, Glogar D, Ruzyllo W, Botker HE, Dudek D, Drvota V, Hesse B, Thuesen L, Blomberg P, Gyongyosi M, Sylven C. Direct intramyocardial plasmid vascular endothelial growth factor-a165 gene therapy in patients with stable severe angina pectoris a randomized double-blind placebo-controlled study: The euroinject one trial. *Journal of the American College of Cardiology*. 2005;45:982-988
60. Stewart DJ, Kutryk MJ, Fitchett D, Freeman M, Camack N, Su Y, Della Siega A, Bilodeau L, Burton JR, Proulx G, Radhakrishnan S. Vegf gene therapy fails to improve perfusion of ischemic myocardium in patients with advanced coronary disease: Results of the northern trial. *Molecular therapy : the journal of the American Society of Gene Therapy*. 2009;17:1109-1115
61. Favaloro L, Diez M, Mendiz O, Janavel GV, Valdivieso L, Ratto R, Garelli G, Salmo F, Criscuolo M, Bercovich A, Crottogini A. High-dose plasmid-mediated vegf gene transfer is safe in patients with severe ischemic heart disease (genesis-i). A phase i, open-label, two-year follow-up trial. *Catheterization and cardiovascular interventions : official journal of the Society for Cardiac Angiography & Interventions*. 2013;82:899-906
62. Rajagopalan S, Mohler E, 3rd, Lederman RJ, Saucedo J, Mendelsohn FO, Olin J, Blebea J, Goldman C, Trachtenberg JD, Pressler M, Rasmussen H, Annex BH, Hirsch AT. Regional angiogenesis with vascular endothelial growth factor (vegf) in peripheral arterial disease: Design of the rave trial. *American heart journal*.

2003;145:1114-1118
63. Stewart DJ, Hilton JD, Arnold JM, Gregoire J, Rivard A, Archer SL, Charbonneau F, Cohen E, Curtis M, Buller CE, Mendelsohn FO, Dib N, Page P, Ducas J, Plante S, Sullivan J, Macko J, Rasmussen C, Kessler PD, Rasmussen HS. Angiogenic gene therapy in patients with nonrevascularizable ischemic heart disease: A phase 2 randomized, controlled trial of advegf(121) (advegf121) versus maximum medical treatment. *Gene therapy*. 2006;13:1503-1511
64. Makinen K, Manninen H, Hedman M, Matsi P, Mussalo H, Alhava E, Yla-Herttuala S. Increased vascularity detected by digital subtraction angiography after vegf gene transfer to human lower limb artery: A randomized, placebo-controlled, double-blinded phase ii study. *Molecular therapy : the journal of the American Society of Gene Therapy*. 2002;6:127-133
65. Giacca M, Zacchigna S. Vegf gene therapy: Therapeutic angiogenesis in the clinic and beyond. *Gene therapy*. 2012;19:622-629
66. Mannell H, Krotz F. Shp-2 regulates growth factor dependent vascular signalling and function. *Mini reviews in medicinal chemistry*. 2012
67. Chong ZZ, Maiese K. The src homology 2 domain tyrosine phosphatases shp-1 and shp-2: Diversified control of cell growth, inflammation, and injury. *Histology and histopathology*. 2007;22:1251-1267
68. Maegawa H, Hasegawa M, Sugai S, Obata T, Ugi S, Morino K, Egawa K, Fujita T, Sakamoto T, Nishio Y, Kojima H, Haneda M, Yasuda H, Kikkawa R, Kashiwagi A. Expression of a dominant negative shp-2 in transgenic mice induces insulin resistance. *The Journal of biological chemistry*. 1999;274:30236-30243
69. Hsu MF, Meng TC. Enhancement of insulin responsiveness by nitric oxide-mediated inactivation of protein-tyrosine phosphatases. *The Journal of biological chemistry*. 2010;285:7919-7928
70. Coulombe G, Leblanc C, Cagnol S, Maloum F, Lemieux E, Perreault N, Feng GS, Boudreau F, Rivard N. Epithelial tyrosine phosphatase shp-2 protects against intestinal inflammation in mice. *Molecular and cellular biology*. 2013;33:2275-2284
71. Wang YC, Chen CL, Sheu BS, Yang YJ, Tseng PC, Hsieh CY, Lin CF. Helicobacter pylori infection activates src homology-2 domain-containing phosphatase 2 to suppress ifn-gamma signaling. *Journal of immunology (Baltimore, Md. : 1950)*. 2014;193:4149-4158
72. Giri H, Muthuramu I, Dhar M, Rathnakumar K, Ram U, Dixit M. Protein tyrosine phosphatase shp2 mediates chronic insulin-induced endothelial inflammation. *Arteriosclerosis, thrombosis, and vascular biology*. 2012;32:1943-1950
73. Dixit M, Zhuang D, Ceacareanu B, Hassid A. Treatment with insulin uncovers the motogenic capacity of nitric oxide in aortic smooth muscle cells: Dependence on gab1 and gab1-shp2 association. *Circulation research*. 2003;93:e113-123
74. Chang Y, Ceacareanu B, Dixit M, Sreejayan N, Hassid A. Nitric oxide-induced motility in aortic smooth muscle cells: Role of protein tyrosine phosphatase shp-2 and gtp-binding protein rho. *Circulation research*. 2002;91:390-397
75. Zhu JX, Cao G, Williams JT, Delisser HM. Shp-2 phosphatase activity is required for pecam-1-dependent cell motility. *Am J Physiol Cell Physiol*. 2010;299:C854-865
76. Mannell H, Hellwig N, Gloe T, Plank C, Sohn HY, Groesser L, Walzog B, Pohl U, Krotz F. Inhibition of the tyrosine phosphatase shp-2 suppresses angiogenesis in vitro and in vivo. *Journal of vascular research*. 2008;45:153-163
77. Lerner-Marmarosh N, Yoshizumi M, Che W, Surapisitchat J, Kawakatsu H, Akaike M, Ding B, Huang Q, Yan C, Berk BC, Abe J. Inhibition of tumor necrosis factor-[alpha]-induced shp-2 phosphatase activity by shear stress: A mechanism to reduce endothelial inflammation. *Arteriosclerosis, thrombosis, and vascular biology*.

2003;23:1775-1781
78. Dixit M, Loot AE, Mohamed A, Fisslthaler B, Boulanger CM, Ceacareanu B, Hassid A, Busse R, Fleming I. Gab1, shp2, and protein kinase a are crucial for the activation of the endothelial no synthase by fluid shear stress. *Circulation research*. 2005;97:1236-1244
79. Kontaridis MI, Liu X, Zhang L, Bennett AM. Role of shp-2 in fibroblast growth factor receptor-mediated suppression of myogenesis in c2c12 myoblasts. *Molecular and cellular biology*. 2002;22:3875-3891
80. Lampe M, Briggs JA, Endress T, Glass B, Riegelsberger S, Krausslich HG, Lamb DC, Brauchle C, Muller B. Double-labelled hiv-1 particles for study of virus-cell interaction. *Virology*. 2007;360:92-104
81. Hofmann A, Wenzel D, Becher UM, Freitag DF, Klein AM, Eberbeck D, Schulte M, Zimmermann K, Bergemann C, Gleich B, Roell W, Weyh T, Trahms L, Nickenig G, Fleischmann BK, Pfeifer A. Combined targeting of lentiviral vectors and positioning of transduced cells by magnetic nanoparticles. *Proceedings of the National Academy of Sciences of the United States of America*. 2009;106:44-49
82. Trueck C, Zimmermann K, Mykhaylyk O, Anton M, Vosen S, Wenzel D, Fleischmann BK, Pfeifer A. Optimization of magnetic nanoparticle-assisted lentiviral gene transfer. *Pharmaceutical research*. 2012;29:1255-1269
83. Mykhaylyk O, Sanchez-Antequera Y, Vlaskou D, Hammerschmid E, Anton M, Zelphati O, Plank C. Liposomal magnetofection. *Methods in molecular biology (Clifton, N.J.)*. 2010;605:487-525
84. Mykhaylyk O, Sobisch T, Almstatter I, Sanchez-Antequera Y, Brandt S, Anton M, Doblinger M, Eberbeck D, Settles M, Braren R, Lerche D, Plank C. Silica-iron oxide magnetic nanoparticles modified for gene delivery: A search for optimum and quantitative criteria. *Pharmaceutical research*. 2012;29:1344-1365
85. Heidsieck A. Simple two-dimensional object tracking based on a graph algorithm. *arXiv:1412.1216*. 2014
86. Rodal SK, Skretting G, Garred O, Vilhardt F, van Deurs B, Sandvig K. Extraction of cholesterol with methyl-beta-cyclodextrin perturbs formation of clathrin-coated endocytic vesicles. *Molecular biology of the cell*. 1999;10:961-974
87. Hart PD, Young MR. Ammonium chloride, an inhibitor of phagosome-lysosome fusion in macrophages, concurrently induces phagosome-endosome fusion, and opens a novel pathway: Studies of a pathogenic mycobacterium and a nonpathogenic yeast. *The Journal of experimental medicine*. 1991;174:881-889
88. Hussain KM, Leong KL, Ng MM, Chu JJ. The essential role of clathrin-mediated endocytosis in the infectious entry of human enterovirus 71. *The Journal of biological chemistry*. 2011;286:309-321
89. Mercan F, Bennett AM. Analysis of protein tyrosine phosphatases and substrates. *Current protocols in molecular biology / edited by Frederick M. Ausubel ... [et al.]*. 2010;Chapter 18:Unit 18 16
90. Menger MD, Laschke MW, Vollmar B. Viewing the microcirculation through the window: Some twenty years experience with the hamster dorsal skinfold chamber. *European surgical research. Europaische chirurgische Forschung. Recherches chirurgicales europeennes*. 2002;34:83-91
91. Wenzel D, Rieck S, Vosen S, Mykhaylyk O, Trueck C, Eberbeck D, Trahms L, Zimmermann K, Pfeifer A, Fleischmann BK. Identification of magnetic nanoparticles for combined positioning and lentiviral transduction of endothelial cells. *Pharmaceutical research*. 2012;29:1242-1254
92. Farese RV, Sajan MP, Standaert ML. Insulin-sensitive protein kinases (atypical protein kinase c and protein kinase b/akt): Actions and defects in obesity and type ii

diabetes. *Experimental biology and medicine (Maywood, N.J.)*. 2005;230:593-605
93. Nelson BA, Robinson KA, Buse MG. Defective akt activation is associated with glucose- but not glucosamine-induced insulin resistance. *American journal of physiology. Endocrinology and metabolism*. 2002;282:E497-506
94. Krotz F, Sohn HY, Gloe T, Plank C, Pohl U. Magnetofection potentiates gene delivery to cultured endothelial cells. *Journal of vascular research*. 2003;40:425-434
95. Mannell H, Hammitzsch A, Mettler R, Pohl U, Krotz F. Suppression of DNA-pkcs enhances fgf-2 dependent human endothelial cell proliferation via negative regulation of akt. *Cellular signalling*. 2010;22:88-96
96. Guzman HR, Nguyen DX, Khan S, Prausnitz MR. Ultrasound-mediated disruption of cell membranes. I. Quantification of molecular uptake and cell viability. *The Journal of the Acoustical Society of America*. 2001;110:588-596
97. Karshafian R, Bevan PD, Williams R, Samac S, Burns PN. Sonoporation by ultrasound-activated microbubble contrast agents: Effect of acoustic exposure parameters on cell membrane permeability and cell viability. *Ultrasound in medicine & biology*. 2009;35:847-860
98. Chen H, Hwang JH. Ultrasound-targeted microbubble destruction for chemotherapeutic drug delivery to solid tumors. *J Ther Ultrasound*. 2013;1:10
99. Tran TA, Le Guennec JY, Bougnoux P, Tranquart F, Bouakaz A. Characterization of cell membrane response to ultrasound activated microbubbles. *IEEE transactions on ultrasonics, ferroelectrics, and frequency control*. 2008;55:43-49
100. Afadzi M, Strand SP, Nilssen EA, Masoy SE, Johansen TF, Hansen R, Angelsen BA, de LDC. Mechanisms of the ultrasound-mediated intracellular delivery of liposomes and dextrans. *IEEE transactions on ultrasonics, ferroelectrics, and frequency control*. 2013;60:21-33
101. Delalande A, Leduc C, Midoux P, Postema M, Pichon C. Efficient gene delivery by sonoporation is associated with microbubble entry into cells and the clathrin-dependent endocytosis pathway. *Ultrasound in medicine & biology*. 2015;41:1913-1926
102. Doherty GJ, McMahon HT. Mechanisms of endocytosis. *Annu Rev Biochem*. 2009;78:857-902
103. Aird WC. Endothelial cell heterogeneity. *Cold Spring Harb Perspect Med*. 2012;2:a006429
104. Reitsma S, Slaaf DW, Vink H, van Zandvoort MA, oude Egbrink MG. The endothelial glycocalyx: Composition, functions, and visualization. *Pflugers Arch*. 2007;454:345-359
105. Kuppers V, Vockel M, Nottebaum AF, Vestweber D. Phosphatases and kinases as regulators of the endothelial barrier function. *Cell and tissue research*. 2014;355:577-586
106. Tabit CE, Chung WB, Hamburg NM, Vita JA. Endothelial dysfunction in diabetes mellitus: Molecular mechanisms and clinical implications. *Reviews in endocrine & metabolic disorders*. 2010;11:61-74
107. Ritchie SA, Ewart MA, Perry CG, Connell JM, Salt IP. The role of insulin and the adipocytokines in regulation of vascular endothelial function. *Clinical science (London, England : 1979)*. 2004;107:519-532
108. Chen L, Sung SS, Yip ML, Lawrence HR, Ren Y, Guida WC, Sebti SM, Lawrence NJ, Wu J. Discovery of a novel shp2 protein tyrosine phosphatase inhibitor. *Molecular pharmacology*. 2006;70:562-570
109. Seo DW, Li H, Qu CK, Oh J, Kim YS, Diaz T, Wei B, Han JW, Stetler-Stevenson WG. Shp-1 mediates the antiproliferative activity of tissue inhibitor of metalloproteinase-2 in human microvascular endothelial cells. *The Journal of*

biological chemistry. 2006;281:3711-3721
110. Song M, Park JE, Park SG, Lee DH, Choi H-K, Park BC, Ryu SE, Kim JH, Cho S. Nsc-87877, inhibitor of shp-1/2 ptps, inhibits dual-specificity phosphatase 26 (dusp26). *Biochemical and biophysical research communications*. 2009;381:491-495
111. Kim JA, Montagnani M, Koh KK, Quon MJ. Reciprocal relationships between insulin resistance and endothelial dysfunction: Molecular and pathophysiological mechanisms. *Circulation*. 2006;113:1888-1904
112. Leinonen E, Hurt-Camejo E, Wiklund O, Hulten LM, Hiukka A, Taskinen MR. Insulin resistance and adiposity correlate with acute-phase reaction and soluble cell adhesion molecules in type 2 diabetes. *Atherosclerosis*. 2003;166:387-394
113. Alcaide P, Auerbach S, Luscinskas FW. Neutrophil recruitment under shear flow: It's all about endothelial cell rings and gaps. *Microcirculation (New York, N.Y. : 1994)*. 2009;16:43-57
114. Maas M, Wang R, Paddock C, Kotamraju S, Kalyanaraman B, Newman PJ, Newman DK. Reactive oxygen species induce reversible pecam-1 tyrosine phosphorylation and shp-2 binding. *American journal of physiology. Heart and circulatory physiology*. 2003;285:H2336-2344
115. Weibrecht I, Bohmer SA, Dagnell M, Kappert K, Ostman A, Bohmer FD. Oxidation sensitivity of the catalytic cysteine of the protein-tyrosine phosphatases shp-1 and shp-2. *Free radical biology & medicine*. 2007;43:100-110
116. Alig SK, Stampnik Y, Pircher J, Rotter R, Gaitzsch E, Ribeiro A, Wornle M, Krotz F, Mannell H. The tyrosine phosphatase shp-1 regulates hypoxia inducible factor-1alpha (hif-1alpha) protein levels in endothelial cells under hypoxia. *PloS one*. 2015;10:e0121113
117. Geraldes P, Hiraoka-Yamamoto J, Matsumoto M, Clermont A, Leitges M, Marette A, Aiello LP, Kern TS, King GL. Activation of pkc-[delta] and shp-1 by hyperglycemia causes vascular cell apoptosis and diabetic retinopathy. *Nature medicine*. 2009;15:1298-1306
118. Wirth T, Parker N, Yla-Herttuala S. History of gene therapy. *Gene*. 2013;525:162-169
119. Peng KW, Pham L, Ye H, Zufferey R, Trono D, Cosset FL, Russell SJ. Organ distribution of gene expression after intravenous infusion of targeted and untargeted lentiviral vectors. *Gene therapy*. 2001;8:1456-1463
120. Pan D, Gunther R, Duan W, Wendell S, Kaemmerer W, Kafri T, Verma IM, Whitley CB. Biodistribution and toxicity studies of vsvg-pseudotyped lentiviral vector after intravenous administration in mice with the observation of in vivo transduction of bone marrow. *Molecular therapy : the journal of the American Society of Gene Therapy*. 2002;6:19-29
121. Mou X, Ali Z, Li S, He N. Applications of magnetic nanoparticles in targeted drug delivery system. *Journal of nanoscience and nanotechnology*. 2015;15:54-62
122. Doreswamy K, Muralidhara. Genotoxic consequences associated with oxidative damage in testis of mice subjected to iron intoxication. *Toxicology*. 2005;206:169-178
123. Alustiza JM, Artetxe J, Castiella A, Agirre C, Emparanza JI, Otazua P, Garcia-Bengoechea M, Barrio J, Mujica F, Recondo JA. Mr quantification of hepatic iron concentration. *Radiology*. 2004;230:479-484
124. Rivadulla C, Foffani G, Oliviero A. Magnetic field strength and reproducibility of neodymium magnets useful for transcranial static magnetic field stimulation of the human cortex. *Neuromodulation: Technology at the Neural Interface*. 2014;17:438-442
125. Yellen BB, Forbes ZG, Halverson DS, Fridman G, Barbee KA, Chorny M, Levy R, Friedman G. Targeted drug delivery to magnetic implants for therapeutic applications. *Journal of Magnetism and Magnetic Materials*. 2005;293:647-654

126. Rathel T, Mannell H, Pircher J, Gleich B, Pohl U, Krotz F. Magnetic stents retain nanoparticle-bound antirestenotic drugs transported by lipid microbubbles. *Pharmaceutical research*. 2012;29:1295-1307
127. Chillon M, Lee JH, Fasbender A, Welsh MJ. Adenovirus complexed with polyethylene glycol and cationic lipid is shielded from neutralizing antibodies in vitro. *Gene therapy*. 1998;5:995-1002
128. Boeckle S, Wagner E. Optimizing targeted gene delivery: Chemical modification of viral vectors and synthesis of artificial virus vector systems. *The AAPS journal*. 2006;8:E731-742
129. Gory S, Vernet M, Laurent M, Dejana E, Dalmon J, Huber P. The vascular endothelial-cadherin promoter directs endothelial-specific expression in transgenic mice. *Blood*. 1999;93:184-192
130. Larcher F, Murillas R, Bolontrade M, Conti CJ, Jorcano JL. Vegf/vpf overexpression in skin of transgenic mice induces angiogenesis, vascular hyperpermeability and accelerated tumor development. *Oncogene*. 1998;17:303-311
131. Lee RJ, Springer ML, Blanco-Bose WE, Shaw R, Ursell PC, Blau HM. Vegf gene delivery to myocardium. *Deleterious Effects of Unregulated Expression*. 2000;102:898-901
132. Wiznerowicz M, Trono D. Conditional suppression of cellular genes: Lentivirus vector-mediated drug-inducible rna interference. *Journal of virology*. 2003;77:8957-8961
133. Kafri T, van Praag H, Gage FH, Verma IM. Lentiviral vectors: Regulated gene expression. *Molecular therapy : the journal of the American Society of Gene Therapy*. 2000;1:516-521

7 Appendix

7.1 Index of Abbreviations

AAV	Adeno-associated virus
AB	Antibody
Ala	Alanine
ALD	Adrenoleukodystrophy
ANOVA	Analysis of variance
APC	Allophycocyanin
APS	Ammoniumpersulfate
AZ	Aktenzeichen
BCA	Bicinchoninic acid
BSA	Bovine serum albumine
cDNA	Complementary DNA
CMV	Cytomegalovirus
Ct	Cycle of threshold
Cys	Cysteine
CytoB	Cytochalasin B
DC	Duty cycle
ddH_2O	Double-distilled water
D_i	Inner diameter
DMEM	Dulbecco's modified Eagle's medium
DMSO	Dimethyl sulfoxide
DNA	Desoxiribonucleic acid
D_o	Outer diameter
DPPC	1,2-dipalmitoyl-sn-glycero-3-phosphocholine
DPPE	1,2-dipalmitoyl-sn-glycero-3-phosphoethanolamine
dsDNA	Double-stranded DNA
DSFC	Dorsal skinfold chamber
dsRed	*Discosoma sp.* red fluorescent protein
DTT	Dithiothreitol
EDTA	Ethylenediaminetetraacetic acid
ELISA	Enzyme-linked immunosorbent assay
env	Envelope protein
ET-1	Endothelin-1
FACS	Fluorescence activated cell sorting
FCS	Fetal calf serum
Fe	Iron
FEE	Field enhancing element
FITC	Fluorescein isothiocyanate
GAPDH	Glyceraldehyde 3-phosphate dehydrogenase
GFP	Green fluorescent protein
Glu	Glutamine
HBSS	Hank's buffered salt solution
HEPES	4-(2-hydroxyethyl)-1-piperazineethanesulfonic acid
HIV-1	Human immunodeficiency virus-1
HRP	Horseradish peroxidase
HUVEC	Human umbilical cord vascular endothelial cells
i.a.	intra arterial

i.p.	intra peritoneal
i.v.	intra venous
ICAM-1	Intercellular adhesion molecule-1
IgG	Immunoglobulin G
IP	Infectious particles
IRES-GFP	Internal ribosome entry site-coupled green fluorescent protein
IVC	Individually ventilated cage
Luc-MMB	Luciferase lentivirus coated MMB
LV	Lentivirus
MAPK	Mitogen activated protein kinase
mc	Monoclonal
MF	Magnetic field
MMB	Magnetic microbubble
MNP	Magnetic nanoparticle
MOI	Multiplicity of infection
MPS	Magnetic particle spectroscopy
mRNA	Messenger ribonucleic acid
MTT	3-(4,5-dimethylthiazol-2-yl)-2,5-diphenyltetrazolium bromide
MβCD	Methyl-β-cyclodextrin
NAD(P)H	Nicotinamide adenine dinucleotide phosphate
NO	Nitric oxide
o.a.d.	Of applied dose
OCT	Optimal cutting temperature embedding medium
PAI-1	Plasminogen activator inhibitor-1
PBS	Phosphate buffered saline
PBS-T	Phosphate buffered saline with tween
pDNA	Plasmid DNA
PECAM-1	Platelet endotheliala cell adhesion molecule-1
PEG	Polyethylene glycol
PEI	Polyethylenimine
PEI-Mag	Polyethylenimine-coated magnetic nanoparticles
PFA	Paraformadehyde
pH	negative of the logarithm to base 10 of the molar concentration of hydrogen ions
PI3K	Phosphoinositide-3 kinase
pNPP	Para-nitrophenylphosphate
PTP	Protein tyrosine phosphatase
PtpI IV	PTP inhibitor IV
pY	Phospho-tyrosine
qRT-PCR	Quantitative real time polymerase chain reaction
RAS	Rat sarcoma
RNA	Ribonucleic acid
ROS	Reactive oxygen species
S1	Safety level 1
S2	Safety level 2
SDS	Sodium dodecyl sulfate
SDS-PAGE	Sodium dodecyl sulphate-polyacrylamide gel electrophoresis
SEM	Standard error of the mean
Ser	Serine
SH2 domain	Src homology 2 domain
SHP-2	Src homology 2 domain-containing protein tyrosine phosphatase-2
SHP-2 CS	Dominant negative phosphatase mutant of SHP-2 (Cys459 to Ser459)

SHP-2 E76A	Constitutively active phosphatase mutant of SHP-2 (Glu76 to Ala76)
SHP-2 WT	Wild type form of SHP-2 (unmodified)
siRNA	Small interfering ribonucleic acid
SO-Mag	Silicon oxide-coated magnetic nanoparticles
SPION	Superparamagnetic iron-oxide nanoparticle
ssDNA	Single-stranded DNA
ssRNA	Single-stranded ribonucleic acid
TBS-T	Tris buffered saline with tween
TEMED	Tetramethylethylenediamine
Tyr	Tyrosine
US	Ultrasound
VCAM-1	Vascular cell adhesion molecule-1
VE-cadherin	Vascular-endothelial cadherin
veff-Luc	Viral enhanced firefly luciferase
VEGF	Vascular endothelial growth factor
VP	Viral particles
VSV-G	Glycoprotein G of the vesicular stomatitis virus
WAS	Wiskott–Aldrich syndrome

7.2 Index of Schemes and Figures

7.3 Index of Tables

7.4 Eidesstattliche Versicherung

Heun, Yvonn

Name, Vorname

Ich erkläre hiermit an Eides statt, dass ich die vorliegende Dissertation mit dem Thema

Lentiviral Magnetic Microbubbles: A guidable tool enabling targeted gene transfer to vascular endothelium *in vivo*

selbständig verfasst, mich außer der angegebenen keiner weiteren Hilfsmittel bedient und alle Erkenntnisse, die aus dem Schrifttum ganz oder annähernd übernommen sind, als solche kenntlich gemacht und nach ihrer Herkunft unter Bezeichnung der Fundstelle einzeln nachgewiesen habe. Ich erkläre des Weiteren, dass die hier vorgelegte Dissertation nicht in gleicher oder in ähnlicher Form bei einer anderen Stelle zur Erlangung eines akademischen Grades eingereicht wurde.

München, 01.12.2017

Ort, Datum UnterschriftDoktorandin/Doktorand

7.5 Publications

Perivascular Mast Cells Govern Shear Stress-Induced Arteriogenesis by Orchestrating Leukocyte Function; Omary Chillo, Eike Christian Kleinert, Thomas Lautz, Manuel Lasch, Judith-Irina Pagel, Yvonn Heun, Kerstin Troidl, Silvia Fischer, Amelia Caballero-Martinez, Annika Mauer, Angela R M Kurz, Gerald Assmann, Markus Rehberg, Sandip M Kanse, Bernhard Nieswandt, Barbara Walzog, Christoph A Reichel, Hanna Mannell, Klaus T Preissner, Elisabeth Deindl; Cell Reports 08/2016; 16(8):2197-207

The tyrosine phosphatase SHP-1 regulates Hypoxia Inducible Factor-1α (HIF-1α) protein levels in endothelial cells under hypoxia; Stefan K. Alig and Yvonn Stampnik, Joachim Pircher, Raffaela Rotter, Erik Gaitzsch, Andrea Ribeiro, Markus Wörnle, Florian Krötz, Hanna Mannell; PLoS ONE 03/2015;10(3):e0121113.

Deficiency of the protein-tyrosine phosphatase DEP-1/PTPRJ promotes matrix metalloproteinase-9 expression in meningioma cells; Astrid Petermann, Yvonn Stampnik, Yan Cui, Helen Morrison, Doreen Pachow, Nadine Kliese, Christian Mawrin, Frank-D Böhmer; Journal of Neuro-Oncology 02/2015;122(3).

Prothrombotic effects of tumor necrosis factor alpha in vivo are amplified by the absence of TNFalpha receptor subtype 1 and require TNF-alpha receptor subtype 2; Joachim Pircher, Monika Merkle, Markus Wornle, Andrea Ribeiro, Thomas Czermak, Yvonn Stampnik, Hanna Mannell, Markus Niemeyer, Volker Vielhauer, Florian Krotz; Arthritis research & therapy 10/2012; 14(5):R225.

Site directed vascular gene delivery in vivo by ultrasonic destruction of magnetic nanoparticles coated microbubbles; Hanna Mannell, Joachim Pircher, Franziska Fochler, Yvonn Stampnik, Thomas Räthel, Bernhard Gleich, Christian Plank, Olga Mykhaylyk, Chiheb Dahmani, Markus Wörnle, Andrea Ribeiro, Ulrich Pohl, Florian Krötz; Nanomedicine: nanotechnology, biology, and medicine 04/2012;8(8):1309-18.

7.6 Danksagung

An dieser Stelle möchte ich von ganzem Herzen all denjenigen danken, die auf die eine oder andere Weise an der Entstehung und Vollendung dieser Arbeit Anteil hatten.

Zuallererst möchte ich mich bei meinem Doktorvater Prof. Dr. med. Florian Krötz bedanken, dafür, dass er mir die Möglichkeit gab an diesem spannenden Projekt und in dieser tollen Arbeitsgruppe zu arbeiten. Desweiteren danke ich Prof. Dr. med. Ulrich Pohl und Prof. Dr. med. Andreas Schober dafür, sich als Zweitgutachter für diese Arbeit bereit erklärt zu haben. Professor Pohl möchte ich insbesondere noch einmal für die fortwährende projektbezogene Unterstützung danken.

Ein ganz besonderes Dankeschön möchte ich meiner Betreuerin und Gruppenleiterin Dr. rer. nat. Hanna Mannell aussprechen. Während meiner gesamten Promotionszeit war sie eine unschätzbare Unterstützung für mich. Danke für die vielen produktiven Diskussionen und aufbauenden Worte.

Auch allen meinen Laborkollegen möchte ich danke sagen, denn nur in einem so entspannten, freundlichen und hilfsbereiten Umfeld wie bei uns kann man sich so wohl fühlen wie ich es getan habe. Kathi, Ramona, Thomas, Joachim, Georg, Philipp, Monica, Mustafa, Jenny, Tanja, Melli… Viele von ihnen sind gute Freunde geworden, mit denen ich während der Arbeit und auch außerhalb eine schöne Zeit verbringen durfte.
Allen hier nicht namentlich erwähnten Kollegen danke ich an dieser Stelle für das großartige Arbeitsklima und die erstklassige Hilfsbereitschaft.

Und auch meiner Familie, die mich immer in allen Angelegenheiten unterstützt hat, möchte ich noch ein riesiges Dankeschön aussprechen.